Development of Sustainable Nano-architectures for Plasmonic Applications

By

Osai Jelani Ross Clarke

A Thesis Submitted to
Saint Mary's University, Halifax, Nova Scotia
In Partial Fulfilment of the Requirements for the Degree of
Masters of Science in Applied Science

December 2016, Halifax, Nova Scotia

Approved:	Dr. Christa L. Brosseau Supervisor
Approved:	Dr. Kai Ylijoki Committee Member
Approved:	Dr. Jacob Hanley Committee Member
Approved:	Dr. Peng Zhang External Examiner
Date:	December 15, 2016

Table of Contents Page #

Chapter 1 introduction

1.1 Preamble 1
1.2 Objectives of Thesis 3
1.3 Scope of Thesis 4

Chapter 2 Literature Review

2.1 Introduction 5

2.2 Sustainable Chemistry 5

2.2.1 Principles of Green Chemistry 7

2.2.2 Tools of Green Chemistry 9

2.3 Sustainable Nanotechnology 11

2.3.1 Green Synthesis of Nanomaterials 12

2.3.2 Bioscaffolds 20

2.3.3 Earth Abundant Metals 23

2.4 Sustainable Plasmonics

2.4.1 Introduction 30

2.4.2 Applications 31

2.4.3 Green Synthesis of Silver Nanoparticles 33

2.4.4 Bioscaffolding for Enhanced Plasmonics 36

2.4.5 CuNPs as Sustainable Alternatives to Au and Ag 37

Chapter 3 Theory

3.1 Introduction 38

3.2 Colloids 38

3.3 Plasmonics 45

3.4 Spectroscopic techniques

3.4.1 Raman Spectroscopy 50

3.4.2 Surface Enhanced Raman Spectroscopy 52

3.4.2.1 Enhancement Factor 54

3.4.3 Electrochemical Surface Enhanced Raman Spectroscopy 55

3.4.4 UV-visible Spectroscopy 56

3.6 Electrochemistry

3.6.1 Bulk Electrolysis 57

3.6.2 Voltammetry 58

Chapter 4 Materials and Methods

4.1 Introduction 60

4.2 Reagents 60

4.3 Instrumentation

4.3.1 Raman Spectrometers 60

4.3.2 Potentiostat 61

4.3.3 UV-Visible Spectrometer 62

4.3.4 Scanning Electron Microscope 62

4.4 Plant Extract Preparation 63

4.5 SERS Substrates

4.5.1 Standard Silver Nanoparticle Preparations 64

4.5.1.1 Sodium Citrate Reduced Silver Nanoparticles (Lee-Meisel method) 64

4.5.1.2 Sodium Borohydride Reduced Silver Nanoparticles (Zhao method) 65

4.5.2 Green Synthesis of Silver Nanoparticles from Plant Extracts 65

4.5.3 Preparation of SERS Substrates 66

4.5.4 Displacement of Capping Agents 66

4.5.5 Preparation of SERS Substrates Using Biological Scaffolds 66

4.5.5.1 Diatomaceous Earth 67

4.5.5.2 Drosophila Wings 67

4.5.6 Electrodeposited Copper Substrates on Screen Printed Electrodes 67

4.5.6.1 SWV Modification of Copper Deposited SERS Substrates 68

4.5.6.2 Bimetallic Cu/Ag SERS Substrates 68

4.5.6.3 Additives in Cu Electrodeposition 69

4.5.7 Immobilization of Probe Molecules 69

4.6 EC-SERS 70

4.7 SERS Analysis 70

Chapter 5 Results and discussion

5.0 SERS on Standard Ag Nano-Substrates 71

5.1 Sustainable SERS Substrates: Green Synthesis of Silver Nanoparticles 78

5.1.1 AgNPs Synthesized using Methanolic Berry Extracts 78

5.1.1.1 Strawberry (*Fragaria x ananassa*) Extract (SBE) 78

5.1.1.2 Haskap Berry (*Lonicera caerulea*) Juice (HBJ) 81

5.1.2 Fruit Peel Extract AgNPs 86

5.1.3 Dandelion Flower Extract AgNPs 89

5.1.4 Plant Extracts Prepared in Water 94

5.1.4.1 Avocado (*Persea Americana*) Pit Extract AgNPs 97

5.2 Bio-Scaffolds 102

5.2.1 Diatomaceous Earth 103

5.2.2 Fruit Fly (*Drosophila melanogaster*) Wings as SERS Templates 113

5.3 Copper SERS Substrates 115

5.3.2 PEG and KCl as Additives 130

Chapter 6 Conclusions and Future Work

6.1 Green Synthesis of Ag Nanoparticles for SERS 135

6.2 Bioscaffolding 136

6.3 Cu SERS Substrates 137

6.4 Final Thoughts 139

References 140

Appendix

Abstract

Development of Sustainable Nano-architectures for Plasmonic Applications

By

Osai Jelani Ross Clarke

Plasmonic nanostructures that are uniform in size and shape are highly desirable for many applications, including plasmon-enhanced solar cells and localized surface plasmon resonance (LSPR) sensing. Unfortunately, such structures are often difficult and costly to fabricate, which limits their widespread application. Therefore, there is great interest in *sustainable* plasmonic architectures that can be manufactured using low cost, energy-efficient fabrication strategies, using earth-abundant metals. The recent progress towards the development of sustainable plasmonic architectures for a variety of applications, including rapid diagnostics and surface-enhanced Raman spectroscopy (SERS) sensing is presented.

Acknowledgments

I would like to thank Dr. Christa L. Brosseau for being my research supervisor. I would also like to thank Dr. Jacob Hanley and Dr. Kai Ylijoki for being on my supervisory committee and Dr. Peng Zhang for agreeing to be my external examiner. In addition, I would like thank both the past and present Brosseau group members for their support and any contributions to my research.

I acknowledge the following agencies for funding various aspects of this research: Natural Sciences and Engineering Research Council, Canadian Foundation for Innovation, Nova Scotia Research and Innovation Trust. I would also like to thank the Department of Chemistry and the Faculty of Graduate Studies and Research at Saint Mary's University.

List of Abbreviations

4,4'-bipy	4,4'-bipyridine
APE	Avocado Pit Extract
BPA	Bisphenol A
BPE Y,I, G	Banana Peel Extract from Yellow, Intermediate and Green Peels
CM	Chemical Mechanism
CTAB	Cetyltrimethyl Ammonium Bromide
CV	Cyclic Voltammetry
DFE	Dandelion Flower Extract
DLVO theory	Derjaguin, Landau, Verwey and Overbeek Theory
DMAB	4,4'-Dimercaptoazobenzene
DSSCs	Dye Sensitised Solar Cells
EC	Electrochemical
EBL	Electron Beam Lithography
EDS	Energy Dispersive X-ray Spectra
EF	Enhancement Factor
ENMs	Engineered Nanomaterials
EM	Electromagnetic Mechanism
FWHM	Full Width at Half Maximum
FIB	Focused Ion Beam
HBJ	Haskap Berry Juice
ISO	International Organization for Standardization
IUPAC	Union of Pure and Applied Chemistry
LSP	Localised Surface Plasmon
LSPR	Localised Surface Plasmon Resonance
MIC	Methyl Isocyanate
OCP	Open Circuit Potential
OPE	Orange Peel Extract
PEG	Polyethylene Glycol
PGM	Platinum Group Metals
PSP	Propagating Surface Plasmon
PVA	Polyvinyl Alcohol
PZC	Potential of Zero Charge
SBE	Strawberry Extract
SDD	Silicon Drift Detector
SDBS	Sodium Dodecyl Benzene Sulfonate
SEM	Scanning Electron Microscopy
SERS	Surface Enhanced Raman Spectroscopy
SHE	Standard Hydrogen Electrode
SP	Surface Plasmon
SPEs	Screen Printed Carbon Electrodes
SPR	Surface Plasmon Resonance
SSV	Sphere Segment Void
SWV	Square Wave Voltammetry

List of Figures

Figure #	Description	Page #
1.1	Flowchart of research objectives	**3**
2.1	Periodic table depicting relative supply status of the elements (reproduced with permission)	**25**
3.1	Percentage of surface atoms as a function of palladium cluster diameter	**39**
3.2	LaMer model of uniform particle formation	**42**
3.3	Electrical double layer structure for colloidal Ag or Cu based on the Stern model.	**43**
3.4	Schematic of interaction energy as function of double layer thickness. Double layer size is decreased by increasing salt concentration.	**44**
3.5	Real and imaginary dielectric functions for gold, silver and silicon	**47**
3.6	Quality factor for different metals as a function of wavelength of incident radiation.	**48**
5.1	SERS spectra of 10 mM p-ATP on citrate reduced AgNPs. The peaks marked by stars are bands assigned to citrate vibrational modes. (30 s, 22.3 mW, 785 nm laser)	**72**
5.2	Cathodic EC-SERS plot of 10 mM p-ATP on citrate reduced-AgNPs. Supporting electrolyte 0.1 M NaF, 532 nm laser, 3 mW, 30 s acquisition.	**73**
5.3	EC-SERS of p-ATP on citrate reduced AgNPs in 0.1 M NaF. A 532 nm laser was used, 3 mW, 30 s acquisition.	**75**
5.4	Extinction profile of citrate and sodium borohydride reduced AgNPs suspended in water.	**77**
5.5	SEM of citrate-reduced AgNPs (left) and $NaBH_4$-reduced AgNPs (right)	**77**
5.6	Extinction profile of strawberry extract reduced AgNPs with varying amounts of 0.1M NaOH. For each trial addition of base, a spectrum was taken immediately (within 5 minutes) and 24 hours later.	**79**
5.7	SERS of 1mM p-ATP on AgNP made from citrate reduction in black and strawberry extract in red. 785nm laser line used. (30 s, 22.2 mW)	**81**
5.8	SERS of 1 mM p-ATP for blueberry extract AgNP and haskap juice AgNPs. 785nm laser line used. (30 s, 22.2 mW)	**82**
5.9	UV-vis extinction profile for haskap juice AgNP and cane sugar AgNPs.	**83**
5.10	SERS of 1mM p-ATP on Haskap juice AgNP and brown sugar AgNPs. 785nm laser line used. (30 s, 22.2 mW)	**85**

5.11	Extinction spectra of BPE AgNP with no heat immediately after the addition of NaOH (black) and 2 hours later (red).	**87**
5.12	SEM image of BPE AgNPs on the left, and histogam of size distribution for 100 NPs on right (Image J software, NIH).	**88**
5.13	SERS of 1mM p-ATP on orange peel extract (OPE) AgNP and banana peel extract (BPE) AgNPs. 785nm laser line used (30 s, 22.3 mW).	**89**
5.14	SEM of dandelion flower extract (DFE) AgNPs on the left and the histogram of size distribution on the right for 50 NPs.	**90**
5.15	SERS of 1 mM p-ATP for all extract synthesized AgNPs including the standard citrate reduced AgNPs. DMAB peaks are noted by a star. 785nm laser was used (30 s, 22.2 mW).	**91**
5.16	EC-SERS of 1 mM 4,4'-bipridine in 0.1 M NaF on a DFE AgNP modified SPE. 785 nm laser was used (30 s, 22.3 mW).	**93**
5.17	SERS of p-ATP on AgNP made from DFE in methanol (red) and in water (black). Both spectra have been baseline corrected using the DeltaNu software. 785nm laser used (30 s, 22.3 mW).	**95**
5.18	The peels of differing degree of ripeness for bananas, from most ripened (yellow) on the left to least ripened (green) on the right.	**96**
5.19	SERS of 1mM p-ATP on green (BPE G), intermediate (BPE I) and yellow (BPE Y) AgNPs. 785 nm laser was used. (30 s, 22.3 mW)	**97**
5.20	SEM of APE synthesised AgNPs on the left and size distribution on the right.	**98**
5.21	SERS of 1mM p-ATP on DFE and APE AgNPs 785 nm laser was used (30 s, 22.3 mW).	**99**
5.22	SERS of 1mM 4,4'-bipyridine on APE AgNPs treated with KCl prior to adding the probe (red) and with no pre-treatment(black)	**100**
5.23	Ten spots on APE SERS substrate treated with 10 mM 4,4'-bipyridine. 785 nm laser, 30 s acquisition, 22.3 mW.	**101**
5.24	SEM citrate-reduced AgNPs (a) & (b) and *in situ* diatom-citrate-reduced AgNPs (c) & (d).	**104**
5.25	SEM of diatom-AgNP 3D SERS substrate directly from the bulk colloidal mixture (A) & (C), and post centrifugation (B) & (D).	**105**
5.26	SERS of 1 mM p-ATP on citrated-reduced silver nanoparticles (black) and on diatom-AgNPs (red). 785 nm laser-line was used (30 s, 22.3 mW (black) 10.6 mW (red)).	**106**
5.27	SERS of 4,4'-bipyridine on citrate reduced diatom-AgNPs using a	**107**

785nm laser line(30 s, 2.93 mW). Each spectrum is the average of 10 spectra collected from 10 different spots on the SERS substrate.

5.28 EC-SERS p-ATP on Ag-diatom SERS substrates made from citrate reduction (532 nm laser 30 s, 3 mW). Asterisks indicate catalytic peaks due to DMAB. **108**

5.29 Cathodic EC-SERS of 0.1 mM 4,4'-bipyridine in 0.1 M NaF on diatom-AgNP substrates made from *in situ* $NaBH_4$ reduction. 532nm laser was used at 3 mW for 30 seconds for each spectrum. **109**

5.30 Plot of EC-SERS measurements of p-ATP collected on diatom-AgNP substrates made from *in situ* $NaBH_4$ reduction. The measurements were taken with a 532 nm laser, power of 3 mW for 30 s at open circuit potential (OCP) in 0.1 M NaF. **111**

5.31 SERS measurements of 4,4'-bipyridine collected on diatom-AgNP substrates made from in situ $NaBH_4$ reduction (A). Linear relationship between the intensity at 1615 cm^{-1} and concentration (B). The measurements were taken with a 785 nm laser (2.93 mW and acquisition time of 30 seconds). **111**

5.32 SEM images of drosophila wings on the left and $NaBH_4$ reduced AgNP coated drosophila wings on the right. **114**

5.33 SERS of 1 mM p-ATP on $NaBH_4$ reduced AgNP-Fruit fly wing substrate (red), on $NaBH_4$-reduced AgNPs (black).(785nm, 30 sec, 10.6 mW (black) and 2.93 mW (red). **114**

5.34 SERS of 1 mM p-ATP on citrate-reduced AgNPs (blue), copper deposits created at -0.3 V for 3 mins in 0.1 M $CuSO_4$ (red), copper deposits created at -0.3 V for 3 mins in 0.1 M $CuSO_4$ followed by SWV (0.00 V to -1.4 V) (black). **117**

5.35 Cu deposits formed from electrodeposition in 0.1 M $CuSO_4$ at a potential of -0.300 V vs Ag/AgCl for 3 minutes (A) and the same substrate after a SWV treatment between 0.000 V and -1.400 V (B). **118**

5.37 SERS of 10 mM p-ATP on Cu substrate made from 0.1 M $CuSO_4$ -0.3 V, 3 minute deposition followed by SWV (0.00 V to -1.4 V) (orange) and $NaBH_4$ AgNP (grey). 785 nm laser, 30 s, 10.6 mW orange, 2.93 mW (grey) (spectral baseline correction performed using NuSpec software) **119**

5.38 Cu deposits produced with a -0.3 V potential for a period of 3 minutes from a purged 0.1 M $Cu(NO_3)_2$ aqueous solution. **121**

5.39	SERS of 1 mM p-ATP on Cu substrate made from 0.1 M $Cu(NO_3)_2$ (-0.3 V, 3 minute deposition (orange) and $NaBH_4$ AgNP (grey)). 785 nm laser, 30 s, 2.93 mW (Spectra are baseline corrected using NuSpec software)	**122**
5.40	SERS of 1 mM p-ATP on Cu substrate made from 0.1 M $Cu(NO_3)_2$ - 0.3 V, 3 minute deposition (orange) and $NaBH_4$ AgNP (grey). 532 nm laser, 30 s, 3 mW (Spectra were baseline corrected using NuSpec software)	**124**
5.41	Ag dendrite deposit on SPE formed during a mixed copper-silver deposition study.	**125**
5.42	SEM of sequentially deposited Cu-Ag deposit using 250 µl 1 x 10^{-4} M $AgNO_3$ (A), EDX of cube deposit face with flower-like growth (B), and EDX of cube without growth (C).	**127**
5.43	SEM of sequentially deposited Cu-Ag using 500 µl 1 x 10^{-4} M $AgNO_3$.	**127**
5.44	EC-SERS of 1mM p-ATP in the cathodic direction on Cu-Ag (500 µl of the 0.1 mM $AgNO_3$) sequential substrates using the 532 nm laser line. 0.1 M NaF was used as the electrolyte.	**129**
5.45	EC-SERS of 1mM p-ATP in the anodic direction on Cu-Ag (500 µl of the 0.1 mM $AgNO_3$) sequential substrates using the 532 nm laser line. 0.1M NaF was used as the electrolyte.	**129**
5.46	EC-SERS of 1mM p-ATP on Cu-Ag sequential substrates at OCP in black, -1V in red and OCP at the end of the anodic collection in blue using the 532 nm laser line. 0.1 M NaF was used as the electrolyte.	**130**
5.47	SEM image of Cu deposit on SPE from an electroplating bath of 0.5 ml 0.2 mM cholesterol-PEG and 10 ml 0.1M $Cu(NO_3)_2$. (-0.3 V Ag/AgCl for 3 minutes).	**133**
5.48	Electrodeposition of Cu from a 10 ml 0.1 M copper nitrate electroplating bath containing 1 ml PEG and 0.05 g KCl. Applied potential -0.3 V for 3 minutes. On the left rosebush-like deposit and on the right cubic deposits shown on and in-between the rosebush deposit.	**133**

List of Tables

Table #	Description	Page #
4.1	Associated spectral window and resolution for the different laser lines and their associated diffraction gratings for the DXR SmartRaman.	**61**
4.2	Quantities of plant parts and solvent required for each extraction	**63**
5.1	SERS peaks for p-ATP and DMAB on silver substrates.[87]	**74**
5.2	SERS Band assignments for 4,4'-bipyridine.[88]	**93**
5.3	Electrochemical potential versus Ag/AgCl and deposition time that was used for the initial trials. Y indicates a Cu deposit was noted, N indicates no Cu deposit was present. All observations were initially made by visual inspection.	**116**
5.4	Combinations of additives investigated for Cu electrodeposition	**131**

Chapter 1 introduction

1.1 Preamble

Plasmonics is the field of study which investigates the unique optical and electronic effects observed when certain nanoscale metals interact with light. At the nanoscale, some metals are able to interact with the electric field of incident electromagnetic radiation via their free conduction electrons. This allows one to enhance the local electric field of the impinging radiation and also manipulate light at the nanometer length scale. The potential applications of plasmonic technology range from improved photovoltaics to targeted cancer therapy.[1,2] However, in order for plasmonics to have a prolonged impact on current technologies, the long-term sustainability of the plasmonic materials must be addressed.

Over the last two decades the field of plasmonics has grown quite rapidly without addressing whether or not current protocols are sustainable. For example, using toxic and/or harsh reducing agents in solution-based synthetic strategies, scientists have been able to produce nanoscale gold and silver metal structures that are fairly monodispersed. While monodispersed nanostructures are ideal in terms of plasmonic performance, using reagents that are potentially harmful to the operator and/or the environment is far from sustainable. By using potent antioxidants found in plant and fruit extracts, similar structures can be produced with little to no detrimental impact.[3-5] This thesis work will explore the green synthesis of silver nanoparticles using a variety of plant extracts, and evaluations of the plasmonic performance in each case will be presented.

Another important issue when it comes to the sustainability of plasmonics is the need for ordered, hierarchical nanostructures in multiple dimensions. Such structures have

optimal and controllable properties. Fabrication of these structures is typically accomplished using high cost, energy intensive lithographic techniques like electron beam lithography (EBL) and focused ion beam (FIB). Such techniques suffer from an additional drawback, they are generally not scalable for large scale applications such as in plasmonic-assisted photovoltaics. A potentially more sustainable route for the production of multidimensional nanoarchitectures is one that relies on the natural nanoscale order present in certain biological materials; this approach is termed bioscaffolding. In this approach, biological materials are used as a scaffold, or template, for the production of highly functional plasmonic materials. This thesis work will explore several different biological materials for this bioscaffold approach that are abundant in nature and exhibit interesting nanoscale order.

Lastly, the coinage metals (Ag, Au, Cu) are well known to be the ideal candidates for plasmonics; however, the field of plasmonics has focused primarily on gold and silver, which offer the promise of stable nanostructures and biocompatibility. However, both Au and Ag are costly, and face earth-abundance limitations in the next 100 years due to current demand and projected use. Copper, unlike the other two coinage metals, is low cost and earth abundant; however, it is more susceptible to surface oxidation and only a handful of copper nanostructures have been reported in the literature. This thesis work will explore controlled electrodeposition for the facile synthesis of plasmonic copper nanostructures as well as bimetallic nanostructure systems.

1.2 Objectives of Thesis

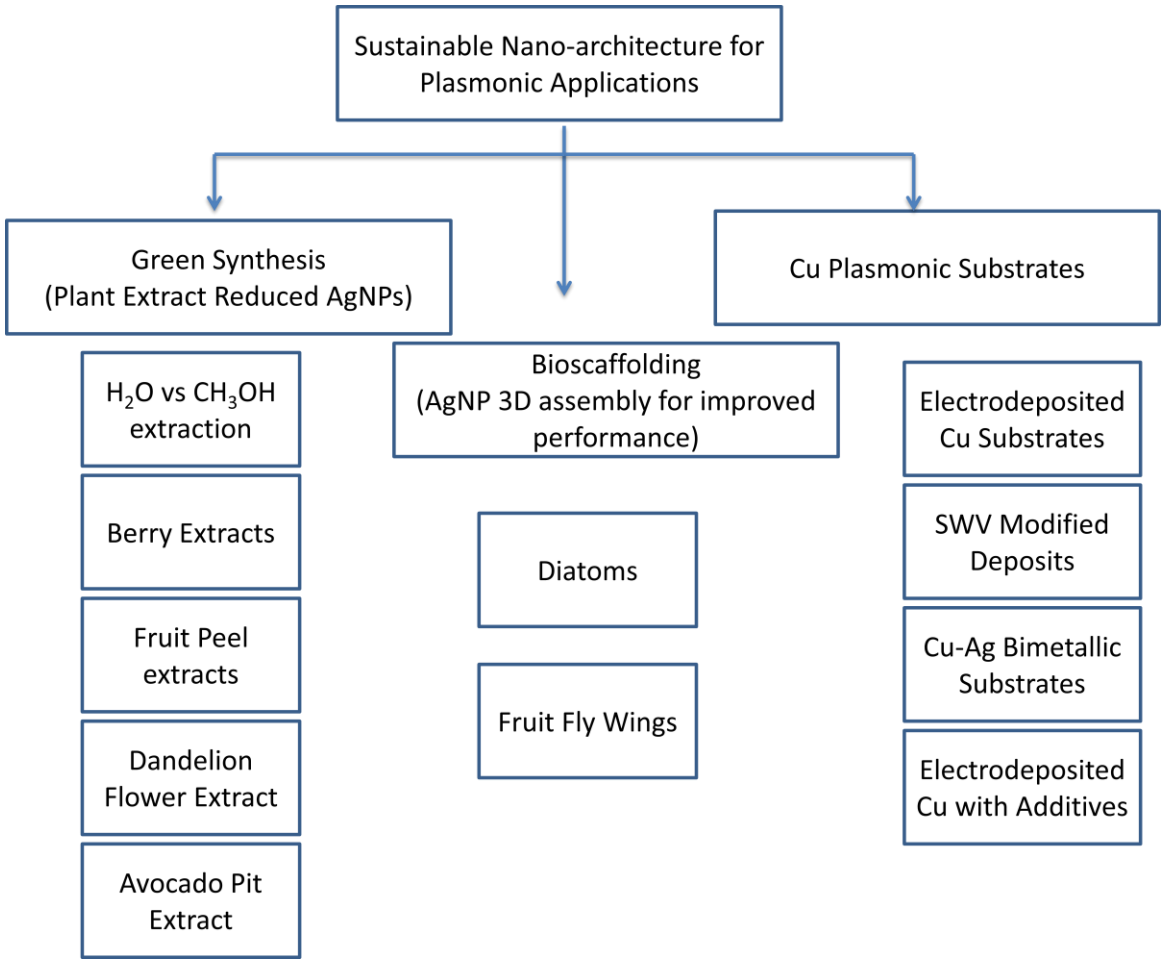

Figure 1.1: Flowchart of research objectives

1.3 Scope of thesis

This thesis is divided into 6 chapters. Chapter 1 introduces the reader to the project and states the objectives and scope of this work. Chapter 2 provides a literature review of sustainable nanotechnology and some applications for those developments. Chapter 3 consists of the prerequisite background theory for the spectroscopic and electrochemical techniques as well as introduces key concepts in colloidal science, plasmonics and catalysis. Chapter 4 reviews the instrumentation, reagents and methodologies for carrying out the experiments.

The experimental results and discussion of findings are provided in chapter 5. Chapter 5 breaks down the sustainable nano-architectures for plasmonic purposes into the 3 components as listed in the previous section. Hence green synthesis, bioscaffolding, and copper nanostructures are all discussed individually. Lastly, Chapter 6 provides the conclusions and future directions for the presented work.

Chapter 2 Literature Review

2.1 Introduction

The aim of this section is to provide the reader with an overview of sustainable chemistry and highlight the tools used to achieve it. The impact of nanotechnology is addressed, showcasing the merit of three strategies; namely green synthesis of nanomaterials, bioscaffold-assisted approach to multidimensional structures and exploring the use of earth abundant metals. The focus then narrows down to a discussion of sustainable plasmonic nanotechnology and its applications.

2.2 Sustainable Chemistry

It is very apparent how chemistry has revolutionised the way people live. Especially since the 20th century with the creation of modern medicines people have been able to outlive predicted life expectancies for many diseases that were once thought to be terminal. Chemistry has significantly contributed to today's society by serving as the foundation from which society meets its energy and consumer demands.[6,7] Despite being among the most impactful sciences, poor communication with the general public has resulted in a situation of distrust.[6] One can say that the media is partly to blame for this as fear mongering tactics associated with the chemical industry has strained relations, but at the same time there are many valid reasons for this public distrust. Prior to the 1980's the chemical industry paid very little attention to generated waste material that was hazardous and polluting, ascribing instead to the simple mantra of "dilution is the solution to pollution."[6] However chemical industrial accidents like that of the Bhopal India catastrophe, where an Indian subsidiary of Union Carbide accidentally leaked a highly

toxic reagent called methyl isocyanate (MIC), which claimed the lives of over 3,000 people and injured more than 40,000 others.[6] In more recent news it has been unearthed that Bayer sold HIV infected haemophilia drugs that were banned in the U.S. to the rest of the world.[8] Another such atrocity was the Love Canal community, which was the site of years of improper disposal of hazardous waste material in the 1940's and later used as a residential community. The extent of the pollution so badly impacted the health of residents that the U.S. government had to intervene. The residents were forced to vacate so that a cleanup, spearheaded by the EPA and funded by a special government program to aid cleanup of hazardous waste material, could be undertaken.[6]

Besides the obvious toll on human health and sustained environmental impacts, there are other pressing matters that chemistry has to also address going forward. The diminishing supply of fossil fuels alongside a growing demand for energy and petrochemical by-products means alternatives to those processes must be found.[4] Those considerations have rallied discussions for sustainable development: a strategy that meets the needs of the current generation without sacrificing the ability of future generations to meet their own needs.[9] Sustainable development can be thought of as a strategic goal utilising many practical approaches consisting of economics, education, business, and society. Under the umbrella of sustainable chemistry one would find renewable energy, industrial ecology, green engineering and last but not least, green chemistry.[10] Sustainable chemistry allows the production of energy from alternative sources, and seeks better waste management through better engineered processes that key into the material and energy embodiments of processes. Green chemistry is vital to these goals as its focus is

aimed at waste reduction, as well as human and environmental safety, as highlighted in the following section. [11]

2.2.1 Principles of Green Chemistry

According to the EPA, green chemistry is the design of chemical products and processes that reduce or eliminate the generation of hazardous substances.[9] If one is aiming to reduce or eliminate the use and generation of hazardous substances, in effect green chemistry is being practiced.[9] The most pivotal part of green chemistry lies in the design phase as it puts the onus on the chemist to intentionally seek out the above mandate and not arrive there accidently. The founders of green chemistry Paul Anastas and John Warner created a series of 12 guiding principles to help one "green" a chemical process.[9-11] The 12 principles of Green Chemistry are as follows:

1) **Prevention**. It is more ideal to prevent waste than to clean it up.
2) **Atom Economy**. Design atom efficient synthetic methods so that all the atoms in the starting material are incorporated into the final product(s).
3) **Less Hazardous Chemical Synthesis**. Where possible, choose synthetic routes that use nontoxic compounds.
4) **Designing Safer Chemicals**. Design new products that preserve efficacy of the function while reducing toxicity
5) **Safer Solvents and Auxiliaries**. Minimise the use of auxiliary reagents and solvents but when necessary they should be innocuous.

6) **Design for Energy Efficiency**. Design processes with minimal energy requirements; if possible processes should be conducted under conditions of ambient temperature and pressure.
7) **Use Renewable Feedstocks**. Preferably use renewable raw materials.
8) **Reduce Derivatives**. Seek to avoid unnecessary blocking groups, protection/deprotection, and all other temporary physical or chemical processes.
9) **Catalysis**. Replace stoichiometric reagents with catalytic cycles.
10) **Design for Degradation**. Design products with biodegradable capabilities such that they do not persist in the environment.
11) **Real-Time Analysis for Pollution Prevention**. Develop real-time and online process analysis methods to monitor the formation of hazardous compounds
12) **Inherently Safer Chemistry for Accident Prevention**. Make use of feedstocks and design strategies that lower the likelihood of accidents.

There are three driving forces for the green chemistry initiative. Societal pressure ensures that companies seek to do better by their clients as they are more likely to support a company they trust.[12] Another driving force is government legislation, which is meant to back the will of the people for less hazardous materials, holding companies responsible for their actions.[12] The final driving force is the obvious economic benefit from using less material and having less waste to manage.[12]

2.2.2 Tools of Green Chemistry

There is no absolute degree of greenness but instead a relative measure of how green a particular process is compared to a previous process is generally the focus of a discussion. One should aim to design processes that abide by as many of the previously mentioned guiding principles as possible. To assist in crafting greener processes there are several tools that one can use, as will be highlighted below.

Use of alternative feedstocks is instrumental to greening processes as they ultimately govern the environmental and health effects arising from the process.[9-11] That being said, it is important that materials be benign to both the people that will come into contact with them and to the environment once disposed of. This choice is one of the more crucial ones as it will determine the market for a particular product as prices may vary based on the amount of work required to refine or obtain a feedstock.[10] The most commonly used feedstocks are petroleum-based which require a very energetic oxidation step in order to make organic products.[10] This is also a depleting feedstock as opposed to a renewable feedstock like alternative agricultural and biological feedstocks. Such alternative feedstocks are already highly oxygenated and so avoid the high energy embodiment of petroleum feedstocks to produce chemical products. Some products, such as certain textiles and plastics, have been derived from renewable starting materials such as soy and hemp.[10]

Alternative reagents have to also be vetted because the starting materials may require certain transformations in order to be made into useful products. The starting material may provide a stoichiometric or catalytic pathway or may just be superior from

an atom economic standpoint.[13] In addition, solvent choice can be added to a tool box of options a chemist has to green a chemical process.[12] For example, some solvents are inherently better than others depending on the desired outcome, but in the pursuit of greening as little of the solvent should escape during the reaction, solvents chosen should be safe to handle, and the best situation is one where no solvent is required.

The trade-offs between performance and risk cannot be overlooked when it comes to pollution reduction and safety considerations.[10] As toxicological studies start to further compliment the design phase, chemists are starting to note not only toxic products but parts of molecules that may have toxic effects. Such toxic functionalities are termed toxophores.[11] An example of a known toxophore is the endocrine-disruptor bisphenol A (BPA) used in the synthesis of plastics.[14] Through real time tracking of BPA transfer from product (e.g. plastic bottle or receipt paper) to human it was discovered that when this toxophore was found in receipt paper it was more likely to be found in dangerously high quantities in people who handled it than those who used BPA containing bottles.[15] Now alternatives like BPA-free receipt paper and electronic receipts help mitigate some of the adverse effects. This is the power of the green chemistry tool box.

Lastly, alternative catalysts can be explored to make the tool box a comprehensive one. Catalysts improve process efficiencies greatly by not only cutting down on process time but eliminating transformations of reagents that would be required in their absence.[13] Certain heavy metal catalysts have been found to have toxic effects.[13] An example of this is the use of cobalt-based catalysts in the production of paints and coatings. The cobalt is used to catalyze the cross-linking of unsaturated fatty acid moieties to chemically dry them for use as binding agents in the paint and coatings.[16] Guebitz and coworkers have

demonstrated a biocatalytic pathway using the enzyme laccase that out performs the cobalt catalyst.[16] There is not always an immediate alternative so it becomes an integral part of the design stage to model processes that halve reduced catalyst loadings. One way in which to reduce catalyst loadings is through the use of high surface-area nano-sized catalysts, such as metal nanoparticles. In addition, there is a great need to move away from catalysts based on earth-limited elements such as the rare earth elements and platinum group metals, and to focus on earth-abundant elements for catalysis, such as iron and nickel.[13]

2.3 Sustainable Nanotechnology

Nanotechnology is the branch of science that makes use of materials that have at least one dimension between 1 – 100 nm.[17] To put things in perspective, the thickness of a strand of human hair can vary from 40,000 – 100,000 nm in diameter. The field of nanotechnology is a rapidly growing field that can attribute its growth to several things: [17, 18] 1) materials at the nanoscale display behaviours that are different from their bulk counterparts and 2) one is afforded a much larger surface area since many more atoms reside at the surface. Nanotechnology has a wide range of application in next generation technologies; as a result the market was estimated to generate $225 billion dollars in 2009 and is forecasted to be a $3 trillion market by the year 2020.[18] Clearly a market with such a path for growth will benefit from sustainability considerations.

The availability of newer material characterisation tools has led to the establishment of several classes of engineered nanomaterials (ENMs) including pure metals like gold and silver, metal oxides like titanium dioxide and zinc dioxide, metal

chalcogens like CdS and CdSe (commonly referred to as quantum dots) and carbon-based nanomaterials such as carbon nanotubes and graphene.[19] By applying the principles of green chemistry to the ENM design process it is possible to get enhanced efficacy with less detrimental environmental and human health impacts. The design process must incorporate starting materials from renewable feedstocks whenever possible. Some ENMs can only be derived from non-renewable starting materials and so it becomes imperative to consider if the elements are in short supply or derived from conflict minerals.[18]

The myriad of applications of ENM makes it necessary to apply the World Commission on Environment and Development's definition of sustainability to the field.[19] The commission has defined sustainability as "development that meets the needs of the present without compromising the ability of future generations to meet their own needs." There are several issues that one is confronted with when considering sustainable nanotechnology. For starters, scientists still deem the field of nanoscience to be in its infancy and therefore one cannot properly gauge a direction for its future.[20] In addition, very little is known about the toxicology of nanomaterials and published data has produced contradictory outcomes.[21]

2.3.1 Green Synthesis of Nanomaterials

Nanoparticle synthesis can proceed through two general approaches: 1) the top-down approach, where one starts with a large structure that is broken down into nanoscale components and 2) the bottom-up approach, wherein one starts with the smallest substituents (atoms, ions) that are then assembled into nanoscale objects.[22,23] Top-down techniques can be grouped into two categories: mechanical or chemical. Mechanical

strategies include milling, extrusion, and grinding. Chemical strategies include evaporation, sputtering, and chemical etching techniques. The bottom-up approach is less energy intensive and resulting structures are closer to being monodipserse.[23] Precipitation and chemical reduction are two widely used bottom-up synthetic routes with the latter being the most common.[3-5]

Metal and semiconducting ENMs will be the focus of the rest of this section. Both types of nanoparticles have synthetic strategies that can be improved upon. In the early 1990's it was shown by Bawendi and coworkers that monodisperse nanoscale semiconductor materials could be produced via a simple pyrolysis procedure.[23] It was this insight that brought about the rational division of the synthetic process into two stages: nucleation and growth. This two stage mechanism has been manipulated to produce nanoparticles of many different shapes and sizes.[23]

The most common way of producing a nanomaterial using the bottom-up approach is *via* the reduction of metal ions in aqueous solution. Once the metal cations are subjected to strong enough reducing agents and a colloidal stabilizer, nucleation of the cations to stabilised metallic species ensues.[23] There are two mechanisms by which metal nanoparticles are formed *via* reduction: the first of which was mentioned earlier 1) *nucleation and growth* - after the reduction of the metal cations to elemental nuclei, the now zero valent nuclei grow/assemble into nanoparticles and 2) *Seed-mediated growth* - metal nanoparticles typically serve as the seeds and are introduced to a growth solution composed of metal ions and capping agents that will facilitate the growth of the secondary metal from the metal ions onto the surface of the seed.[3,23]

It is clear that if one wants to obtain monodispersed nanoparticles that the nucleation rate must be high so as to prevent the formation of new nuclei after the first nucleation burst; this is referred to as the saturation point.[23] If complete nucleation is achieved in one burst, metal precursors only deposit on the existing particles in the growth phase.[24,26] This would result in all nuclei being exposed to growth conditions for approximately the same time, hence they would be approximately the same size. The concentration of the metal precursors (metal cations) affects how quickly one is able to get to the saturation point. The higher the concentration of precursor, the faster the saturation point is achieved.[23,5]

Capping agents are used in colloidal synthetic strategies to stabilise the nanostructures in several ways: imposing size constraints, controlling morphology, and protecting nanostructures from aggregation. Most capping agents used to date are heteroatom-functionalised long chain hydrocarbons.[3] Some examples of typical capping agents include oleic acid, oleyamine, trioctylphosphine, and dodecanethiol. These molecules bind very strongly to the surface of metal ENMs. This allows the synthesis of nanoparticles with near monodispersity that can be self-assembled into highly ordered patterns.[3] Despite these advantages, capping agents can be difficult to remove from the surface of the nanoparticles, which can impact their properties. Some capping agents have been noted to have negative environmental impacts. An alternative would be to use more weakly bound capping agents, such as polymers. Polymer capping agents can be removed with less energy intensive processes. This is often a requirement when one thinks of catalysis. The more unoccupied surface area there is to support catalytic function the better. Hutchings and coworkers found that polymer capping agents such as polyvinyl

alcohol (PVA) used to cap gold nanoparticles can be removed by simply using hot water.[24] This facilitates their later use for catalysis where it is evident that CO_2 conversion increased by upwards of 50% after polymer capped nanoparticles were washed with hot water.[24]

Dendrimers are another type of capping agent that can be used in colloidal nanoparticle synthesis. A dendrimer is a synthetic polymer with tree-like branching that can support small substrates at their centres. Those substrates are the precursor building blocks for what will eventually become a nanoparticle. The real benefit of the dendrimer capping agents is the ability to produce small nanoparticles with narrow size distribution in the absence of a strong capping agent. Hence, dendrimer capping agents can also be removed easily as Yamamato and coworkers have demonstrated with the use of dendrimers to make TiO_2 nanoparticles.[25]

Block co-polymers have been utilized as capping agents that give one the ability to control the size of the nanoparticles with low polydispersity.[3] The most common block copolymer used in colloidal nanoparticle synthesis is poly (acrylic acid)-block-polystyrene (PAA-b-PS). This block co-polymer has been shown to be toxic, so before using such a capping agent the trade-offs have to be assessed.[3]

Green capping agents are ideally those that are nontoxic, exist in nature, and can be separated fairly easily for reuse or disposal. Polysaccharides are a popular choice as a green capping agent as they are water soluble, low-cost, and generally environmentally friendly. In addition, polysaccharides can also be easily removed from the nanomaterial surface due to weak binding affinity. Dextran has been shown to have great promise as a

capping agent in the production of iron oxide nanoparticles; in addition it can also serve as a reducing agent. The polysaccharides are mostly desirable for their environmentally benign feature.[3] Additional green capping agents include proteins and peptides.[26] Cubic and tetrahedral Pt nanoparticles have been shown as possibilities emanating from the distinct adsorption abilities of peptides to nanoparticle precursors.[26]

The vast majority of nanoparticle synthetic strategies utilize a chemical reduction and therefore the reducing agent plays a key role in the type and quality of nanoparticles that may result. Many reducing agents that are currently used are toxic and have negative environmental impacts.[3] Some of the more commonly employed reducing agents include sodium borohydride ($NaBH_4$), hydrazine (N_2H_4), and formaldehyde. All three are noted as being flammable and hydrazine and sodium borohydride are both dangerous to the environment.[3] This means additional steps have to be taken in order to safely manage the use of such reducing agents especially given the fact that experimentally the reducing agents are used in stoichiometric excess, which means their harsh reducing behaviour can persist after the synthesis.[3] Another commonly used reducing agent in nanoparticle synthesis is H_2 gas but this is relegated more or less to use in research laboratories. This is the case because industrial applications try to avoid the potential explosive combustion of H_2 gas under high pressure with air. The dangers associated with the above reducing agents warrant a search for safer more benign alternatives. One of the first alternatives has been mentioned above already: polysaccharides. The hydroxyl groups give the polysaccharides their reducing nature. The use of polysaccharides provides a green alternative for nanoparticles used in pharmaceutical and biomedical applications since they do not often exhibit significant cytotoxicity.[3] β-D-glucose, negatively charged

heparin, and starch are just a few examples of polysaccharides that have been used to make metal nanoparticles.[3]

As mentioned previously, proteins and peptides have been shown to be effective reducing agents for nanoparticle synthesis. The protein reducing agents were subcategorised under two headings based on their origin: microbial synthesis and photosynthesis.[3] Microbial synthesis relies on bacteria, fungi, actinomycetes, yeasts, and viruses to be used as bio-factories for nanoparticle synthesis. Those biofactories stem from the microbe's ability to chemically detoxify most metals. Bacteria have been demonstrated to aggregate and reduce Ag ions within their cell poles producing a wide variety of nanoparticles with large size distributions.[3] Fungi have a larger percentage of proteins that make them more efficient biosynthetic microbial pathways for nanoparticle synthesis. The nanoparticles from fungi typically have a smaller size distribution than those from bacteria.[3] Viruses have also displayed some promise for the production of metal nanoparticles. The nanostructures derived from viruses can be tethered to a number of functional units that have been utilised in battery electrodes and supercapacitors.[3]

The size of the microbial factories imparts a complexity that makes it difficult to establish a mechanism and thus more finely control the nanoparticle synthesis. To better establish a mechanism for those more complicated microbial systems, protein extracts derived from unicellular algae have been used to make Ag nanoparticles. In this work it was determined that the hydroxyl groups in the tyrosine amino acids were solely responsible for the reduction of silver ion to metallic silver.[27] From this same work it could also be shown that the anisotropic growth of Ag into nano-plates was attributed to the carboxyl groups present in the amino acids aspartic acid and glutamic acid.[27] The

work by Wang and coworkers showed that the reducing ability of the amino acids was heavily dependent on its binding affinity to the metal and also showed that the characteristic reducing nature of an amino acid was heavily affected by neighbouring amino acids when present in a peptide.[28]

The photosynthetic reducing agent refers to the ability of green plants and their components to reduce metal ions to nanoscale metal particles.[23] Plant extracts consisting of polysaccharides, proteins, amino acids and enzymes provide reducing capability with environmental benignancy just like microbial pathways. The real bonus is the fact that the plant extracts are easy to produce and store compared to the analogous microbial reducing agents that often require complicated microbial isolation, culturing and maintenance.[23] One can make use of this photosynthetic pathway from extracts derived from stems, flowers, fruits, peels, roots, leaves and seeds.[5] The organoleptic properties of plants and fruit are closely linked to their reducing ability. The bright colours of fruit and the varying colours of leaves are all due to different phytochemicals; the green in kale is glucosinolates, the orange in carrots are α and β carotenes while the red-purple in berries are largely attributed to anthocyanins.[23] Essentially, any phytochemicals in the extracts with recognised antioxidant properties can be utilised for the reduction of metal cations.[5]

It is imperative to note the importance of solvents in the greening of any synthetic pathway. A rational selection of solvent is part and parcel of the design phase as solvents are used as a medium for dissolution of precursors, transferring heat and dispersing synthesised nanoparticles. If a solvent is required then water is generally preferred.[29] This is typically the case as water is non-toxic and non-flammable. In terms of energy savings it may be useful to consider other solvents given that water has the highest heat capacity

of known liquids and hence requires significant energy to raise its temperature.[3] Supercritical fluids have been thought of as energy saving alternatives as properties like diffusion coefficient and thermal conductivity can be simply manipulated by moving the system from gas like to liquid like.

It has been demonstrated that the dielectric constant of supercritical water can be varied around the supercritical point to achieve supersaturation which allows for small sized nanoparticles to be formed.[3] Supercritical carbon dioxide is also energy efficient in fact it is noted as being energetically superior to supercritical water, as well as being non-flammable and nontoxic.[3] Additionally, supercritical carbon dioxide reduces the coffee ring effect noted in the evaporation of most liquid solvents, yielding ordered lattices of nanoparticles. Ionic liquids are also good alternatives as they are non-volatile relative to commonly used organic solvents.[3] Ionic liquids can also serve as capping agents; stabilising the resulting nanoparticles.[3] There has been a fair amount of research done on heating ionic liquids with more environmentally friendly technologies like microwave and ultrasound methods.[3] These techniques can be used on ionic liquids because of their high ionic charges, high polarities and high dielectric constants that allow fast and homogenous temperature elevation.[3]

Plant-mediated synthesis of metal nanoparticles is an active research area as it often results in more biocompatible structures that can be used in many biomedical applications. One of the current problems is that those strategies lack known routes for the production of monodispersed nanostructures.[30] In addition, these “greener” strategies may end up having unfavourable attributes compared to conventional routes depending on the intended application. Thick surface layers stemming from the plant matter have

been noted to encase / protect the surface of those nanostructures.[31] Such layers are referred to as the biogenic corona.[31] The size of the corona will vary in thickness based on its origin (root, leaf, seeds etc.) and will also be affected by the extract production and nanoparticle formation parameters like temperature, pressure, pH, and duration.[30, 31]

2.3.2 Bioscaffolds

While most people perceive functional nanomaterials to be modern day constructs, nature is also full of such materials.[32] Naturally derived nanomaterials offer several advantages such as inherent stability, long-range order and biodegradability. Examples include the complex structures found in leaves, feathers and shells.[38] When biomaterials are used as a scaffold for the fabrication of functional materials it is referred to as bioscaffolding or biotemplating.[32]

A key advantage of using natural biomaterials as scaffolds comes from their inherent complexity, a structural sophistication that has come about through millions of years of evolution.[32, 33] For example the beautiful iridescent colours of some butterfly wings are due not to pigments or colorants but instead to periodic nanostructures; this is referred to as structural color. Some desert plants incorporate nanostructures to provide superhydrophobic surfaces to reduce energy dissipation, while nanostructures in photosynthetic organisms like diatoms have unique optical properties that allow for greater light absorption.

There are three main ways in which material scientists have explored biotemplating/bioscaffolding to date:[32] 1) replication: using chemical and physical processes like casting and nanolithographic processes to construct replicas of desirable morphologies, 2) assembly: using the naturally occurring nanostructures as building

blocks, attaching them through electrostatic, metal-ligand, and intermolecular interactions and lastly 3) encapsulation: bio-nanostructures are incorporated into existing manmade materials. These structures can be separated into four categories: hierarchical porous structures, periodic porous structures, hollow structures, and nanostructures. Such bio-templated materials have been employed for CO_2 reduction, solar cells, lithium ion batteries (LIBs), photocatalytic hydrogen generation, photocatalytic degradation and chemical sensing.[32]

Diatoms are single cell photosynthetic algae that have a photonic crystal-like structure and can be found in almost all aquatic environments in great quantities.[34-38] Diatoms possess a unique outer structure composed of a hierarchical nanoscale series of pores on a silicified (silicon dioxide) cell wall referred to as the frustrule.[34] Frustules give diatoms their photonic crystal-like structure and enhance their ability to harvest light efficiently; so much so that scientists believe diatoms are responsible for 20-40% of the Earth's oxygen.[35,37] The diatom structure can be used as a scaffold, making use of the periodicity in their frustules since the incident electromagnetic radiation is going to experience diffraction with the same periodicity.[37] This ability has been employed to enhance the function of dye sensitised solar cells (DSSCs) since there is an increased path length for the incident light, which in turn allows more time for it to be absorbed by the dye.[32]

Butterfly wings display ideal characteristics for this type of nanomaterial fabrication as they consist of scales with a honeycomb-like structure that traps incident light. The light entrapment occurs because of the high refractive index that permits total internal reflection.[39-42] This feature is common to many naturally occurring structural

colours. Peacock feathers and butterfly wings display a change in colour with viewing angle which is due to the presence of nanoscale structures.[42, 43]

Biotemplates have been made even more functional through genetic modifications. This is the case for M13 viruses whereby alterations to their genomes have made it possible to incorporate nanowires (Co_3O_4 and hybrid $AuCo_3O_4$) as reported by the Blecher group.[32] The incorporation of such nanowires could be directly applicable to the improvement of lithium ion batteries as they provide a much greater surface area for Li ion exchange which would allow the batteries to charge more quickly and store more charge.[32]

The simplest way to make use of naturally occurring templates is *via* casting techniques. This is a normal occurrence when dealing with insect wings.[39-42] Insect wings are removed from the insect and coated with a thin metal film. Afterwards, the biological matter is chemically removed through dissolution. The deposition of Au on butterfly wings has been achieved in the literature by electron beam evaporation onto the surface of the wing,[41] and the same is true for diatoms.[42] A different approach was taken for the biotemplating of crab shells, which show a similar nanoporous feature; a combination of hard templating and surfactant self-assembly was used. Xia and coworkers removed all organic matter in the crab shell *via* calcination, where the shell is exposed to a high temperature.[44,45] Once this was complete, the crab shell was ground into a fine powder, and a combination of a resin and a block copolymer were used to impregnate the nanoscale features.[44,45] Once the assembly was complete, the crab shell material was dissolved using hydrochloric acid.[44] Mirkin and colleagues biotemplated diatoms in a similar fashion. Diatoms were calcified, followed by deposition of a 5 nm layer of

metallic titanium followed by a 30 nm layer of silver.[46] The final step used HF to remove the underlying diatom structure. Sandhage and coworkers established protocols for making very precise inorganic replicas of diatoms. Similar replicas were also made out of carbon.[47] It was obvious from the results of carboxylate-functionalised replicas that the hierarchical arrangement of micro and nanopores in the biotemplate favorably influence catalytic behaviour.[47] The carbonaceous replica of the diatoms were used as support material for the enzyme glucose oxidase with protoamine (GOx-PA).[47] The enzyme glucose oxidase catalyses the conversion of β-D-glucose to D-glucono-1,5-lactone. The results indicate that the catalytic activity increases 2-3 times for the diatom carbon and gold replicas compared to commercial carbon black or gold supports.[47]

2.3.3 Earth Abundant Metals

Some elements have relatively high prices that can stem from one of two things: there is a high embodied energy associated with the refining of their crude precursors or sometimes the general supply is low. In the world of economics the ratio of supply to consumer demand governs the price of products. This is not always true in the real world as is the case with endangered elements like helium.[48] The endangerment of any element does not generally mean that it will disappear from the face of the earth (except for helium) but rather that future demand will far outweigh the supply. For example, helium is the second most abundant element in the universe, however due to historically low prices and limited recapture technologies, helium is what is referred to as an *endangered element*. The notion of element endangerment comes about when one considers the current uses for a particular element and projected growth of use, versus the currently available sources (i.e. operational mines, post-consumer recycling rates, etc.). Figure 2.1

highlights the elements in the period table that face earth-abundance limitations in the next 100 years. The platinum group metals (PGM), which includes Pd, Rh, and Pt, are all used for catalysis and all have problematic supplies. Platinum in particular was traditionally used in great excess in automobile catalytic converters. Unfortunately, there has not been significant headway in finding alternative metals that can remove carbon monoxide, hydrocarbons, and nitrogen oxide from exhaust fumes with comparably high efficiencies.[57] Therefore, many of the catalytic technologies requiring Pt have resorted to incorporating as little as possible into their designs. For Pt, nanotechnology has bettered the situation by providing larger surface areas to accomplish the same catalytic goals with less platinum. However, as demand for vehicles grows globally, this too will reach a limit due to the known availability of Pt.

Another example of an earth-limited element is the rare earth element neodymium (Nd). Neodymium is used to make powerful magnets used in acoustic devices like speakers and headsets, and more recently smartphones.[49] Per unit volume Nd provides the greatest magnetic strength of any known permanent magnet. The distribution of elements worldwide is heterogeneous; China possesses greater than 95% of the rare earth elements, Nd included, the Democratic Republic of the Congo has the majority of known supplies of Co, (PGM) have their largest deposits in South Africa and Russia.[49] Distributions like these can lead to geopolitical unrest.[48]

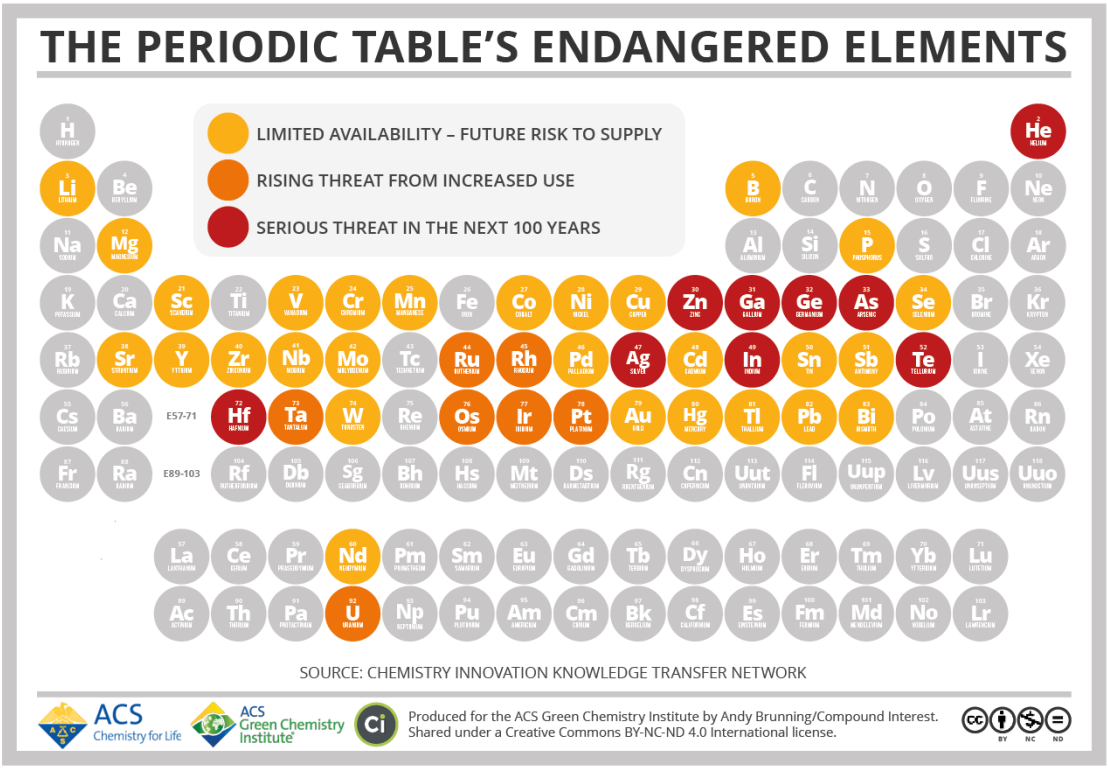

Figure 2.1: Periodic table depicting relative supply status of the elements (Reproduced with permission).[48]

A careful study of Figure 2.1 highlights a concern for the field of plasmonics both Au and Ag face earth-abundance issues, and the case is quite dire for Ag. Silver is the most electrically and thermally conductive element and it is used for a multitude of applications including mirror coatings, electronic circuitry, and photovoltaic panels. In 2015, for example, it was estimated that 100 million ounces of silver were used for solar energy purposes. As a result, there has been great interest in exploring lower cost and more sustainable plasmonic metals, and at present the best available substitute is copper.

Copper nanostructures have been synthesized via a wide range of approaches ranging from solution based methods to thermal and electrochemical techniques. In terms of solution based methods one can proceed *via* a hydrothermal synthetic method or a

chemical precipitation method.[50] In the hydrothermal synthetic method the reactions are conducted in water in a sealed, pressurised container. By completing the synthesis with temperatures just above the critical point, scientists have prepared several different Cu structures requiring very minimal post treatment. This synthetic strategy is simple, green, and has several advantages: [50] 1) most inorganic salts are water soluble, 2) water is a green and relatively cheap solvent, 3) small coordinating molecules can be introduced to modulate crystal growth, and 4) nanocrystals may exhibit oriented growth patterns due to strong water dipoles. Experimental conditions including copper concentration, pH, growth time, and temperature also play significant roles in determining the shape, size and overall quality of the Cu nanostructures.[50] The hydrothermal process for copper nanoparticle synthesis is usually a two-step process whereby copper hydroxide particles are first formed by the reaction of a cupric salt with a strong base such as NaOH. The copper hydroxide particles are then thermally dehydrated in an autoclave to make copper nanostructures.[50] This was demonstrated by Neupane and colleagues illustrating a fair amount of control over the final particle size and shape.[51]

Cu nanostructures can be made by employing different copper salts and a variety of additives.[50] One dimensional (1D) Cu nanostructures were made by mixing $CuCl_2$, NaOH and cetyltrimethyl ammonium bromide (CTAB) prior to introduction into an autoclave. Once heated with thorough mixing, the mixture was placed in the autoclave with glucose. Cu, CuO, and Cu_2O nanorods were made via those protocols.[50] The formation of the rods is attributed to the growth directing surfactant CTAB.[50]

Solution-based chemical precipitation methods may be more accessible, however, since high pressures are not required. One simply needs to introduce a reducing agent to a

copper salt solution, this will form the monomers that will subsequently aggregate into nanostructures. The resulting particles from such a standard preparation are approximately 10 nm in size. The morphology can be significantly altered by varying the choice of copper salt and strong base; $Cu(NO_3)_2 \cdot 3H_2O$ with NaOH produced nanoparticles, $Cu(OAc)_2 \cdot H_2O$ with NaOH resulted in nanobelts while $Cu(NO_3)_2 \cdot 3H_2O$ with Na_2CO_3 formed nanoplatelets.[50] By the addition of polyethylene glycol (PEG), varying length CuO nanorods were reported for the precipitation strategies.[50] The molar ratio of OH^-/Cu^{2+} in the PEG studies was critical to the resulting structures. If the molar ratio of OH^-/Cu^{2+} was 4 or higher, CuO nanowire bundles would form. However, lower molar ratios did not produce nanostructures. Additionally, when the right ratios were used in the absence of PEG, dendritic structures were formed, also indicate how crucial the combinations of reagents are to the final resultant structure.[51,52] Additives are known to affect nucleation and growth in the solution-based synthetic strategies by adjusting the surface energies. Ionic surfactants like sodium dodecyl benzene sulfonate (SDBS) and CTAB can adsorb onto the surface of CuO nanocrystals and reduce the interfacial tension between the nanocrystallising phase and the surrounding solution, resulting in diverse structures.[50] On the other hand, non-ionic surfactants like PVP and PEG exercise their influence on the nucleation and growth by serving as templates: once the nanocrystals have oriented themselves only certain growth patterns are supported.[50] This is evident in several examples: urea that promotes the growth of urchin like particles, PEG + CTAB create bamboo leaf-like structures, and PVP directs the growth of CuO into hierarchical nanochains.[52]

Electrochemical methods are highly sought after for their speed, low cost and overall simplicity. It was noted in the work done by Li and coworkers, how one could alter the surface of a copper electrode electrochemically, forming nanostructures.[53] In this work, a polished Cu disk was used as the working electrode, Pt foil as the counter electrode, and saturated mercurous sulfate as the reference electrode in a supporting electrolyte. The system was treated with square wave voltammetry (SWV) from 0 V to -1.4 V. At the more positive applied voltages, the Cu surface is composed of oxides and sulfates that are then completely reduced to Cu particles which can then diffuse and move on the surface to attain the lowest surface energy configuration. This action allows the controlled shaping of the Cu electrode into micro and nanoscale features depending on the parameters of the SWV and concentration of sulfuric acid. A shorter time period and more concentrated sulfuric acid solutions displayed more nanoscale freatures.[53]

Another electrochemical approach to producing nanostructured Cu is via a process called dealloying. Chen and coworkers investigated the production of nanoporous copper through the selective dealloying of $Cu_{30}Mn_{70}$ ribbon.[54] This ribbon alloy was chosen as it met two criteria: there were homogeneous single phases and large electrochemical potential differences between the Cu and the alloy components.[12] The standard redox potential of Cu and Mn are 0.342 V and -1.135 V (vs. the standard hydrogen electrode (SHE)), respectively.[54] The Cu-Mn ribbon was made by a rapidly cooling a Cu-Mn melt made by a melt spinning method to avoid phase separation.[54] It was determined that an electrolyte of HCl could support uniform nanoporosity. However, if the concentration of HCl was too high the Cu could dissolve and migrate forming large irregularities in

morphology. With a dealloying potential of 0.2 V vs SHE the Mn could be selectively removed in 0.025 M HCl, resulting in copper nanocubes.[54]

The Bartlette group successfully coupled electrodeposition with nanolithographic techniques in what is referred to as copper sphere segment voids.[55] Bartlett and coworkers demonstrated that nanoporous copper could be generated by the electrodeposition of Cu onto polystyrene spheres layered on a solid substrate. Following electrodeposition, the spheres were removed with DMF by soaking for 2 hours. This removal provided nanoscale voids, hence the name sphere segment void (SSV). In order to achieve the most ideal deposition, parameters such as applied potential, solution concentration, and additive properties were optimised. The applied potential needed to provide fast nucleation to generate a large number of nuclei to achieve a small enough grain size, and the deposition time was short so as to avoid the formation of copper oxide.[55] A series of different potentials were explored in order to facilitate Cu deposition. When a potential was employed that brought about a visible deposit in 3 minutes it was noted that deposits were far from smooth. This is due to the fact that at even at low overpotentials, preferential deposition can occur.[55] To overcome this problem the Bartlett group turned to additives as seen in the solution based strategies. Polyethylene glycol (PEG), when introduced as an additive in the electrodeposition of Cu is known to act as an inhibitor preventing the formation of dendritic growth, and when used in conjunction with KCl it improves the overall quality of copper deposits.[55]

Even more fundamental than additives to the electrodeposition of copper are the effects of concentration of the copper salt and the supporting electrolyte and the effect of temperature. Keswani and colleagues looked at the effect each of these listed parameters

had on deposition. It was found that the electrodeposition was much steadier at elevated temperatures.[56] This could be seen by a plot of current density versus deposition time for temperatures of 25 °C and 65 °C measured at an overpotential of -0.25 V vs Hg/Hg_2SO_4. Keswani notes a massive drop in current density over time recorded for the cell near room temperature, while for the elevated temperature trial the current drop was more subtle. The current drop was much smaller at the elevated temperature because of the improved diffusivity of Cu ions at higher temperature leading to improved mass transport. The diffusion coefficient of Cu ions increases by a factor of ~2.5 from 25 °C to 65 °C.[56] It could also be noted from Keswani's work that the greater the current density the faster the deposition rate. Current densities of 39 mA/cm^2 produced smooth deposits compared to current densities of 207 mA/cm^2 that produced a nodular deposit.

2.4 Sustainable Plasmonics

2.4.1 Introduction

Plasmonics is a branch of nanotechnology that focuses on the ability of some nanoscale metals to interact with the oscillating electric field component of incident electromagnetic radiation. The free conduction electrons present in the metal collectively oscillate in response to this, generating a surface plasmon resonance (SPR) condition. The nature of the interaction between the metal and light is largely governed by the complex dielectric function of the metal. In order to have significant plasmonic character, Mei theory predicts that the metal should have a negative real and small imaginary component of this complex dielectric function.[2] For visible radiation, this requirement is best satisfied by three metals: Ag, Au and Cu.[1] In plasmonics, Ag and Au are by far the most common choices. Plasmonic metals allow one to harvest and manipulate light at the nanometer

length scale, which has application in several areas including sensing, communications and alternative energy. One particular application of interest to chemists is surface enhanced Raman spectroscopy (SERS), which is elaborated on in Chapter 3. Briefly, SERS is the improved sensitivity of the vibrational spectroscopic technique known as Raman spectroscopy that takes advantage of the enhanced electric field on or near certain nanoscale metals. SERS activity can therefore be used as a tool to measure plasmonic performance of coinage metal NPs.

2.4.2 Applications

Plasmonic nanomaterials have the ability to concentrate, amplify, and manipulate light at the nanometer length scale, offering up many possibilities for applications ranging from biomedicine to information technology advancement. Biomedical applications are to date the most explored application of plasmonics. DNA sequencing is typically done with dyes that are susceptible to photodegradation.[1] However, this can be done with plasmonic NPs with even greater sensitivity because of the large absorption cross-section associated with the surface plasmons. A simple model of this would entail functionalising the plasmonic NPs with target nucleotides, and to functionalise a sensing substrate with complementary oligonucleotides specific to the DNA strands one wants to detect.[1] When DNA-modified NPs are introduced to the sensing surface, if the complementary strands are present, binding will occur, allowing the retained DNA strands to be identified by the surface plasmons.[1] Similarly, plasmonic NPs can be used for cell labelling to identify cancer cells. It is known that cells can accumulate noble metal NPs but when they are functionalised with specific antibodies like the monoclonal anti-epidermal growth factor receptor the affinity for malignant cells is over 6 times greater than for non-malignant

cells.[1] Furthermore, it has been shown that the characteristic surface plasmon absorption band accumulated in the malignant species is sharper and redshifted compared to their non-malignant counterparts.[1] Besides cancer detection, cancer therapy is also possible with plasmonic nanotechnology as the particles can be energized so precisely that they plasmonically elevate the temperature of their local environments. Temperature increases as little as 5-10 °C over normal biological conditions are enough to selectively destroy abnormal cells.[1] Scientists have also made use of the plasmonic heating character for purposes of drug delivery. Conventional drug delivery protocols call for the encapsulation of a drug in a coating that prevents interaction with non-target cells. When the drug arrives at the target region the drug can then be released at a desired rate. This can be improved by having a polymer coating that is temperature activated.[1]

Plasmonics can also assist in improving the current energy crisis. Photovoltaic devices are all based on the same simple principle: electron-hole pairs are created through the absorption of light and are separated into junctions leading to charge accumulation that is ultimately used to provide electricity. A major issue with modern solar cells is that large cell thicknesses are needed to absorb enough incident radiation.[1] Unfortunately, this thickness requirement increases chances of recombination of the electron-hole pairs which results in large inefficiencies in energy conversion, and in addition increases the weight and cost of the device. Plasmonic nanostructures can improve energy conversion efficiency in several ways: 1) at the surface of the photovoltaic device the NPs can scatter incident light, thereby increasing the path length and the chances of it being absorbed and 2) the NPs can be placed at the semiconductor junction such that incident light is concentrated and locally amplified.[1] It should also be noted that surface plasmonic

activity can be tuned for optimal activity at a particular wavelength through careful size and shape selection of the NPs, something that is not so easily achieved through the use of dyes.[1]

Information technology can also stand to make considerable gains through the integration of plasmonics *via* fast propagation of optical signals without Ohmic losses experienced by current electrical signal transduction.[1] Light is typically manipulated by dielectric materials but this manipulation is limited to a focus of $\lambda/2$ due to the diffraction limit.[1, 2] Metals have not typically been used for focussing light due to their short light penetration depth.[1] Surface plasmons have set in motion new strategies for light manipulation, reading, and writing information at size scales much smaller than their wavelengths. Plasmonics can also be used in next generation camouflage technology as the ability to control light so precisely can be used to make the background of an object appear on its surface giving the illusion of invisibility.[1]

2.4.3 Green Synthesis of Silver Nanoparticles

The most common way to prepare AgNPs is *via* the citrate reduction of Ag^+ from $AgNO_3$ into colloidal Ag, first reported by Lee and Meisel in 1982.[57] In this synthesis, citrate serves as both the reducing and capping agent. A 1% v/v sodium citrate solution is introduced to boiling $AgNO_3$ and left to boil for an hour. The resulting Ag nanoparticles (AgNPs) generally exist in a wide range of shapes and sizes that make it difficult to correlate an observation to specific structural properties of the Ag. There is some degree of control that is afforded to scientists: if one works at a pH = 5.7 the reaction is slow and the majority of colloidal Ag is triangular or polygonal while if done at pH = 11 the

reaction is fast and one gets mostly nanoscale rods and spheres.[58] This happens because the citrate is deprotonated at higher pH and can coordinate to the Ag^+ more strongly, preventing the randomness observed at very low pH.[58] Ideally, if one had to select an experimental pH one would want to use working conditions just above the pKa of citrate, which is 6.4. This improves the uniformity of resulting AgNPs. At very high pH, OH^- participates in shaping the metal structures and sample polydispersity can result.[59] At very low pH the nucleation and growth happens very slowly resulting in anisotropic silver nanostructures. To optimise this synthetic approach further it is suggested that the reaction first take place at high pH, which favors rapid nucleation, and then the system be driven to a low pH which supports slow growth.[58] Uniform silver spheres are expected to result with the improved balance of the nucleation and growth stages.[58]

To get more uniform noble metal NPs scientists have typically moved away from citrate and employed harsher reducing agents like $NaBH_4$ with capping agents such as polyvinyl alcohol to control the size, shape, and stability of NPs.[30] Unfortunately, many of these newer reducing and capping agents are not considered green.[3] As a result there has been great interest over the past several years in the area of green synthetic methods for producing monodisperse metal NPs.

Plant extracts consist of secondary metabolites such as phenolic acids, flavonoids, alkaloids, and terpenoids that act as antioxidants and are therefore capable of reducing Ag^+ ions into AgNPs[30]. Recent studies in the literature have shown this to be an active area of research.[35] The sweet chilli pepper leaf extracts one such example, which is composed of proteins, enzymes, polysaccharides, amino acids, and vitamins. This cocktail acts as both a reducing and capping agent. The sweet chili pepper leaf extract

was shown to produce large AgNPs at lower pH and small AgNPs at higher pH.[30] Fast nucleation at high pH leads to small NPs, and slow nucleation at low pH leads to large NPs. Higher reaction temperatures also tend to produce smaller nanoparticles.[30] Additionally, different extracts support certain morphologies such as lemongrass leaf extract which was shown to form gold nanotriangles by Sastry *et al.*[60] Rege and coworkers demonstrated that the network of veins in magnolia leaves can be used to make noble metal nanoparticles from the capillary flow of metal salts through the leaf vasculature.[61] The petiole of the leaves were dipped into metal salt solutions, and once the nanoparticles had formed, the tips of the leaves were combusted completely to facilitate the recovery of the nanoparticles *via* varying sedimentation rates exploited by centrifugation in water.[61] The AgNPs produced were very monodisperse but at 9 nm were too small for most plasmonic applications. However, the AuNPs were used for the catalytic conversion of p-nitrophenol to p-aminophenol.[61] It can be noted that the majority of plasmonic nanoparticles made via living plants or their extracts are not often used for SERS as the biological capping agents are difficult to remove and thus hinder SERS sensing applications.[30] In green synthetic approaches using plant extracts, the thick, organic capping material is referred to as a biogenic corona.[31] Since SERS has a very short decay length (~5 nm): the distance within which one can enjoy the enhancement from the nanoscale metal particles.[62] This corona on the surface of the nanoparticles blocks analyte access to the surface, thus, pushing the limits of the surface distance dependence and reducing one's ability to obtain SERS spectra.[62]

2.4.4 Scaffolding for enhanced plasmonics

As mentioned previously, the synthetic fabrication of well-defined nanoporous structures is often energy intensive, expensive, and not scalable.[63] Luckily, nature offers many options of micro and nano scale materials that can be used as scaffolds for this purpose. The plasmonic nanostructures incorporated into the lattices of nano/micro porous templates allow for the creation of super lattices: a situation where the guided mode resonances of a photonic crystal overlap with the localised surface plasmon resonance (LSPR).[37] The 3D aspect facilitates a greater volume of surface plasmons (more nanoparticles) in the irradiated area (Raman laser area) that can further enhance SERS signal.[37] This is noted by Ren and coworkers who were able to illustrate more sensitive and reproducible SERS detection in diatom-AuNP substrates than for non-diatom associated substrates.[34] Diatoms are typically pretreated in order to facilitate binding of the metal nanoparticles to its surface. One commonly used pre-treatment uses complementary DNA strands. The surface of the diatom is treated with one strand and the metal is functionalized with the complementary strand.[36] Another popular pre-treatment allows the NPs to attach to the diatom via a peptide bond. NPs are functionalised with carboxylic acid groups and the amino groups present on the diatom surface facilitate amide bond formation through dehydration.[36]

A slightly different approach is taken to get improved SERS from the more delicate cicada wing. In recent work, the cicada wing was first coated in TiO_2 using a dip-coating technique, followed by electron beam evaporation of Ag onto the wing. With those protocols Xu and colleagues were able to get uniform signal, improved limits of detection, and were able to demonstrate quantitative detection.[41] Furthermore, it was

shown that when the wing was coated with Au the substrates could be recycled with $NaBH_4$ after detection of thiols.[41]

2.4.5 CuNPs as a Sustainable Alternative to Au and Ag for Plasmonic Applications

The vast majority of plasmonic applications utilize Au and Ag, which is problematic from a sustainability point of view for the aforementioned reasons. While theoretically Cu should be as good as Au for plasmonics, practical limitations exist. For example, copper is generally coated with an oxide layer, which has the effect of dampening the plasmon resonance, and in addition there is a lack of reported Cu nanostructures in the literature. Work done by Bartlette and colleagues on copper sphere segment voids, introduced previously, is one such attempt where uniform nano-featured copper was used for SERS analysis of pyridine.[55] The uniform Cu substrates reported in this work gave a relatively weak SERS response due to the presence of the PEG additive that stabilises the surface. The electrochemically altered surfaces of a copper electrode by the Keswani group mentioned earlier, was also evaluated for its plasmonic ability.[56] Nano-roughened surfaces like those produced by Keswani, while weakened by the presence of an oxide layer, further demonstrates the potential of copper for plasmonics.[56] A major challenge is successful passivation of the Cu nanostructure surface without compromising the surface plasmon strength.[53]

Chapter 3 Theory

3.1 Introduction

This section provides the necessary theoretical background for concepts central to this thesis work as well as an introduction to the instrumentation used in this project. This chapter starts with a focus on colloidal systems, such as metal nanoparticle sols, and in particular explores colloidal synthesis, stability and properties of colloids. The fundamentals of plasmonics is then discussed, including an introduction to plasmon-assisted catalysis. Finally, the theory necessary to understand the instrumentation utilized in this thesis work is presented, namely Raman spectroscopy and electrochemistry.

3.2 Colloids

According to the International Union of Pure and Applied Chemistry (IUPAC), colloids are heterogeneous systems that consist of particles that have at least one dimension in the approximate range of 1 nm to 1µm or discontinuities in a medium within that size range.[64] The discontinuities or particles are referred to as the dispersed phase while the medium is the continuous phase. In terms of the scope of this thesis only metal colloidal sols, where nanoscale metal solids are dispersed in a liquid medium, will be considered. Since the metal nanoparticle systems explored in this thesis work are all sols, a brief discussion of the properties of colloidal systems is warranted.

When the size of a material is reduced to nanoscale dimensions there is a much higher percentage of molecules/atoms at the surface. For example, for Pd clusters, when the cluster diameter is 1.2 nm, 76% of the Pd atoms are present as surface atoms, as can be seen in Figure 3.1.[65]

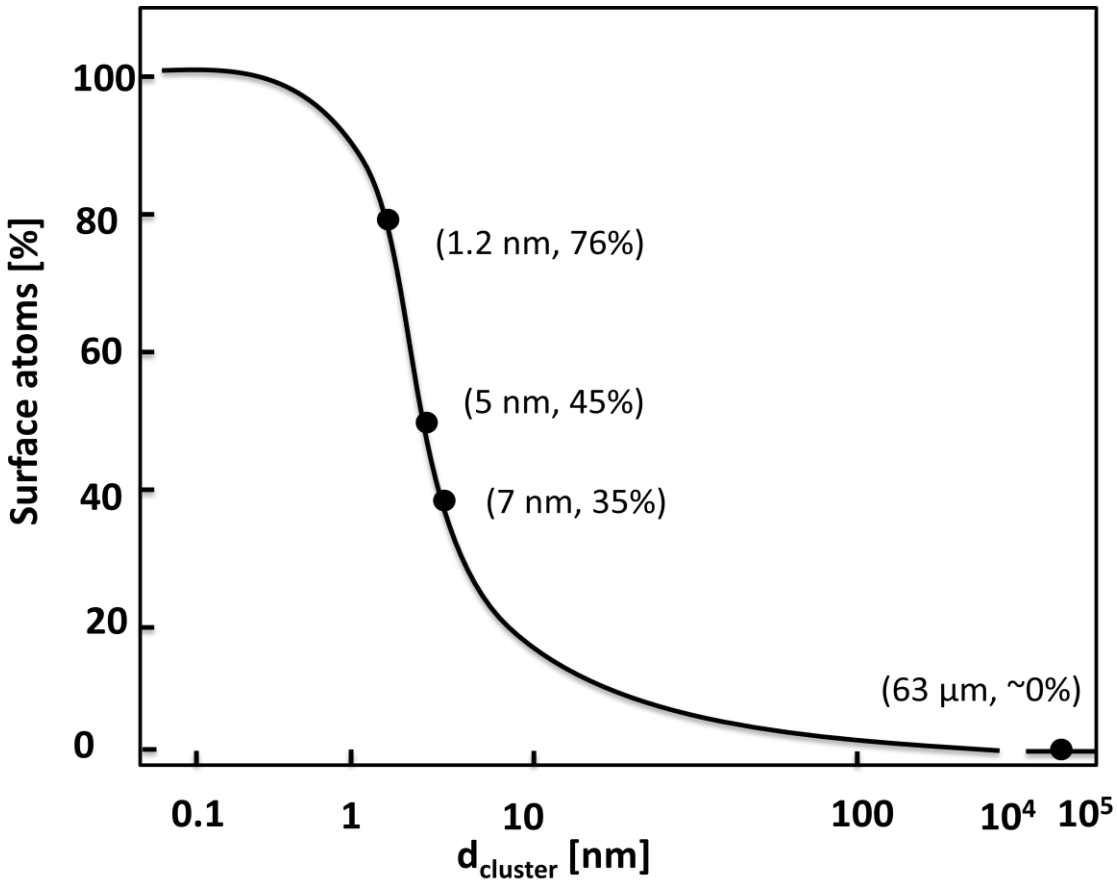

Figure 3.1: Percentage of surface atoms as a function of palladium cluster diameter (Adapted from reference 65).

Atoms at the surface are surrounded by fewer neighbouring atoms compared to atoms in the bulk, which results in an unequal distribution of energy at the interface between the bulk and the surface. This extra energy is described as the surface energy, γ.[66] The surface energy is the energy (G) required to create a unit of new surface area (A) as a function of temperature, pressure, and number of atoms in the structure.

$$\gamma = \left(\frac{dG}{dA}\right)_{ni,T,P} \qquad 3.1$$

When the surface area is fixed, its energy can be reduced by:[66]

1) *Surface relaxation* - the sub-surface atoms are all bonded to one another. Those bonds can be thought of as attractive forces. This attractive force gets reduced by acting to pull the surface atoms inward. The atomic layer remains unchanged while the distance between the surface layer and the subatomic layer is reduced. The relaxation mechanism is more apparent in less rigid systems and thus occurs more readily in liquid phases. The reduction in bond length is noticeable in nanoparticles.[66]

2) *Surface restructuring* - this mechanism is possible when there is more than one dangling bond on each of the surface atoms which can be combined with the dangling bonds of their neighbours to stabilise the surface. An example of this is silicon nanostructures. The [100] index facet is greater in surface energy than both the [110] and [111] facets but after restructuring, the [100] facet is observed to be the most stable.[66]

3) *Surface adsorption* – by chemically or physically attaching groups to the surface the surface energy can be reduced. This can be accomplished by functionalising surfaces with materials that are stable in the continuous phase. Often a capping agent will be used in colloidal nanoparticle synthesis to add constraints on size and shape through selective adsorption on particular low-index facets.[66]

Colloidal synthesis consists of three phases: a supersaturated solution, nucleation, and growth.[79] To achieve supersaturation, the concentration of the solute must be greater than the equilibrium concentration, or the temperature must be brought down below the phase transformation point. Supersaturated solutions have a high Gibbs free energy.[66, 67] To lower this energy, a solid phase is created termed the nuclei. The reduction of the Gibbs free energy is the driving force for both nucleation and growth.[66] Segment I of the

LaMer model for nucleation and growth in Figure 3.2 shows a linear increase in precursor (metal ion) concentration with time; no significant nucleation occurs as the concentration of precursor ions has not reached the concentration of precursor at which the solution is saturated enough to overcome the energy barrier to nucleation (C_{min}).[66, 67] Once C_{min} is reached (segment (II)), nucleation ensues rapidly, referred to as the nucleation burst. Once the concentration of the precursor drops back below C_{min} nucleation stops. In segment (III) only growth of existing nuclei occurs since the concentration of the precursor is below self-nucleation levels.[67] This growth will persist until the precursor concentration dips below the initial saturation concentration, C_s. This growth period can be viewed as heterogeneous nucleation because the precursors at concentrations below C_{min} will nucleate at existing metal particle surfaces through diffusion.[66] This model was developed in the 1950s and is still the most widely used model to describe nucleation and growth. Strategies to adjust NP size have been derived from the LaMer model. It stands that fast nucleation leads to many small NPs, while slow nucleation will produce larger particles.[66] More precise models for nanoparticle growth are lacking due to a lack of experimental data.[66]

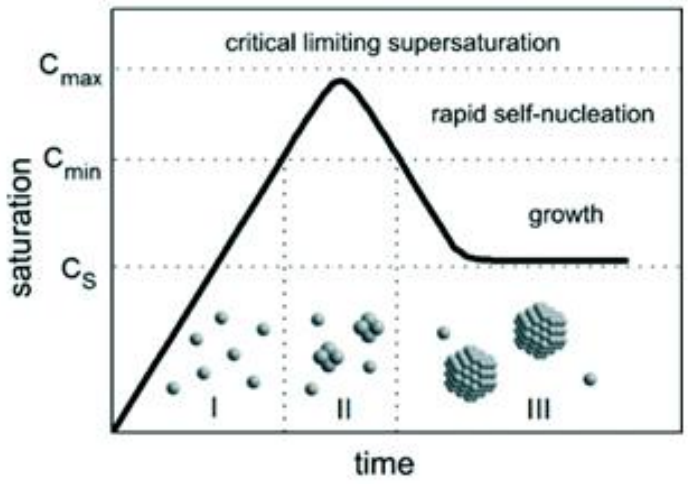

Figure 3.2: LaMer model of uniform particle formation[67] (Reproduced with permission).

When a colloidal metal sol is made using polar solvents as the dispersion (continuous) medium, a surface charge will develop.[68] This surface charge will generate an electrostatic potential between the metal surface and electrolyte ions, which drives the separation of the anions from the cations near the surface of the metal.[66] The electrical potential at the surface (Ψ_0) will be greater than the electrical potential a distance from the surface (Ψ) and gets weaker with increased distance. One can expect the colloidal metal particles to adsorb ions to their surface in an effort to neutralise this charge. This complete passivation of the metal surface by ions of opposite charge was the first electrical double layer model postulated, called the Helmholtz model. The Helmholtz model however falls short as it ignores the thermal motion of the ions and the role of solvent molecules.[66, 68] A more comprehensive model of the electrical double layer is the Gouy-Chapman model, which is based on a Boltzmann distribution of ions near the surface of the metal.[66] The Gouy-Chapman model describes a diffuse layer of ions that progressively neutralise the surface of the metal as one moves away from the surface. The

Gouy-Chapman model however does a poor job at accommodating the actual size of the ions. [66]

The Stern model includes a consideration of ion size for the first layer of adsorbed ions.[68] This first layer is referred to as the Stern layer and the region outside this is the diffuse layer where the Gouy-Chapman model still holds.[68] The double layer and the Stern layer are separated by the Helmholtz plane. (Figure 3.3)

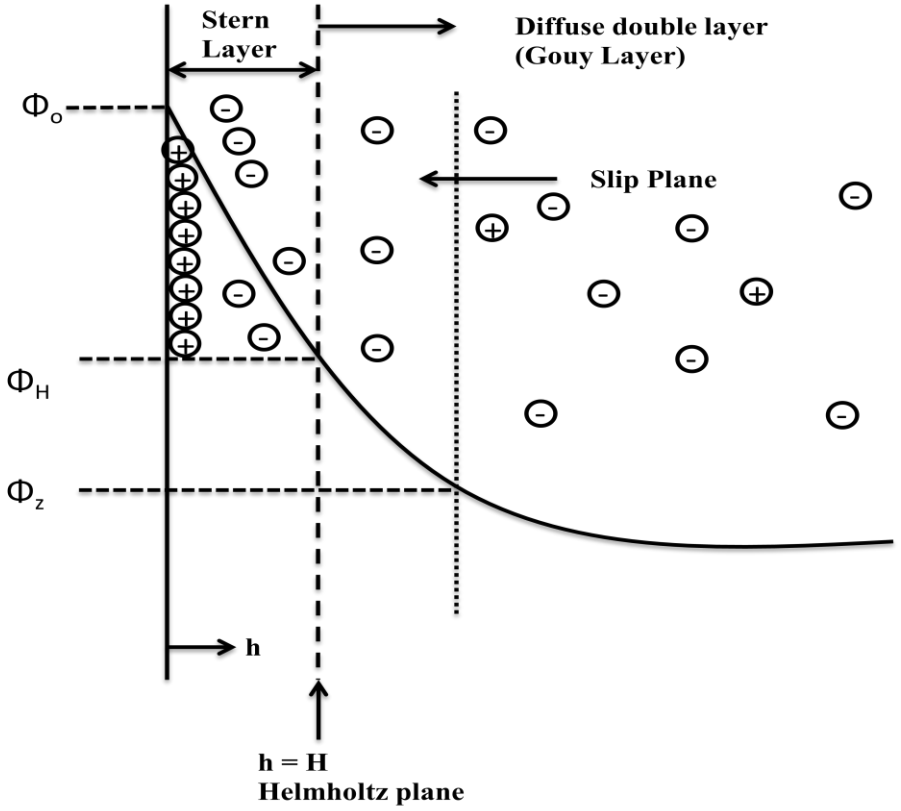

Figure 3.3: Electrical double layer structure for colloidal Ag or Cu based on the Stern model (adapted from reference 68).

The interaction of two colloidal metal nanoparticles can be best explained through DLVO theory, named after the 4 scientists who independently developed the model; Derjaguin, Landau, Verwey and Overbeek.[66] When two NPs approach each other, their electrical double layers overlap and an electrostatic repulsion results.[67] According to DLVO theory,

structures as small as NPs experience a negligible gravitational force effect. However, they constantly collide with one another *via* Brownian motion, which causes van der Waals attractive forces to become significant.[66,67] The attractive forces reduce the potential energy of the system through aggregation of the particles. The repulsive force serves as a barrier to aggregation. As the double layer is thinned out by high electrolyte concentration, the electrostatic repulsion-induced barrier to aggregation is reduced through charge-screening.[66] The energy requirement to achieve aggregation is therefore lowered, making every collision a possible point of merger. Figure 3.4 shows this decrease in repulsive force as a function of double layer thickness. This balance of attractive and repulsive forces for colloidal systems is key to their stability; in some cases colloidal systems are undesirable and measures can be taken to favor attractive forces over repulsive forces, thus forcing aggregation, such as the addition of charged ions, heating or stirring of the sol.

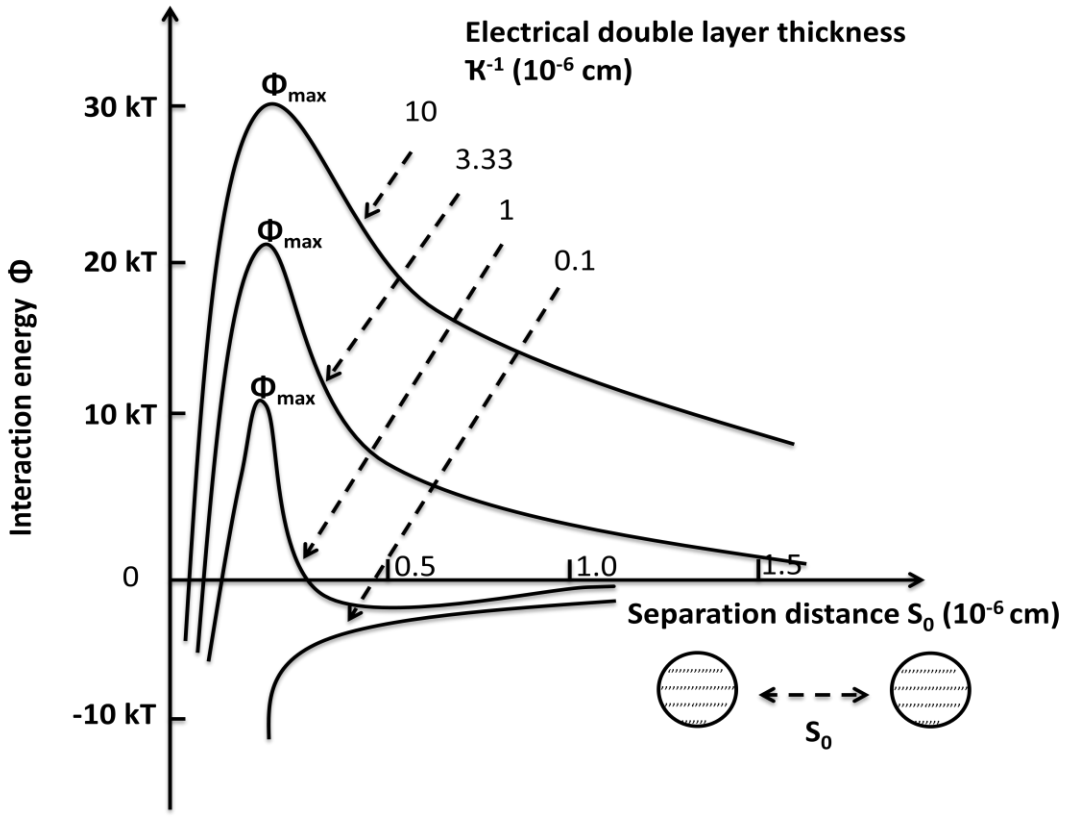

Figure 3.4: Schematic of interaction energy as function of double layer thickness. Double layer size is decreased by increasing salt concentration. (adapted from reference 66).

3.3 Plasmonics

A plasma is a gas of charged particles and is considered the 4th state of matter.[69] Some metals at the nanoscale exhibit plasma-like properties at their surfaces. A single quantum of a plasma oscillation is called a *plasmon*. When the plasmon oscillation occurs at the surface of a nanoscale metal it is referred to as a surface plasmon (SP).[69] If the frequency of the charge density wave of the SP matches the frequency of the oscillating electric field of the incident radiation, surface plasmon resonance (SPR) can result.[69] A consequence of SPR is a great enhancement of the electric field at or near the surface of the metal.[69] Since this SPR condition requires the presence of free electrons, discussions of plasmonic materials are generally confined to metals. The nature of the SPR available for a particular metal is strongly dictated by the real and imaginary components of the complex dielectric function of that metal. Additionally, the shape and size of the nanostructured metal will dictate the frequency at which the surface plasmons oscillate. Furthermore, the proximity of nanostructures to one another can have varying plasmon coupling effects.[69]

There are two types of SPs: the first is a localised surface plasmon (LSP). The LSP is noted in metal structures that are nanoscale in all dimensions.[2] The second type is the propagating surface plasmon (PSP) and this is a characteristic of the metal structure; PSPs only occur in metals that are nanoscale in only one dimension.[2] Hence, very thin metal films are capable of supporting a PSP, forming the basis for surface plasmon resonance spectroscopy. As this thesis deals only with the generation and utilization of localized surface plasmons from zero-dimensional nanostructures, the discussion will be focused there.

The dielectric function is often used to characterise the optical properties of bulk materials as a function of the frequency of incident electromagnetic radiation, and is denoted by the symbol ε.[1, 2] Dielectric function is related to the index of refraction by $n = \sqrt{\varepsilon}$.[82] Optical materials like lenses and prisms have positive real number indices of refraction and dielectric functions. For non-transparent objects, those same values are complex numbers; this is the case for metals. Those values are ultimately the result of the electronic structure of a material.[1, 2] The complex dielectric function is then composed of real and imaginary components, denoted as ε_r and ε_i, respectively. The real dielectric function component (ε_r) refers to the degree to which a material is polarized by incident radiation, and the imaginary dielectric function (ε_i) refers to the ability of the polarised material to absorb energy.[8] According to Mie theory, only metals are capable of supporting LSPRs. Mie theory can be used to calculate the extinction cross-section (C_{ext}) of a metal, which is a measure of a particular metal's ability to both absorb and scatter incident light at a certain wavelength, λ, as highlighted in equation 3.2. When C_{ext} is large, the metal supports a strong SP, and this only occurs for metals that have a negative real component and a small, positive imaginary component of the complex dielectric function.[2] As shown in Figure 3.5, in the visible wavelength regime this is only true for certain metals such as Ag, Au, and Cu.

$$C_{ext} = \frac{24\pi^2 R^3 {\varepsilon_m}^{3/2}}{\lambda}\left[\frac{\varepsilon_i}{(\varepsilon_r + 2\varepsilon_m)^2 + {\varepsilon_i}^2}\right] \qquad 3.2$$

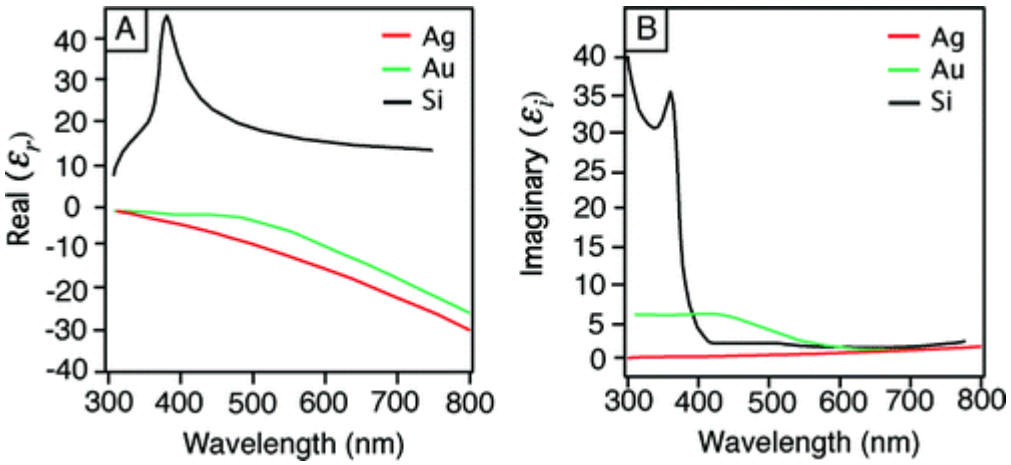

Figure 3.5: Real and imaginary dielectric functions for gold, silver and silicon.[2] (Reproduced with permission)

Furthermore, the strength of the SP that certain metals can exhibit varies considerably, and this can be evaluated by calculating the quality factor, or Q-factor, which compares both the real and imaginary components of the complex dielectric function for a metal. The value of the Q-factor as a function of incident wavelength is plotted for several metals in Figure 3.6.[2] Ag displays the most useful plasmonic behaviour as it has the highest Q factor over most of the vis-NIR range. Au and Cu are also good but suffer from d-band interference below ~600 nm.[2] Lithium is also potentially useful, but practical use is limited due to reactivity. Al supports SP in the deep-ultraviolet, and is potentially of interest as a material for UV-SERS.

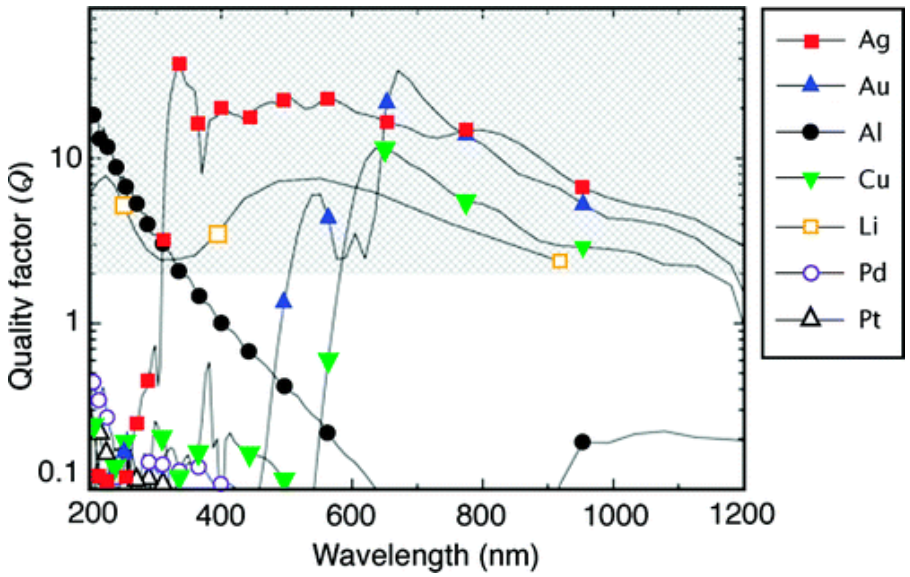

Figure 3.6: Quality factor for different metals as a function of wavelength of incident radiation.[2] (Reproduced with permission)

The size of the nanoparticle is also critical since each metal has its own penetration depth for incident light waves.[69,70] With decreasing wavelength of incident radiation the penetration depth rapidly decreases for the coinage metals, this can help to explain the large drop observed in Q-factor in Figure 3.6. The average penetration depth for the coinage metals is about 30 nm, with Ag having a much larger penetration depth of approximately 80 nm at resonant frequencies.[70] Constraints on size upper limits of plasmonic nanostructures are also in part due to the occurrence of multipole excitations.[1] In small NPs only dipoles are formed when they interact with light, which manifest themselves as LSPR modes. In larger particles there is more room for polarization, which means multiple poles can be supported that at first will lead to a broadening of the LSPRs, then at large enough diameters radiative damping occurs.[1] Both the broadening and the dampening lead to the attenuation of enhanced electric fields.[1] When NPs are exceedingly small, the absorption cross-section far exceeds the scattering cross-section

which leads to NPs better suited for plasmonic heating (~ < 10 nm).[71] Hence, there exists an optimal size range (diameter) for metal nanoparticles when plasmonic applications are being explored, which is generally between 20-100 nm for the coinage metals.[71]

The interparticle spacing of NPs also has an effect on the overall electric field strength.[2] LSPs can start to interact once the NPs are about 2.5 diameters from one another.[72] This interaction is very intense at small separation lengths (~1 nm).[72] The electric field strength enhancement is maximised within such proximity and is exploited in SERS, where the greatest enhancements are appreciated in gaps the size of individual molecules; such gaps are referred to as "hot spots".[70] Hot spots have also been observed in nanostructures that have sharp corners or edges; this is attributed to the lightening rod effect.[2] In addition, NPs in 3D assemblies are capable of much stronger optical modulations than those in 2D arrays.[69]

More recently, it has been discovered that plasmonic nanoparticles are also capable of catalysing certain reactions. This is referred to as surface plasmon-assisted catalysis, or SPAC.[71,73,74] The catalysis is afforded by the decay of SPs, which can happen one of 2 ways; through a radiative path where the NPs act like a nanoscale antenna, scattering incident radiation, or through a non-radiative channel where the NPs absorb the incident radiation.[71] The absorption may result in heat generation as alluded to earlier by electron-phonon coupling, or it can produce high energy electrons termed "hot electrons" that can be transferred to an unoccupied resonant energy level of a molecule on or in very close proximity to the NP surface.[71,73,74] This has been demonstrated for *para*-aminothiophenol (p-ATP), which is catalyzed to p,p'-dimercaptoazobenzene (DMAB) when present on coinage nanostructures and irradiated with incident light of appropriate

energy. This catalytic transformation is evaluated for the sustainable plasmonic architectures developed in this thesis work.

3.4 Spectroscopic techniques

3.4.1 Raman Spectroscopy

One of the spectroscopic techniques that can benefit from the enhanced localised fields described above is Raman spectroscopy. Raman spectroscopy is a form of vibrational spectroscopy based on the inelastic scattering of light. The scattering process happens between a photon and a molecule. The incident radiation assumes a different frequency after the interaction; the frequency difference is characteristic of the molecular vibrations. The shift in frequency of the scattered photons can be greater than (anti-Stokes shift) or less than (Stokes shift) the frequency of the incident photons, and the direction of the shift is governed by whether the illuminated species of interest is in a vibrational excited state or the ground state.[75,76] By removing the Rayleigh (elastic) scattered component, and observing only the Raman scattered component (generally Stokes scattering), one can obtain the vibrational spectrum of the sample being analyzed, which is complementary to the more common infrared spectroscopy.

In Raman spectroscopy, the vibrational frequencies are reported as Raman shifts from UV-visible incident photons while in infrared spectroscopy these frequencies are based on the absorption of incident infrared light, and detected as the ratio between incident and transmitted infrared radiation. This affords different selection rules for Raman and infrared spectroscopy.[76] For a molecule to be IR active there needs to be a change in the dipole moment during the vibration and in the case of Raman activity there

needs to be a change in polarizability.[76, 77] As a result, vibrational modes can be Raman active and IR inactive or vice-versa, or they can be active for both.

Unlike in infrared spectroscopy, where chromophores tend to have similar absorption strengths, the ability of a chromophore to scatter light well, and hence produce an appreciable Raman signal, is highly dependent on several factors. For example, molecules that have extensive pi bonds (delocalized electrons) typically give intense Raman spectra as their electron clouds are more susceptible to perturbation by an incident electric field such as in the case of benzene. Water, and glass, with only single bonds, are weak Raman scatterers.[76, 77] As a result, many biologically relevant systems present in aqueous environments can be potentially investigated with Raman spectroscopy in affordable glass cells. This is very difficult to do using infrared spectroscopy due to the strong infrared absorption of both water and glass. In addition, electron-rich atoms, such as heteroatoms and metals, tend to give good Raman signal due to enhanced scattering.

Despite the advantages that Raman spectroscopy can offer compared to infrared spectroscopy, the inherent signal weakness due to the low occurrence of the inelastic scattering processes (~1 in 1 million photons) has resulted in a lagged development for routine chemical analysis. As a result, Raman spectroscopy has only proven useful for the analysis of bulk materials or very concentrated solutions. This limitation however, was overcome by the discovery of surface-enhanced Raman spectroscopy (SERS) in the late 1970's. SERS was the first successful application of localized surface plasmons, and represented the birth of modern day plasmonics. SERS will be described in detail in the following section, and is a major focus of this thesis work.

3.4.2 Surface Enhanced Raman Spectroscopy

In the mid-1970's it was observed by Fleischmann and coworkers that there was a large improvement of the Raman spectra for pyridine adsorbed onto the surface of an electrochemically roughened silver electrode.[75] While Fleishmann originally attributed the increased signal intensity to simple surface area increase, Van Duyne and Jeanmaire[78] and Albrecht and Creighton[79] independently reported in 1978 that that the source of the enhancement was not due to surface area increase only, but that the majority of the signal increase was in fact due to an enhanced electromagnetic field on the surface of the nanoscale metal features. The idea of *localized* surface plasmon resonance was born. In subsequent years, the fundamental ideas concerning the origin of the SERS signal have been well studied, and continue to evolve. Generally, however, there is a consensus on the contributions to the enhancement, which involves both a chemical (charge-transfer) mechanism as well as an electromagnetic mechanism based on the presence of the localized surface plasmon resonance.[75]

The chemical enhancement in SERS can come about in two ways: 1) the polarizability changes of the adsorbed molecules on the metal surface provide an increased Raman scattering cross section compared to free molecules and 2) electron transfer between the adsorbate and the metal substrate can occur, driven by the incident radiation, which facilitates the excitation of electrons from the HOMO to the LUMO in the molecule.[2] Theoretical predictions estimate that the chemical mechanism (CM) contributes $\sim 10^2$ to the overall enhancement.[2]

The electromagnetic enhancement mechanism is associated with the SPs already discussed in the plasmonics section.[1] The electromagnetic enhancement occurs as the

incident radiation on the metal surface is amplified by being in phase with the induced local field, which can then be scattered by the molecules on or in close proximity to the metal surface.[75] This enhancement can also occur *via* the scattered radiation of the molecule being coupled to the metal surface instead of the incident radiation being enhanced. It should be noted that both of these pathways for electromagnetic enhancement happen simultaneously and, unlike for the chemical enhancement, the molecules of the analyte do not have to be in direct contact with the metal to experience this enhancement.[2, 75] Theoretical predictions suggest that the electromagnetic mechanism (EM) contributes the most to SERS, approximately 10^4-10^{10}. Combining both the CM and EM contributions, one can see that the Raman signal for a desired analyte can be increased by 10^6-10^{12} times simply by incorporating coinage metal nanoparticles into the system. This level of signal enhancement makes single molecule detection a possibility, as has been illustrated for certain systems.[75]

It should be mentioned that decay length of the LSPR, although tunable (with shape, size and spacing of metal nanoparticles), ranges from 5 - 15 nm.[62] Therefore, the electromagnetic enhancement can only be experienced through short distances. Additionally, within the decay length, a decrease of SP strength of ~ $1/r^{10}$ where r is the radius of the nanoparticle, is noted as a function of the distance between the analyte and the nanoparticle.[80] Hence, one would ideally want an analyte to make direct contact with the metal nanoparticle to make the most of this distance dependance.[80]

3.4.2.1 Enhancement factor (EF)

To assess the total enhancement that can be obtained from a particular SERS substrate, the enhancement factor (EF) is calculated, which is a value that embodies the contributions from both the EM and CM. The enhancement factor can be computed as follows:

$$EF = \frac{I_{SERS}/N_{Raman}}{I_{Raman}/N_{SERS}} \quad 3.3$$

where I_{SERS} and I_{Raman} represent the integrated intensities for the same vibrational mode for the SERS and Raman measurements, respectively. N_{SERS} and N_{Raman} represent the number of probe molecules that contribute to the signal for SERS and Raman, respectively.

For the calculation of N_{SERS} it is assumed that a monolayer of the probe molecule is formed on the SERS substrate and it is only this layer that contributes to the observed SERS signal.[81] Therefore, N_{SERS} can be calculated as follows:

$$N_{SERS} = \frac{RA}{\sigma} \quad 3.4$$

where σ is the surface area, or footprint, of the probe molecule. R is the roughness factor of the substrates: a small positive number integer that represents the increased surface area for the nanoscale surface. Lastly A is the surface area illuminated by the laser. For SERS substrates made of nanospheres, R is the product of half the area of a sphere and the inverse area of a circle with the same diameter as the sphere.[81]

$$R = \frac{1}{2}(4\pi r^2)\frac{1}{\pi r^2} = 2 \quad 3.5$$

For normal Raman spectroscopy a concentrated sample is required from which many probe molecules contribute to the Raman signal.[81] Hence, when calculating N_{Raman} the concentration and effective volume of sample the laser probes is important. Firstly, one needs to determine the volume of illuminated sample that contributes to the signal. Since the area of the laser spot can be determined by working parameters, finding out the depth of the contribution becomes important.[81] By rendering a depth profile where the laser is kept in the same position and a silicon wafer is moved back and forth through the focal point of the laser the focal volume can be ascertained. [81] This measurement, known as a scanning knife edge measurement, shows that the signal intensity is highest at the focal point, and exhibits a continuous decay in signal in either direction away from the focal point. By dividing the integrated area under this Raman intensity depth profile by the maximum intensity, the value for the effective layer size (h) can be computed. The volume of the sample that contributes to the Raman signal can now be calculated by multiplying the illuminated area (A) by h. N_{Raman} can be established as follows

$$N_{Raman} = AhcN_A \qquad 3.6$$

where c is molar concentration and N_A is Avogadro's constant.The EF for SERS substrates consisting of uniform nanospheres can therefore be summed up as follows:[81]

$$EF = \frac{I_{SERS}}{I_{Raman}} \frac{hcN_A\sigma}{2} \qquad 3.7$$

3.4.3 Electrochemical Surface Enhanced Raman Spectroscopy (EC-SERS)

By coupling SERS with an applied electrochemical potential one can possibly obtain further enhancement from a SERS substrate. This technique is referred to as electrochemical surface enhanced Raman spectroscopy (EC-SERS). Both mechanisms

responsible for SERS enhancement (chemical and electromagnetic mechanisms) can be influenced by the applied potential.[98] For example, alteration of the applied potential allows one to manipulate the Fermi level of the metal, thus allowing for enhanced charge-transfer between the metal and the adsorbate. In addition, manipulation of the surface charge through applied voltage can help to drive adsorbates to the surface, thereby increasing the SERS signal due to proximity considerations. Other factors including surface redox processes and potential-induced reorientation of adsorbates can also help to explain potential-dependent changes in SERS signals. It stands that SERS substrates in an electrolyte will have both an alternating electromagnetic (EM) field associated with the SPs as well as a static electrochemical (EC) field both established in the double layer between the surface of the SERS substrate and the electrolyte. [76]

3.4.4 UV-visible spectroscopy

UV-vis absorption spectroscopy can be used to obtain quick insight into the shape, size, and polydispersity of colloidal NPs.[1] Since the NPs all have a particular scattering and absorption cross-section, they interact with the radiation in a fairly well understood manner. Energy is conserved, thus any energy lost by incident radiation at the surface of the NPs through absorption and scattering processes can be measured.[1] This measurement is called an extinction measurement, and is measured using traditional UV-vis spectroscopy. The extinction of the incident radiation is due to both scattering and absorption processes, and is therefore most accurately referred to as an extinction spectrum. Larger NPs absorb in more red shifted (longer λ) portions of the visible spectrum while smaller NPs are generally more blue shifted. If one has a large NP size distribution it is expected to have a broad absorption peak (large FWHM) and if very

monodispersed the absorption peak is expected to be narrower (small FWHM).[1] In addition, anisotropic nanoparticles can display multiple peaks; for rods two peaks are observed, one due to the longitudinal plasmon resonance and another due to the transverse plasmon resonance. UV-vis measurements of colloidal metal sols offer a quick and easy way to monitor reaction progress and colloid stability. In addition, since the extinction, and therefore the observed color, is dependent on factors such as size, shape and aggregation, this forms the basis of many visual readouts in diagnostic sensors, including home pregnancy tests that utilize Au nanospheres for the "red" positive indication.

3.6 Electrochemistry

3.6.1 Bulk electrolysis

Bulk electrolysis is an electroanalytical technique wherein one holds either the current (amperometric coulometry) or potential (potentiostatic coulometry) constant and measures the other variable as a function of time to determine the amount of analyte present through a change in its oxidation state.[82] In this thesis, potential control (constant voltage) is used to electrodeposit metal onto a carbon working electrode. When the redox system under investigation can proceed spontaneously it is referred to as Galvanic, and offers the user close to no control over the morphology of the deposits.[82] Galvanic deposition is therefore not ideal for the present studies. Hence, electrolytic (non-spontaneous) processes, where one can control the electrodeposition, are generally preferred for making metal nanostructrues.[68]

Electrodeposition of metal cations involves application of an external potential to attract and reduce the cation at the surface of the electrode; in this thesis work both Ag^{+}

and Cu^{2+} were explored. The first step involves formation of an adatom on the substrate, which can then migrate on the surface in search for a more energetically favourable site.[68] The first layer deposited will determine the arrangement of subsequent deposits.[68] Heterogenous nucleation at the electrode has two limiting cases. Firstly, *instantaneous nucleation* is most probable when applying very high potentials.[68] This will result in deposits resembling nodules, dendrites or, at extremely high potentials: powders with low adhesion.[92] The second case is *continuous nucleation*.[68] Continuous nucleation can occur when there is equal nucleation energy at all nucleation sites. It should be noted that this is idealistic and that in practice there will be less energy in cracks and surface defects of the electrode.[68, 83] Low applied potentials allow more time for ordered crystalline deposits to form.

To obtain better quality electrodeposits, additives are often used but knowledge of their function is generally lacking. Smoother deposits can be made by using organic compounds and surfactants.[83] Some examples of additives that have been explored for this purpose include polyethylene glycol (PEG) and KCl, as was highlighted in the literature review. Different ratios of additive can impact grain size of the deposit and some additives may even inhibit dendritic growth.[83]

3.6.2 Voltammetry

Voltammetric methods are widely employed electroanalytical techniques. In these methods, one measures current as a function of an applied potential, generating a plot called a voltammogram. Voltammetric methods are one of the most sensitive techniques in analytical chemistry, capable of parts per billion detection units for heavy metals.[82] Under conditions of complete concentration polarization, the current in the

electrochemical cell is measured. Under this condition, the rate of the reduction or oxidation is limited by the mass transfer of the analyte to the electrode. Voltammetry differs from the potentiostatic coulometry discussed earlier as it does not take measures to reduce concentration polarization, such as constant stirring to improve mass transport of the analyte to the electrode surface.[68] The simplest of these voltage-time functions (excitation signals) is the linear scan. A square wave excitation signal was used in this work; voltammetry of this waveform is termed square wave voltammetry (SWV).

When a smooth electrode is exposed to SWV conditions, the surface of that electrode can be partially shaped by the quick potential pulses that will oxidize and reduce the analyte and / or the metal many times in one run.[53] This is sometimes used to introduce nanoscale features in a smooth metal electrode and in this work SWV was used to increase the nanoscale features of the electrodeposited copper.[53]

Chapter 4 Materials and Methods

4.1 Introduction

This section starts with a description of the reagents used in this thesis work. Next, the instrumentation that was utilised in this work is outlined including Raman spectrometers, UV-vis spectrophotometer, and potentiostat/galvanostats. The methodology used to make the SERS substrates and subsequently characterise them is then noted.

4.2 Reagents

$AgNO_3$ (>99%), $Cu(NO_3)_2$ (99.999%), $CuSO_4$ (99.999%), $NaBH_4$ (≥99%), NaCl (99%), NaOH (99.99%), KCl (≥99%), chitin, and Celite (diatomaceous earth) were all purchased from Sigma Aldrich (St, Louis, MO, USA) and were used without further purification. All solutions were prepared using Millipore water (≥ 18.2 MΩcm). All glassware used was placed in an acid bath composed of neat H_2SO_4 overnight, and was then rinsed with Millipore water thoroughly prior to use.

4.3 Instrumentation

4.3.1 Raman Spectrometers

Two Raman spectrometers were used in this work. The first was a DeltaNu Advantage 785 Raman spectrometer, produced by Intevac, Santa Clara, CA. This spectrometer uses a 785 nm diode laser and an air cooled CCD detector. The spectrometer is operated with NuSpec software for signal acquisition processing and manipulation of parameters. For further spectral processing and data analysis Origin 8.6 (OriginLab Corporation, Northampton, MA) was utilized. The DeltaNu spectrometer has a resolution of 4.0 cm^{-1}.

The second Raman spectrometer was a DXR SmartRaman Raman spectrometer produced by Thermo Fisher Scientific Inc. (Madison, WI, USA). The DXR SmartRaman has two laser lines: a 532 nm (diode-pumped solid state laser) and NIR 780 nm (frequency-stabilised single mode diode laser). Both lasers came with two different gratings as shown below in Table 4.1.

Table 4.1: Associated spectral window and resolution for the different laser lines and their associated diffraction gratings for the DXR SmartRaman.

Laser line / nm	Grating	Spectral window / cm^{-1}	Resolution / cm^{-1}
785	High resolution	50- 1800	3.0
785	Low resolution	50 – 3300	5.0
532	High resolution	50- 1800	3.0
532	Low resolution	50 -3500	5.0

4.3.2 Potentiostats

EC-SERS and electrochemical measurements including cyclic voltammograms were obtained using a WaveNow USB potentiostat produced by Pine Research instrumentation (Durham, NC, USA).[84,85] The instrument is controlled using the Aftermath Data Organizer software (version 1.2.4361) produced by the same company. The electrodes used in this work were all screen printed carbon electrodes (SPEs) sourced from Pine Research Instrumentation. The SPEs used were all 5 mm x 4 mm rectangular carbon working electrodes, with a carbon counter electrode and a Ag/AgCl

reference electrode. The electrodes are connected to the electrochemical cell and potentiostat through a mini-USB cell cap connector. A second potentiostat was used for the electrodeposited SERS substrates, which was a Model 263A Potentiostat/Galvanostat produced by Princeton Applied Research (Oakridge, TN, USA). The software required for operation of this potentiostat was Electrochemistry Power Suite 258 also provided by Princeton Applied Research.

4.3.3 UV-Visible Spectrophotometer

Absorption measurements were obtained using an Ocean Optics USB2000+ fiber optic spectrometer. This instrument was used to record the extinction spectra for the colloidal sols. A sample of the sol was placed in a quartz cuvette and irradiated using a UV-visible deuterium light source.

4.3.4 Scanning Electron Microscope

The shape and size of the metal nanostructures evaluated in this project were ascertained using a TESCAN MIRA3 LMU field emission SEM (Warrendale, PA, USA). This FE-SEM has a tungsten electron gun and is fitted with both a back scatter and a secondary electron detector. Energy dispersive X-ray spectra (EDS) were collected using an INCA X-max 80 mm^2 EDS system that uses a silicon drift detector (SDD). This was used to obtain qualitative information regarding the composition of the SERS substrates. The metal nanoparticles were imaged by depositing a drop of the colloidal sol onto a 5 x 5 mm silicon wafer obtained from Ted Pella, Inc. (Redding, CA, USA). All biological materials explored for bioscaffolding in this thesis work were secured to carbon tape and coated with carbon prior to imaging. Electrodeposited SERS substrates were simply cut out of the screen printed electrode and the working electrode was then secured to carbon

tape and the exposed plastic edges were also covered with carbon tape to reduce charging effects from the plastic during imaging.

4.4 Plant Extract preparation

All plants and fruits were obtained locally, either from local parks or from local grocery stores. Extracts were all prepared using different parts of the plant and fruits. Certain parts of the plant required larger quantities to be used. Table 4.2 lists the part of the plant an extract was produced from and the quantity of plant material that was required.

Table 4.2: Quantities of plant parts and solvent required for each extraction.

Part of plant	**Quantity used in extract**	**Amount of solvent / ml**
Dandelion Flowers	10 flowers, ~4.5g	140
Strawberries	6 berries ~32g	50
Haskap Juice	N/A, used directly	N/A, used directly
Brown Cane Sugar	12g	100
Haskap Berries	10 berries	100
Blue Berries	10 berries ~32g	100
Orange Zest	~32g	50
Banana Peels	50g	100
Avocado Pit	1 pit	100

All parts of the plant to be used were first thoroughly washed with Millipore water. The dandelion flowers and avocado pits were both placed into the oven at 135°C for 30 minutes and then were allowed to cool before the following protocols were followed. After being heated the avocado pit tough exterior was easily removed by hand and discarded. Plants/fruits were placed into a laboratory blender with the corresponding amounts of solvent as listed in Table 4.2. The mixtures were then blended for 60-100 seconds until no further change could be noted in consistency. The blended materials

were filtered twice, first through 3 layers of cheesecloth to remove of large particulates, and afterwards the extract was filtered *via* gravity filtration using Whatman filter paper #1. The extracts were first prepared using methanol as the solvent and later studies were conducted in Millipore water as the solvent in an effort to render the synthesis more green.

4.5 SERS Substrates

4.5.1 Standard Silver Nanoparticle Preparations

All SERS substrates prepared in this body of work were compared to the standard colloidal AgNPs in terms of both signal intensity and signal uniformity, as well as in their ability to support plasmon-assisted catalysis. The two most utilised methods by our research group to make non-sustainable SERS substrates are as follows; the first is based on the Lee-Meisel method[57] and the second is adapted from Zhao *et al*.[73]

4.5.1.1 Sodium citrate reduced silver nanoparticles (Lee-Meisel method)

0.9g of $AgNO_3$ was dissolved in 500 ml of Millipore water and brought to a vigorous boil with constant stirring. The beaker was kept covered with a watch glass and the synthesis was done in a dark space so only a minimal amount of light could reach the photosensitive Ag^+. Once vigorously boiling, 10 ml of 1 % w/w% trisodium citrate was added to the reaction vessel and allowed to boil for an additional 30 minutes. The colloidal Ag sol was then allowed to cool before centrifuging at 3600 rpm 10 times, each time discarding the supernatant and adding a new 1 ml aliquot of colloidal Ag. The centrifuge used in this work was a Galaxy 16 by VWR (Missassauga, ON, Canada).

4.5.1.2 Sodium Borohydride Reduced Silver Nanoparticles (Zhao method)

To a 3-neck flat bottom flask the following was added: 95.0 ml ultrapure water, 1.0 ml of 0.1 M $AgNO_3$, 3.4 ml of 5% w/w trisodium citrate, 600 µl of 0.17 M citric acid and 200 µl of 0.1mM $NaBH_4$. The solution was allowed to react for 1 minute before being stirred and was heated to boiling under reflux. The $NaBH_4$ was made in cold water and was only added after the rest of the reaction mixture was boiling and then the mixture was allowed to boil for 60 additional minutes. The colloidal Ag was centrifuged at 8000 rpm in 14 tubes containing 1430 µl each. The supernatant was discarded and the pellets were combined into a fresh tube and centrifuged at the same speed for a second time. The supernatant was once again discarded and the pellet diluted to 50 µl with ultra-pure Millipore water using a micro pipette.

4.5.2 Green Synthesis of Silver Nanoparticles from Plant Extracts

The Lee-Meisel method described above was adapted for the plant/fruit extract Ag colloid synthesis. 100 ml of 1 mM $AgNO_3$ solution was prepared and allowed to boil with vigorous stirring in the fume hood, protected from light. Once the solution was boiling, 2 ml of an extract was then added to the reaction vessel. The reaction was then allowed to boil for a further 30 minutes. The mixture was then taken off the hotplate and 0.1 M NaOH was added dropwise until the color of the mixture turned dark red-orange (approximately 30 drops). Once the desired color was achieved, 1 ml aliquots of the colloidal Ag were put into individual centrifuge tubes and were centrifuged at 10,000 rpm for a period of 15 minutes. The supernatant was removed and the pellets collected into 2 tubes that were centrifuged a second time at the same speed for the same amount of time.

The final resulting pellet, which was essentially a AgNP paste, was then used to prepare the SERS substrates.

4.5.3 Preparation of SERS substrates

To the rectangular surface of an SPE working electrode, 5 µl of the colloidal Ag pellet was spread evenly and allowed to air dry in the dark. Once dried this was repeated twice more. Each layer was allowed to dry before the next layer was added. This was done for the standard Ag, extract reduced Ag, and for any biotemplated SERS substrates unless otherwise noted.

4.5.4 Displacement of capping agents

The capping agents employed to protect and stabilize NPs can become problematic for sensitive SERS detection. This is because the capping agents are generally bound strongly to the metal surface, and can therefore dominate the SERS signal and/or block surface access for target analytes. Simple steps can be taken to remove the capping agents; a particularly effective method and the method used in this thesis work is outlined here. AgNP-modified SPEs were placed in a 1 mM KCl solution for 30 minutes followed by careful rinsing with Millipore water. Due to the nature of the strong specific adsorption of Cl^- onto Ag, the Cl^- is capable of displacing the capping agents, after which the probe molecules could be introduced and detected. This treatment was carried out for the Lee-Meisel method and on some of the extract synthesized AgNP substrates when used to detect non-thiolated probe molecules.

4.5.5 Preparation of SERS substrates using biological scaffolds

All biotemplates were imaged *via* SEM to identify any desirable nano/micro features before they were explored as possible SERS substrates.

4.5.5.1 Diatomaceous earth

Diatomaceous earth is siliceous in nature and is composed of many single cell diatoms. Two approaches were used for templating with diatomaceous earth, which is commercially available in a purified form as Celite®. The first was to directly incorporate Celite® into the Lee-Meisel synthesis reported in section 4.5.1.1. To the 500 ml of Millipore water, 0.200 g of Celite® was added and the rest of the steps were followed.

The second approach required the electrodes to be treated with Celite® first, followed by a 3-layer addition of AgNPs. 0.02 g/ml Celite® was centrifuged for at low speed (1000 rpm) for 5 mins. The supernatant was discarded and the Celite® pellet was re-suspended in an equal volume of water. 5 µl of re-dispersed Celite® was then deposited onto an SPE. Once this had dried, two more layers were applied.

4.5.5.2 Drosophila wings

Wings were removed from freshly deceased fruit flies (*Drosophila melanogaster*) obtained from the biology laboratory at Saint Mary's University. Wings were rinsed with water and then carefully placed on the SPE working electrode with a pair of tweezers so they would occupy as much of that surface as possible. Three layers of the Lee-Mesiel AgNP were then drop coated onto the wings, allowing each layer to dry before a subsequent layer was applied.

4.5.6 Electrodeposited copper substrates on screen printed electrodes

Single step chronoamperometry was performed to deposit metallic Cu from both $CuSO_4$ and $Cu(NO_3)_2$ salts. The first set of studies relied only on 0.1 M $CuSO_4$. An applied potential of -0.1 V for 1 minute was applied to the working electrode. The time was increased until visual deposits formed on the electrode or 20 minutes had elapsed,

whichever came first. This was repeated for applied potentials of -0.3 V and -0.5 V for a variety of times so that an ideal deposition potential and time could be determined. $Cu(NO_3)_2$ was used to conduct the same studies to see if there was a difference when the nature of the counter ion and ionic strength was varied.

4.5.6.1 SWV modification of copper deposited SERS substrates

After the copper deposits were formed square wave voltammetry (SWV) was used to add nanoscale detail to these deposits. The SWV was set in the range of 0.0 V to -1.4 V Ag/AgCl, scan rate of 0.2 mV/s, pulse amplitude 2 mV, 1402 points using the Princeton Applied Research 263A Potentiostat/ Galvanostat.

4.5.6.2 Bimetallic Cu/Ag SERS substrates

Bimetallic copper-silver SERS substrates were made *via* electrodeposition onto the SPE in two different ways. Firstly, a 0.1 M copper (II) nitrate solution and a 1×10^{-4} M silver nitrate solution were made. Both solutions were purged with a stream of argon for 15-20 minutes. To 10 ml of the copper nitrate solution, 1ml of the silver nitrate was added with stirring at 200 rpm. The copper-silver deposits were formed under chronoamperometric conditions using a one-step profile and the scan definition of -0.300 V vs Ag/AgCl for 180 seconds. This will be referred to as the mixed method in the results and discussion.

The second set of bimetallic Cu-Ag substrates were made by first forming the copper deposits at the same applied potential and time as described above using an electroplating bath with only 10 ml of 0.1 M copper (II) nitrate while the bath was being stirred at 200 rpm. Different volumes ranging from 100 µl to 2 ml of 1×10^{-4} M silver nitrate were then added to the electroplating bath and a potential of 0.3 V for 180 seconds

was applied again. This will be referred to as the sequential method in the results and discussion.

4.5.6.3 Additives in Cu electrodeposition

Combinations of different additives were used to evaluate their effect on the deposit size. Polyethylene glycol (PEG) and KCl were the two additives investigated initially, as these two additives had been reported previously in the literature.[55] To the varying volumes of PEG and KCl were added to the electroplating bath and an applied potential of -0.3 V for a duration of 180 s was applied.

4.5.7 Immobilization of probe molecules

In order to compare the SERS performance of the many substrates explored in this work, a common molecule was chosen as the Raman reporter, or probe molecule, for this work. In SERS, a Raman reporter molecule is simply a molecule that has an excellent Raman signal and strong binding to coinage metals, which can be used to evaluate the SERS response for different surfaces. Generally these probe molecules are either thiol or pyridine based. For this work, *para*-aminothiophenol (p-ATP) and 4,4'-bipyridine (4,4'-bipy) were both chosen as probe molecules; p-ATP has the added benefit of allowing one to evaluate catalytic activity through the formation of the oxidative product (DMAB), as described previously. 5 µl of the probe molecule of interest at the desired concentration (generally 0.1 or 1.0 mM, aqueous) was introduced to the surface of a modified SPE. This was allowed to dry and samples were evaluated for SERS shortly after.

4.5.6 EC-SERS

Modified screen printed electrodes were placed in the electrochemical cell, which was a standard glass vial. 0.1 M NaF was used as the supporting electrolyte and was purged with argon prior to use. Once the deaerated electrolyte was added to the electrochemical cell containing the SPE, the open circuit potential (OCP) spectrum was collected. This spectrum is an important reference as it represents the SERS signal achievable at the resting potential of the metal (i.e. SERS without any electrochemical perturbation). The system was then brought from 0 V to -1 V in increments of 0.1 V, and at each applied potential a SERS spectrum was collected. Driving the system to further negative potentials is referred to as the cathodic sequence (cathodic direction), while returning to the more positive potentials is referred to as an anodic sequence (anodic direction).

4.6 SERS Analysis

An acquisition time of 30 s was used for collecting Raman spectra with both the 785 nm and 532 nm laser lines. With the 785 nm laser a power of 21 mW was employed while with the 532 nm laser a power of 3 mW was used unless otherwise stated. In all cases SERS and Raman spectral data were corrected for both power and time in order to be directly comparable.

Chapter 5 Results and Discussion

5.0 SERS on Standard Ag Nano-Substrates

AgNPs produced *via* citrate reduction of Ag^+ from aqueous silver nitrate is recognised as one of the simplest ways to obtain SERS substrates. These SERS substrates generally lack size and shape homogeneity and as a result the signal rendered from spot to spot on the surface may vary significantly. Citrate is also problematic as the reducing agent / capping agent since it has a strong Raman signature that can obscure the signal coming from target analytes. In addition, the presence of citrate on the surface increases the distance between the analyte and the AgNP, reducing the possibility for maximum signal enhancement due to the very short decay length for the electromagnetic enhancement for SERS. Figure 5.1 shows the SERS spectra of a monolayer of *para*-aminothiophenol (p-ATP) on citrate reduced AgNPs. The peaks indicated by asterisks are very dominant and are attributed to the citrate molecule as opposed to the p-ATP probe molecule; since both are present on the surface, both molecules contribute to the observed signal.

Despite this disadvantage, citrate-reduced silver nanoparticles continue to be one of the most widely utilized platforms for SERS studies, having been used by many others to study a variety of different compounds.[2] One of the most common Raman reporter molecules is the simple thiol *para*-aminothiophenol (p-ATP), which is utilized in this thesis work to evaluate the multitude of SERS substrates. In particular, in addition to being an excellent Raman probe, p-ATP undergoes plasmon-assisted catalysis to 4,4'-dimercaptoaminobenzene (DMAB) (Scheme 1), which can be followed *in situ* using SERS. Additionally, since this catalytic process is an oxidation, EC-SERS is particularly

well suited to explore this reaction, as the oxidation can be reversed electrochemically, and followed spectroscopically.

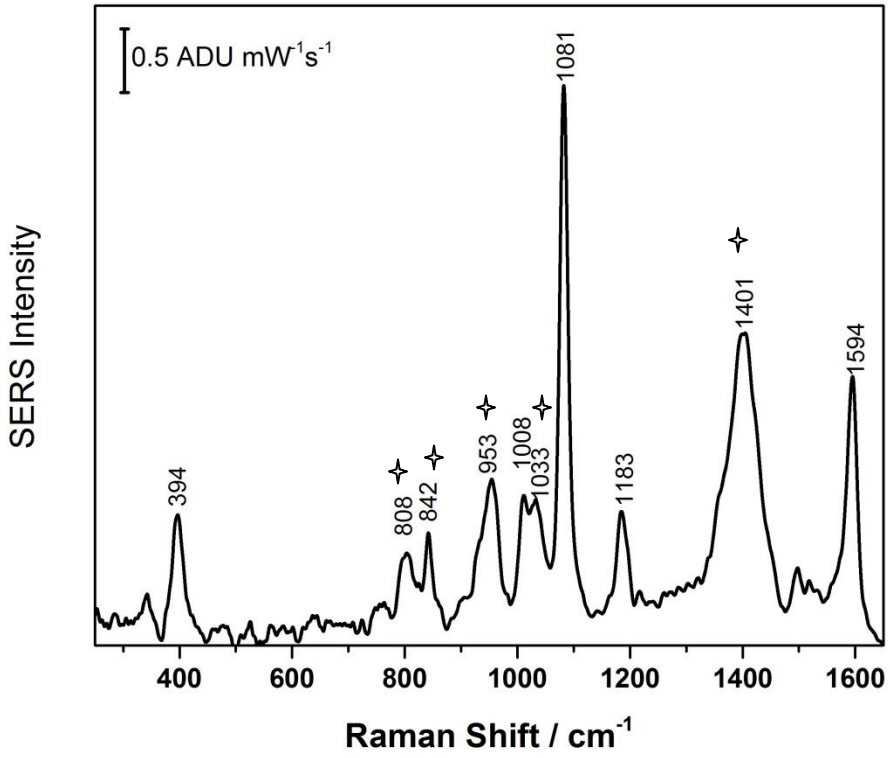

Figure 5.1: SERS spectra of 10 mM p-ATP on citrate reduced AgNPs. The peaks marked by stars are bands assigned to citrate vibrational modes. (30 s, 22.3 mW, 785 nm laser)

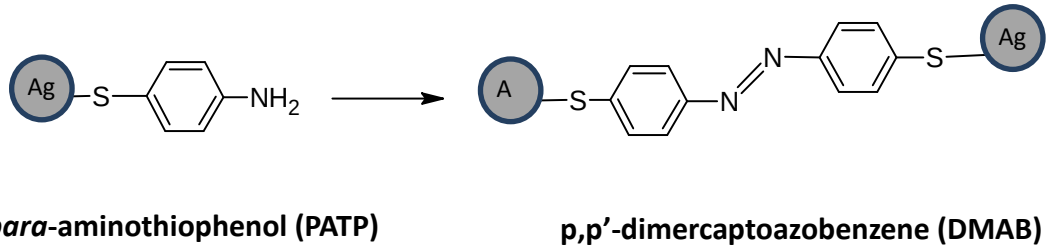

Scheme 1: Plasmon assisted catalytic conversion of p-ATP to DMAB.

Figure 5.2 shows the added benefit of doing an EC-SERS spectroelectrochemical analysis. The SERS spectra collected at open circuit potential (OCP) shows the spectral

fingerprint for both p-ATP and DMAB. However, as the applied potential approaches -1.0 V vs. Ag/AgCl the peaks associated with the catalytic product DMAB at 1141, 1390 and 1443 cm^{-1}, as marked by asterisks (*), progressively diminish until they eventually dissappear. This observation is consistent with the electrochemical reduction of the DMAB product back to p-ATP; only peaks due to p-ATP are observed at -1.0 V. A complete assignment of the bands due to both p-ATP and DMAB is presented in Table 5.1.

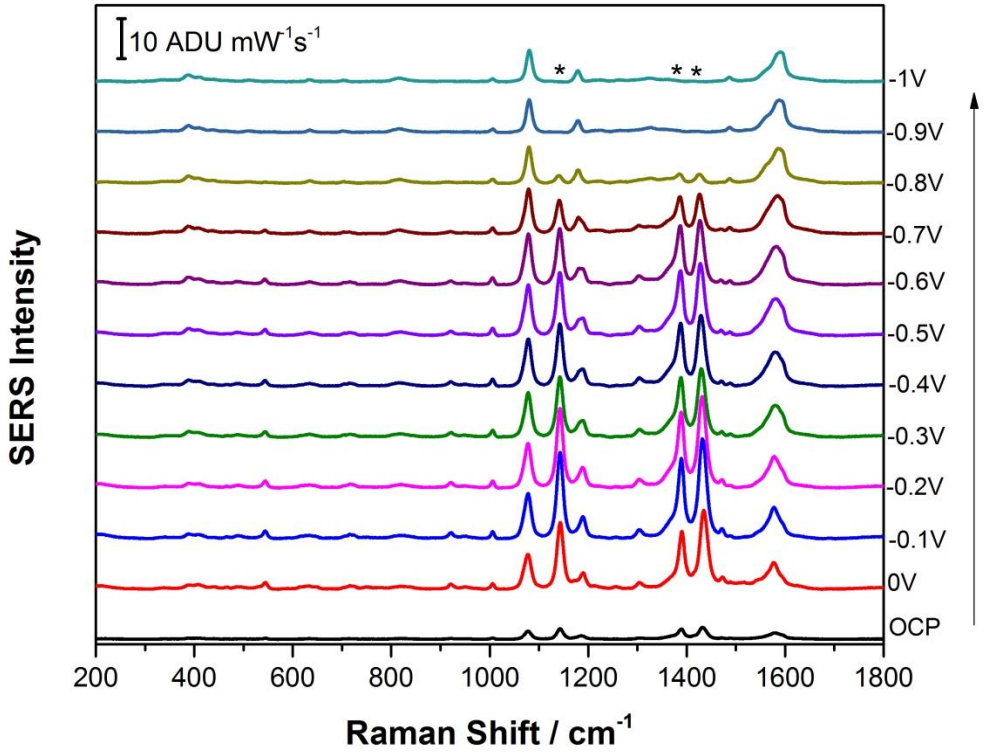

Figure 5.2: Cathodic EC-SERS plot of 10 mM p-ATP on citrate reduced-AgNPs. Supporting electrolyte 0.1 M NaF, 532 nm laser, 3 mW, 30 s acquisition.

Table 5.1: SERS peaks for P-ATP and DMAB on silver substrates.[87]

Molecule	SERS peak / cm^{-1}	Relative intensity	Peak assignment
P-ATP	390	w	ν(C-S)+ δ_{ip}(C-C)$_{Ar}$
DMAB	**486**	**w**	**ν(C-S)**
P-ATP	542	vw	δ_{ip}(C-C)$_{Ar}$+ ν(C-S)+ δ_{ip}(C-H)$_{Ar}$
DMAB	**714**	**w**	**γ(C-C)$_{Ar}$**
P-ATP	920	vw	$\delta_{ip,as}$ (C-C)$_{Ar}$
P-ATP	1005	w	γ_{as}(C-H)
P-ATP	1080	m-s	δ_{ip}(C-H)$_{Ar}$
DMAB	**1141**	**vs**	**$\delta_{ip,as}$(c-h)(ortho)[b]**
P-ATP	1192	m	δ_{ip}(C-H)
P-ATP	1308	m	ν(N-N)+ $\delta_{ip,s}$(C-H)
DMAB	**1390**	**m-s**	**ν_{as}(C-C)$_{Ar}$+$\delta_{ip,as}$(C-H)$_{Ar}$ + ν(N-N)**
DMAB	**1434**	**s**	**$\delta_{ip,s}$(C-H)+ ν(N-N)**
P-ATP	1490	w	δ_{ip}(C-C)$_{Ar}$+ $\delta_{ip,s}$(C-H) + ν(C-N)
P-ATP	1590	m-s	ν(C=C)$_{Ar}$

[a]*ν*, stretching; δ, in plane bending; γ out of plane bending; s, symmetrical; as, asymmetrical; ip, in-plane; Ar, aromatic ring; intensity: vs, very strong; s, strong; m, medium; w, weak; vw, very weak.[87]

After returning to open circuit potential from -1.0 V (anodic direction), the signal peaks due to DMAB not only return but become more intense as shown in Figure 5.3. This enhancement of signal is largely due to the electrochemical oxidation of p-ATP to DMAB at the Ag electrode surface, which would be expected. However, the fact that peaks due to the oxidation product were already present at OCP (cathodic), prior to the application of any voltage is further proof that plasmon-assisted catalysis does in fact occur.

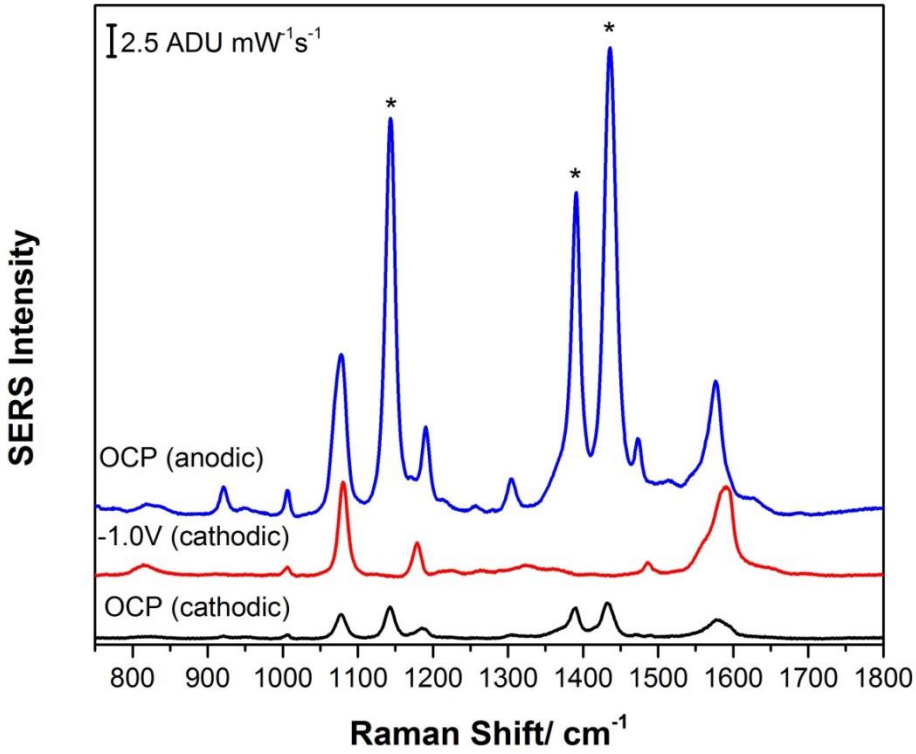

Figure 5.3: EC-SERS of p-ATP on citrate reduced AgNPs in 0.1 M NaF. Peaks marked by an asterisk belong to the DMAB. A 532 nm laser was used, 3 mW, 30 s acquisition.

The point of pursuing sustainable plasmonic architectures is not just to show that they are possible, but to ensure that these new platforms can function as well as or better than the standard plasmonic substrates. One of the preliminary checks for whether or not colloidal AgNPs are actually formed for a particular synthetic route or not is through

observation of the extinction spectra. If a peak is spotted at ~ 450 nm (±100 nm), it is generally a good indication that AgNPs are present. Figure 5.4 shows the extinction spectra for two of the commonly used methods to make AgNPs: the Lee-Meisel method using citrate and the Zhao method which uses $NaBH_4$. It can be noted that the extinction peak for the $NaBH_4$-reduced Ag is narrower (lower FWHM) and is blue-shifted relative to the citrate-reduced AgNPs. The decreased peak broadness reflects a narrower size distribution of the $NaBH_4$-reduced AgNPs, which can be corroborated from the SEM images shown in Figure 5.5. Additionally, the peak associated with the $NaBH_4$ method is centered at a lower wavelength (blue-shifted) since the average size of these nanoparticles (~46 nm) is smaller than for the citrate reduced AgNPs (~95 nm).[88]

A central goal of the first part of this thesis work was to evaluate green synthesised AgNPs using similar methods and to test the resultant plasmonic performance, and make comparisions to these standard AgNPs.

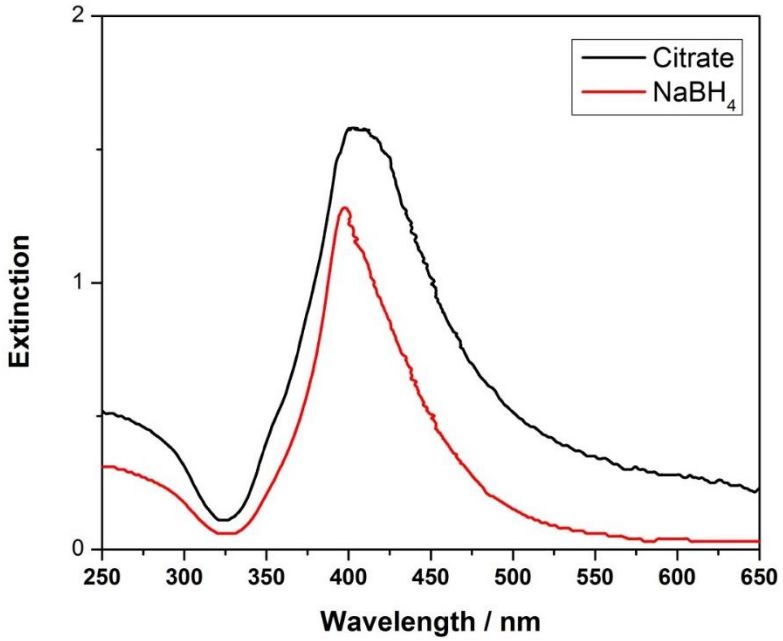

Figure 5.4: Extinction profile of citrate and sodium borohydride reduced AgNPs suspended in water.

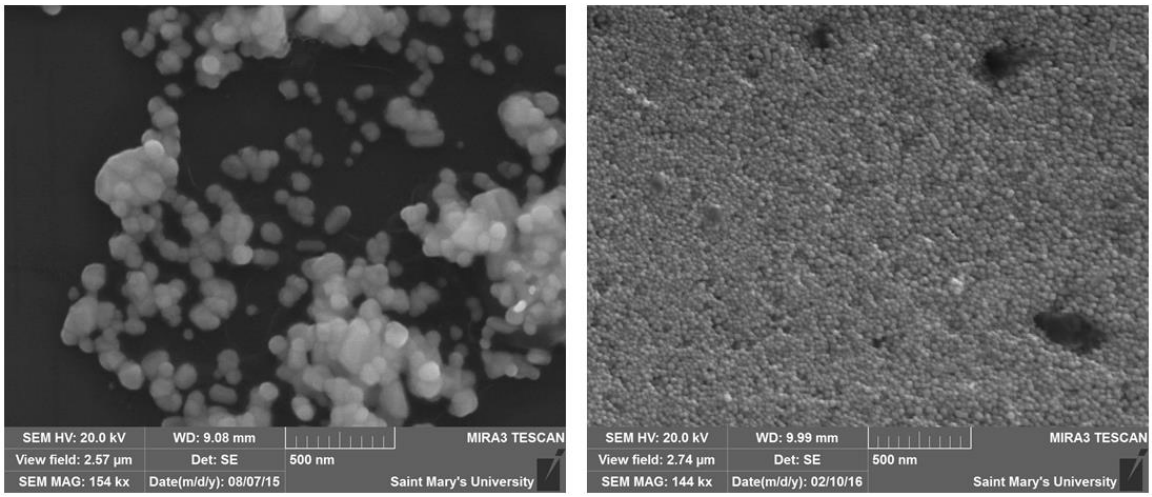

Figure 5.5 SEM image of citrate-reduced AgNPs (left) and $NaBH_4$-reduced AgNPs (right)

5.1 Sustainable SERS Substrates: Green Synthesis of Silver Nanoparticles

5.1.1 AgNPs Synthesized using Methanolic Berry Extracts

In order to replace the standard reducing agents used in silver nanoparticle synthesis with greener substitutes, one avenue that has been explored has been plant and fruit extracts that are rich in antioxidants. Antioxidants, as highlighted earlier in the literature review, are molecules that are easily oxidized (thus protecting important biomolecules from harmful oxidation) and therefore are good reducing agents. Simply put, these antioxidant species can take on the role of reducing agent in the synthesis of metal nanoparticles, rendering the process greener. In this section, several different berry extracts were explored, all with reported high levels of antioxidants.

Early on with the green synthetic strategies it was noted that a few drops of NaOH (0.1 M) was required before a UV-vis extinction profile indicating the presence of colloidal Ag could be noted through the appearance of a broad peak centered around 400 nm and a corresponding yellow-orange colour. pH adjustment is commonly utilized in AgNP syntheses in order to improve the kinetics of the reaction[68, 89]

5.1.1.1 Strawberry (*Fragaria x ananassa*) Extract (SBE)

Strawberries are rich in anthocyanin antioxidants, which are also responsible for their bright red colour.[90-92] The fact that strawberry extract components are rich in antioxidants composed of conjugated ring systems make it an interesting candidate for silver ion reduction, hence it was the first berry extract evaluated.[93] The strawberry extract was prepared using methanol as the solvent following the procedure outlined previously. When added to the 0.1M $AgNO_3$ solution, the reaction mixture went from colourless to a reddish-pinkish, due to the red colour of the strawberry extract itself. At

that point the extinction spectra for the solution remained weak in the region that would indicate the formation of AgNPs. Only after addition of a few drops of 0.1 M NaOH was a peak due to AgNP formation noted. This result is shown in Figure 5.6. Here it is evident that the addition of base had a significant influence on the formation of the NPs. With 10 drops of 0.1M NaOH there is a very shallow peak that shows up immediately; after 24 hours there is an increase in the signal intensity which is reflective of a greater amount of AgNPs. With the addition of 30 drops of base this effect is even more dramatic. The SEM images of the strawberry extract AgNPs were unfortunately poor because of the thick biogenic nanoparticle corona that capped the nanoparticles.[31]

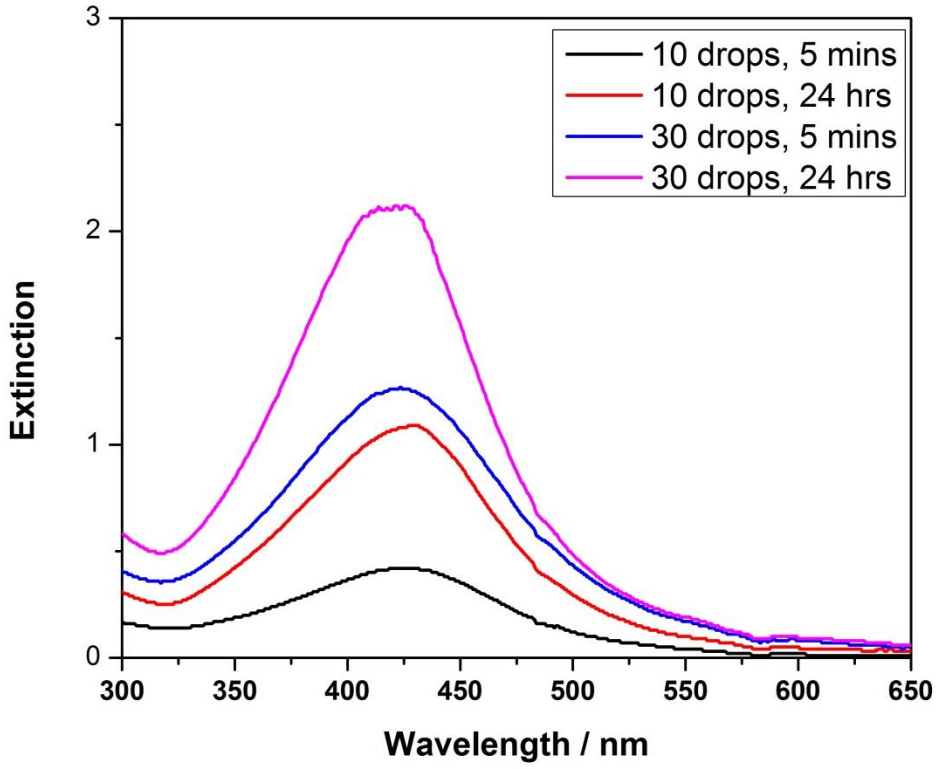

Figure 5.6: Extinction profile of strawberry extract reduced AgNPs with varying amounts of 0.1 M NaOH. For each trial addition of base a spectrum was taken immediately (within 5 minutes) and 24 hours later.(1 drop ~ 25 µl)

The strawberry extract (SBE) synthesised AgNPs were used for SERS of *para* aminothiophenol (p-ATP). As outlined above, this probe molecule will not only tell one whether the green synthesized colloidal silver was SERS active but also allows one to evaluate the extent to which plasmon-assisted catalysis is possible for these particular AgNPs. Figure 5.7 displays the SERS spectra from a traditional citrate reduced SERS substrate and one made using AgNPs produced using the SBE obtained with a 785 nm laser at a power of 22.3 mW for 30 seconds. There are two things worth mentioning at this point. Firstly, the citrate used to reduce and cap the nanoparticles in the Lee-Mesiel colloidal Ag appears to have a greater spectral interference than the capping agents (biogenic corona) on the SBE reduced-AgNPs. Secondly, this surface layer of capping agent can have repercussions on the catalytic properties of the metal nanoparticle since it will increase the distance between the reactant and the source of hot electrons / holes provided by the metal.[74, 87] The SERS signal for the citrate reduced AgNP shows several peaks representing a partial finger print of the citrate molecule namely: 1401 cm^{-1} v_{as} (COO), 1033cm^{-1} v_s(C-O), 940 cm^{-1} v_s (C-C), 842 and 808 cm^{-1} v_s (CCCC-O). [94]

The broad citrate peak at 1401 cm^{-1} overlaps with the 1390 and 1434 cm^{-1} peaks of the catalytic product (DMAB). It is apparent from Table 5.1 that there are three strong peaks that can be used to identify DMAB. If one takes a closer look at Figure 5.7 it is evident that the 1144 cm^{-1} DMAB peak is present on the SBE AgNP SERS substrate. It can be argued that this peak is very weak and not conclusive of the presence of DMAB. Hence, p-ATP peaks were used to judge the overall plasmonic sensitivity of the SBE synthesized AgNPs. When compared to the citrate reduced-AgNPs, the p-ATP signal was more intense for the SERS spectra obtained from the SBE AgNPs. Figure 5.7 clearly

shows that SBE AgNPs are viable for SERS and could be considered a good sustainable SERS substrate.

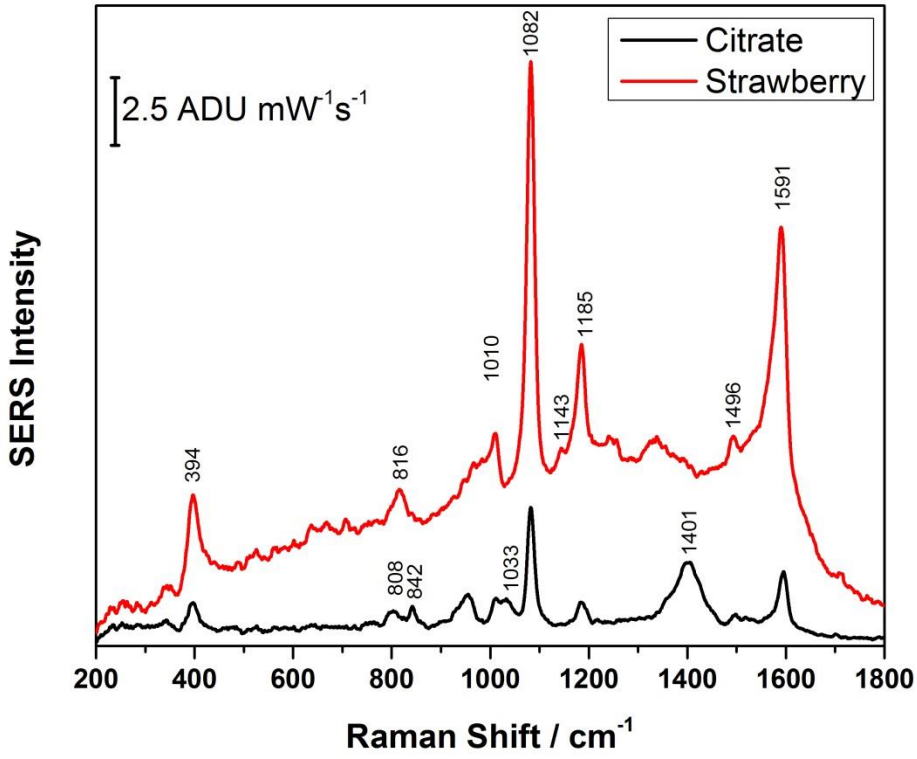

Figure 5.7: SERS of 1mM p-ATP on AgNP made from citrate reduction in black and strawberry extract in red. 785nm laser line used. (30 s, 22.2 mW)

5.1.1.2 Haskap Berry (*Lonicera caerulea*) Juice (HBJ)

The haskap berry has been reported to be one of the most impressive fruits grown in Canada with respect to its antioxidant content; even the very antioxidant-rich blueberry pales in comparison to the haskap berry in terms of antioxidant potency.[95] To evaluate haskap berry juice (HBJ) as a potential green method for producing AgNPs the same procedure was followed as for the strawberry extract. However in the case of the haskap

berries its availability was severely limited due to high demand and so the more readily available haskap juice was initially used. Figure 5.8 compares the SERS spectra for a monolayer of p-ATP on the AgNP surface, when the AgNPs were prepared using the haskap berry extract, as well as blueberry extract for comparison. The haskap berry extract was slightly better in terms of the plasmonic performance of the AgNPs, however some measurable background was observed. Similar to the citrate reduced AgNPs both the blueberry and haskap juice AgNPs did not appear to support any significant catalysis of p-ATP to DMAB.

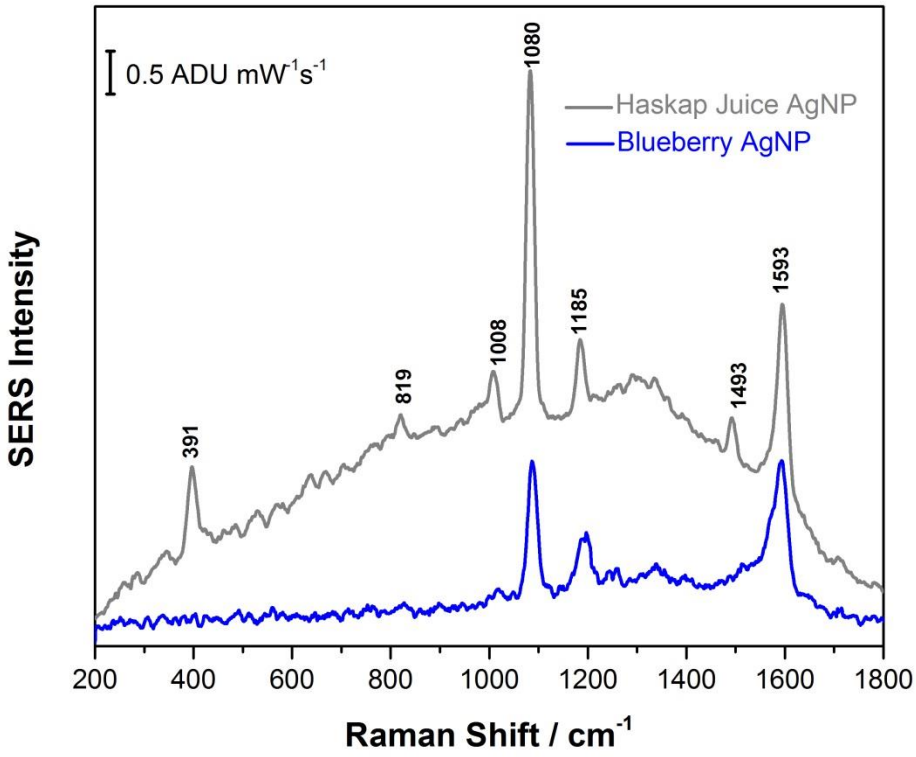

Figure 5.8: SERS of 1 mM p-ATP for blueberry extract AgNP and haskap juice AgNPs. 785nm laser line used. (30 s, 22.2 mW)

While examining whether the greater antioxidant content of the haskap berry makes it a better reducing/capping agent than other berries, one has to note that the haskap juice was a commercial product, which had added cane sugar to make the juice more palatable. Since the sugar can also act as a mild reducing agent, the next logical thing to do was to assess the contribution of brown cane sugar to the synthesis of the nanoparticles. Extinction spectra were obtained for both syntheses are shown in Figure 5.9. The haskap berry AgNPs appear to be less plentiful and less monodisperse than the cane sugar AgNPs.

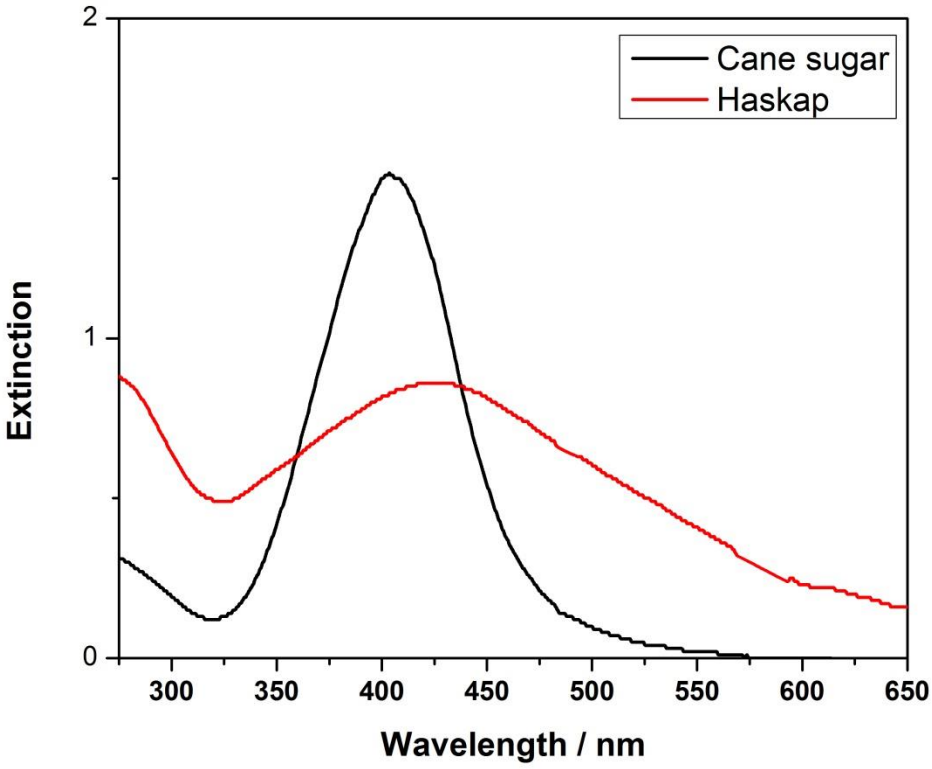

Figure 5.9: UV-vis extinction profile for haskap juice AgNP and cane sugar AgNPs.

Despite the lower FWHM and greater intensity extinction profile of the cane sugar, the SERS for the cane sugar reduced AgNP substrates were significantly weaker in intensity than the haskap juice AgNPs noted in Figure 5.10. Furthermore, the cane sugar AgNPs yielded no catalytic DMAB peaks. From a green chemistry perspective less is more, so if one of the components of the haskap juice can make more SERS-active AgNPs than the complete cocktail then it would be a greener strategy to use that component. However, the performance of the more monodispersed cane sugar AgNPs did not translate into improved SERS performance compared to that of the haskap juice AgNPs. From these observations, it can be noted that sugar is a contributing factor in many of the green extracts but performs better in a cocktail that includes antioxidants. The reduced SERS signal of cane sugar could be a consequence of the multiple hydroxyl groups in the cane sugar that participate in Ag^{+} reduction that are retained as capping agents.[5] Although the sugar molecules can be easily removed as noted in the literature review with hot water, this step was not pursued given that thiols (i.e. p-ATP) have very strong affinities for Ag and would normally displace the more weakly bound sugar molecules.[87] Later on pure haskap berries were obtained and it was found that those silver substrates were less SERS active than the AgNPs produced by the HBJ. The berry extracts were altogether discontinued as sustainable strategies for producing AgNPs as they were all known food sources.

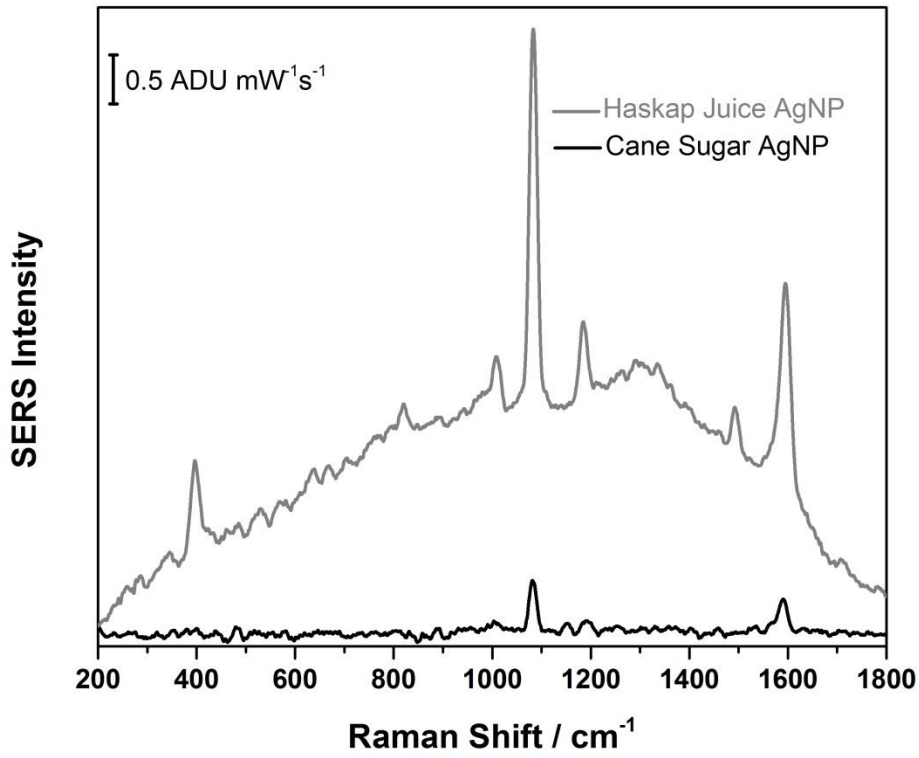

Figure 5.10: SERS of 1 mM p-ATP on Haskap juice AgNP and brown sugar AgNPs. 785nm laser line used. (30 s, 22.2 mW)

The two dark berries (blueberry and haskap berry) show promise for production of SERS active AgNP substrates. However, only the haskap juice AgNPs demonstrated better performance than the standard citrate-reduced AgNPs. Thus, it could be stated that haskap berry juice offers a greener pathway for the production of silver nanoparticles that results in a better performing product than the non-green approach. One issue however, is that berries are a food resource, and hence their use in this synthetic strategy competes directly with a food item, and is therefore not particularly sustainable. The rest of this section will therefore explore extracts derived from natural materials which are generally considered to be waste products, such as fruit peels, pits and weeds.

5.1.2 Fruit peel extract AgNPs

Orange (*Citrus sinensis*) and banana (*Musa*) peels both represent food waste materials, and as such both were evaluated in this thesis work for the synthesis of colloidal silver. For both fruit peels, the extracts were first prepared using the procedure outlined previously. It should be noted that while all the other green synthetic strategies presented so far required heat to produce NPs in a timely fashion, the banana peel extract (BPE) was complete within 2 hours, at ambient temperature. This added advantage makes the process greener since less energy is utilized during the reaction. It has been shown in the literature that BPE can be used to make AgNPs but these are often only used for antimicrobial purposes.[96, 97] Additionally, the banana peel extracts in the literature have mostly employed heating to obtain the extracts and in some cases heat is applied again during AgNP formation.[96, 97] Figure 5.11 shows the extinction profile for the BPE AgNP obtained from a two hour reaction at room temperature. In this case, polymeric components including lignin, cellulose, hemicelluloses, and pectins that make up the banana peels are believed to reduce and cap the AgNPs.[96]

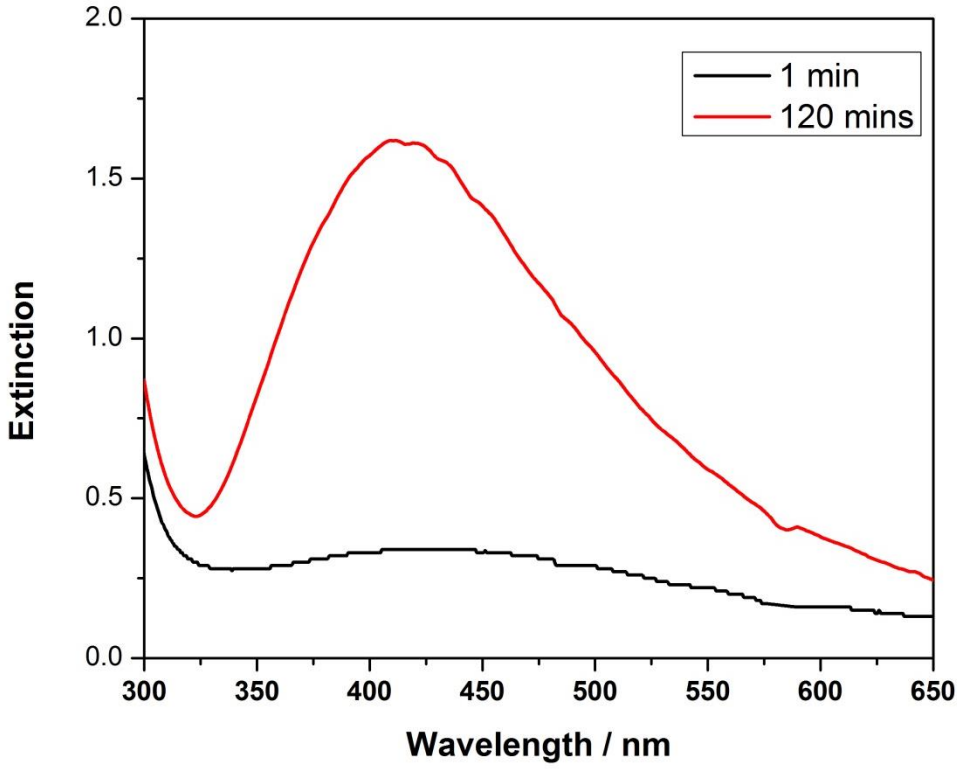

Figure 5.11: Extinction spectra of BPE AgNP with no heat immediately after the addition of NaOH (black) and 2 hours later (red).

Just like the berry NPs, the BPE AgNP extinction peak after 2 hours is broader than the absoption profiles of the standard AgNPs shown in Figure 5.4, hence the BPE AgNPs had a greater size distribution. Fortunately, the biogenic corona associated with the BPE AgNPs was not too thick and SEM images of the AgNPs could be obtained. The SEM and histogram of the size distribution of 100 NPs are shown in Figure 5.12. The mean AgNP diameter was 59 nm with a standard deviation of 28 nm. This large standard deviation is consistant with the large FWHM shown in Figure 5.11.

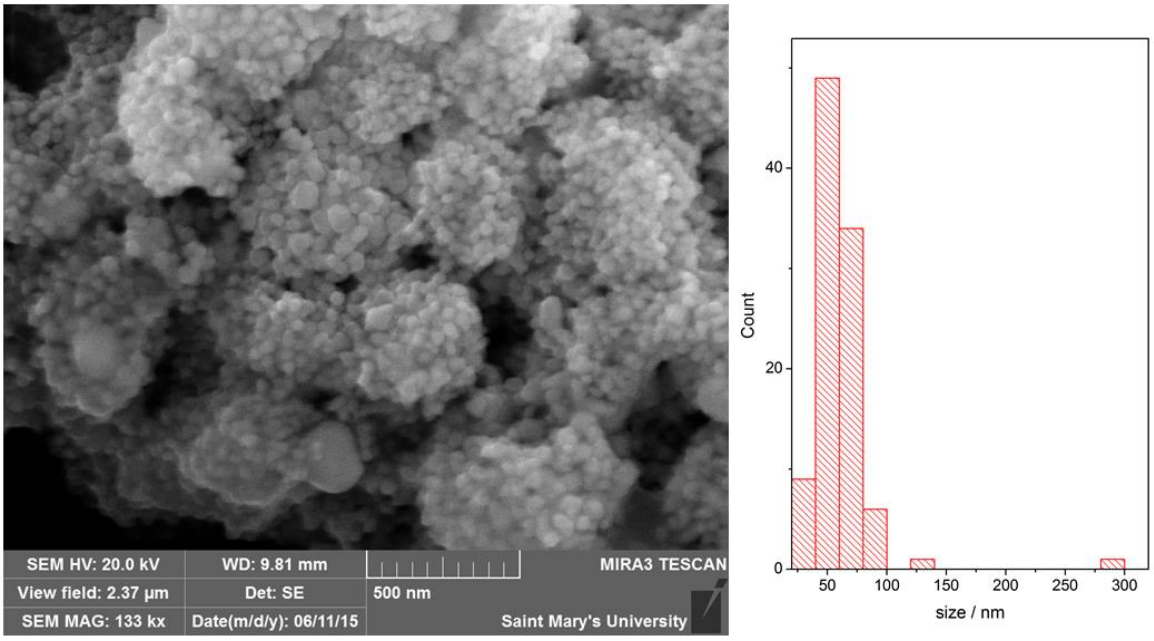

Figure 5.12: SEM image of BPE AgNPs on the left, and histogam of size distribution for 100 NPs on right. (Image J software, NIH)

The other peel extract used to synthesise colloidal silver was the orange peel extract (OPE). It displayed a similar extinction profile to the BPE AgNPs but to achieve this it required heating near the boiling point for the full 30 minutes as outlined in the experimental section. The OPE AgNPs could not be imaged *via* SEM because of the thick biogenic corona. Figure 5.13 shows the SERS spectra of 1mM p-ATP recorded on both the BPE and OPE AgNPs SERS substrates, for comparison. The spectra obtained were similar in vibrational fingerprint as well as intensity. The catalytic peaks for DMAB could be identified in the SERS spectra obtained on both the BPE and OPE synthesized AgNPs.

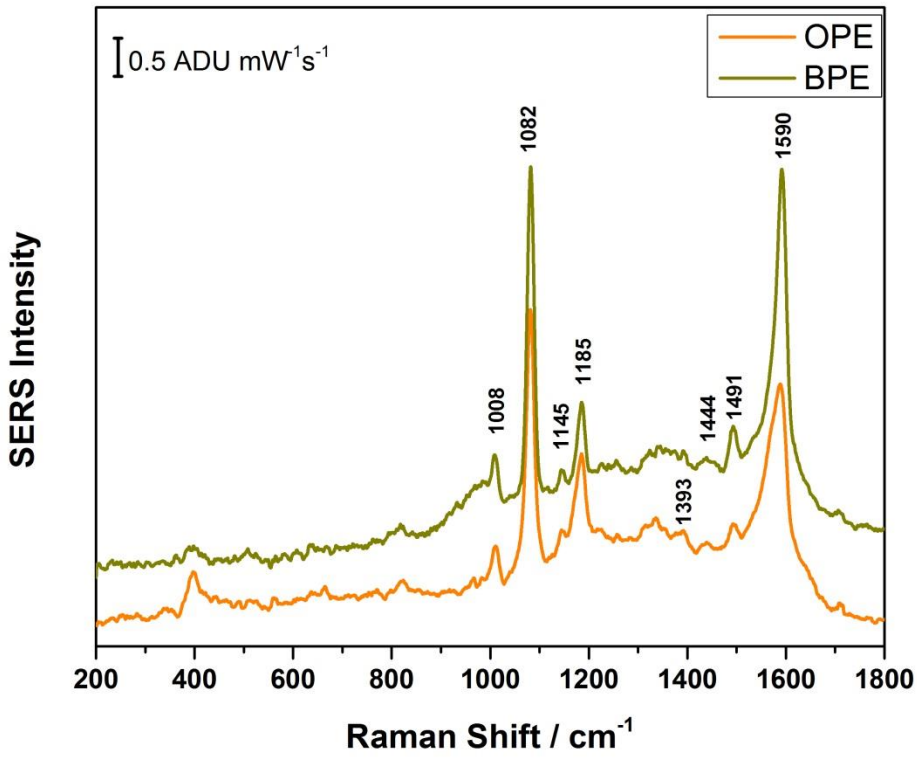

Figure 5.13: SERS of 1 mM p-ATP on orange peel extract (OPE) AgNP and banana peel extract (BPE) AgNPs. 785nm laser line used (30 s, 22.3 mW).

5.1.3 Dandelion flower extract AgNPs

Dandelion flowers (*Taraxacum officinale*) have been reported to be a potent source of antioxidants, and are frequently used for healthcare teas and tincures. As a weed and general nuisance plant in Canada, it was natural to select dandelion flowers for study as part of this thesis work. Dandelion flowers were collected, washed, and dried, and the dandelion flower extract (DFE) was then prepared in methanol and used and used as the reductant for AgNP synthesis. The extinction profile for these AgNPs (not shown) was broader than that of the citrate NPs but the SEM images (Figure 5.14) indicated that the AgNPs were more monodisperse, with a mean size of 21 nm, and standard deviation of 6

nm; in fact, the DFE AgNP were much more uniform than the standard citrate reduced nanoparticles. The contradicting results of the extinction profile for the citrate vs DFE reduced AgNPs and their corresponding SEM images can be the case as the SEM preparation uses pre-concentrated AgNPs. During centrifugation, there is a partial size separation due to varying sedimentation rates of AgNPs while the UV-vis extinction profile is an ensemble average of all the AgNPs in the path of the light source prior to any separation. In addition, a biogenic corona was not easily visualized on the surface of the nanoparticles.

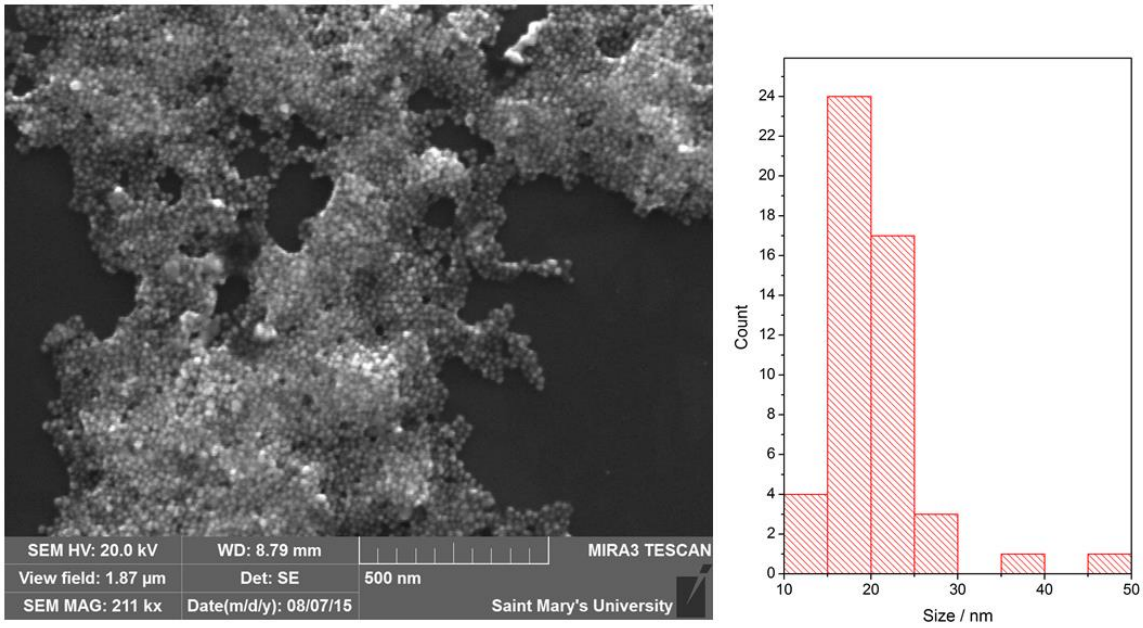

Figure 5.14: SEM of dandelion flower extract (DFE) AgNPs on the left and the histogram of size distribution on the right for 50 NPs.

The SERS response for 1 mM p-ATP for the green substrates as well as the standard citrate AgNPs can be found in Figure 5.15. Immediately upon inspection of Figure 5.15 it can be observed that the signal is far more intense for the DFE AgNPs than for the rest of the AgNPs evaluated thus far. One can also appreciate that the DFE AgNPs SERS response for p-ATP has more associated background signal than the other

AgNPs. This is believed to be due to an intrinsic florescence emanating from the DFE organic material capping the AgNPs.[5,70] In addition, the DFE AgNPs were the only nanoparticles to show efficient catalytic conversion of p-ATP to DMAB, as noted by the peaks labelled with an asterisk in Figure 5.15.

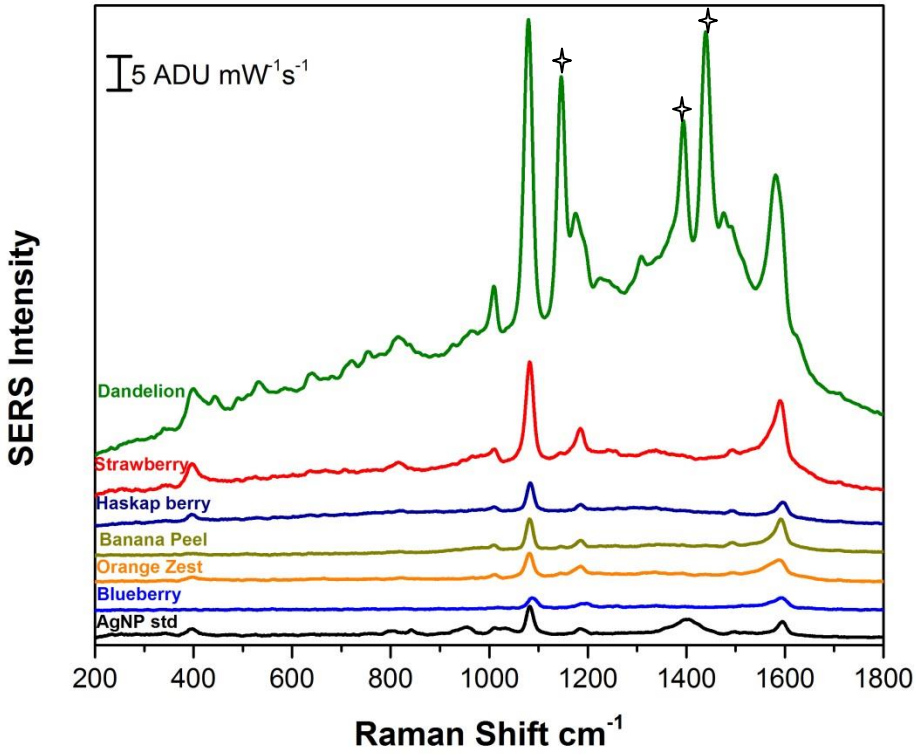

Figure 5.15 : SERS of 1 mM p'ATP for all extract synthesized AgNPs including the standard citrate reduced AgNPs. DMAB peaks are noted by a star. 785nm laser was used. (30 s, 22.2 mW)

Sulfur can adsorb very strongly to silver and can in the process displace any organic capping agent.[96] While this property is beneficial to obtaining a SERS response for thiolated probe molecules this can also render the SERS substrate not useful for sensing anything that is not a thiol. With this in mind, 4,4'-bipyridine was also evaluated

as a probe molecule for all the green SERS substrates presented thus far. Only the DFE AgNP were able to provide a SERS finger print for 4,4'-bipyridine, and even this signal was difficult to obtain. Since DFE AgNPs were decent for non-sulfur terminated molecules like 4,4'-bipridine, these substrates were further used to explore electrochemical-SERS (EC-SERS). A SERS response was measured at each applied potential. The peak assignments are listed in Table 5.2 for 4,4'-bipyridine. All the peaks associated with 4,4'-bipyridine can be noted in the blue spectrum collected at -1.0 V. The OCP spectrum represents the SERS spectrum obtainable in the absence of an externally applied electrical potential. The potential of zero charge (PZC) for Ag(poly) is at -0.95 V vs Ag/AgCl, and so at OCP (-0.1 V) and -0.5 V in Figure 5.16 the surface charge of the Ag substrates is positive in both cases.[98,88] As the potential changes the relative intensities of the SERS peaks was observed to change. This shows that DFE AgNPs can have improved SERS performance with an applied potential, which makes it the most successful green synthetic strategy from extract obtained in methanol thus far.

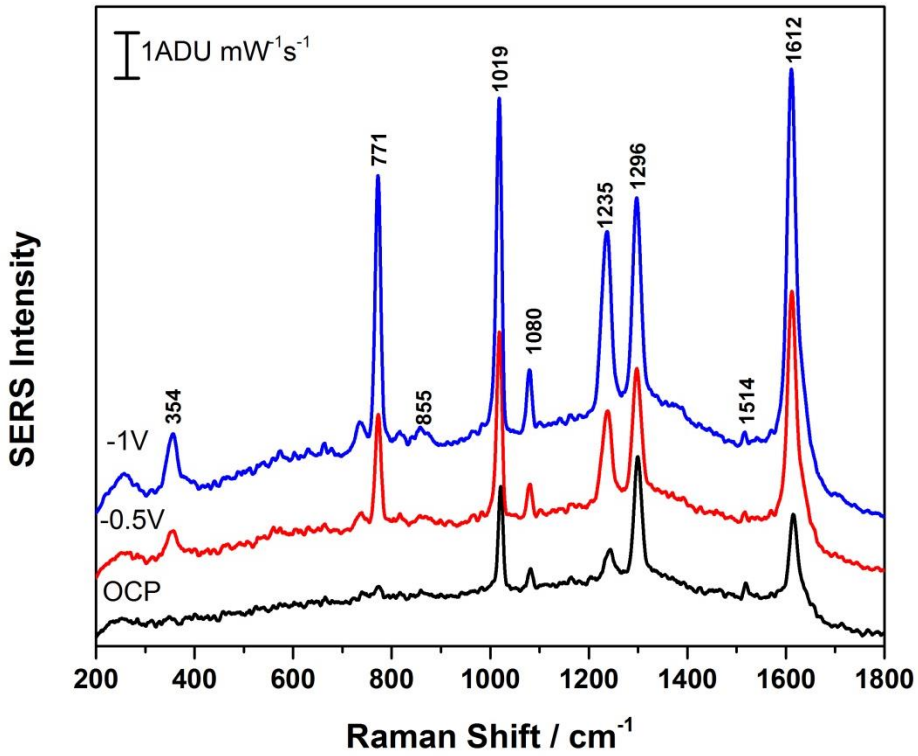

Figure 5.16: EC-SERS of 1 mM 4,4'-bipridine in 0.1 M NaF on a DFE AgNP modified SPE. 785 nm laser was used (30 s, 22.3 mW).

Table 5.2: SERS Band assignments for 4,4'-bipyridine.[88]

SERS peak / cm^{-1}	Band Assignment
852	CH o.p. bending
1022	Ring breathing
1229	CH i.p. bending
1293	Inter-ring stretching
1511	CH i.p. bending +ring stretching
1610	Ring stretching

5.1.4 Plant Extracts Prepared in Water

It has so far been demonstrated that the plant / fruit extracts explored in this thesis work are capable of generating SERS-active silver substrates. Most of the published work in this area has focused on a simple proof-of-concept study that a particular extract can indeed produce AgNPs with a certain size distribution and in some cases the study might go a step further and demonstrate their antimicrobial activity.[4] Most of the extracts are obtained *via* the use of alcohol pulverisation followed by gravity filtration or a more energy intensive microwave extraction.[99, 100] Whatever the process, the vast majority of these publications utilize methanol or ethanol as the solvent, which is not as green as water. Hence, in this work the use of water as an alternate solvent for the production of the plant extracts was evaluated. From this point forward only extracts obtained from non-food sources were used.

There is very little difference in the SERS activity between AgNP substrates made from DFE extract obtained using methanol as the solvent compared to that obtained using water (Figure 5.17). All the peaks from DMAB are still clearly visible, therefore the efficacy with regards to the plasmon-assisted catalysis is protected. Upon closer examination it can be appreciated that the catalytic peaks are more intense in the black spectrum belonging to the substrates made from DFE in water. Therefore, the use of alcohol is not necessary to extract the useful reducing and capping agents from the dandelion flower. In fact, methanol may extract compounds not directly used in the synthesis, which may attenuate the SERS response due to the formation of the biogenic corona from components present in the methanol extract.

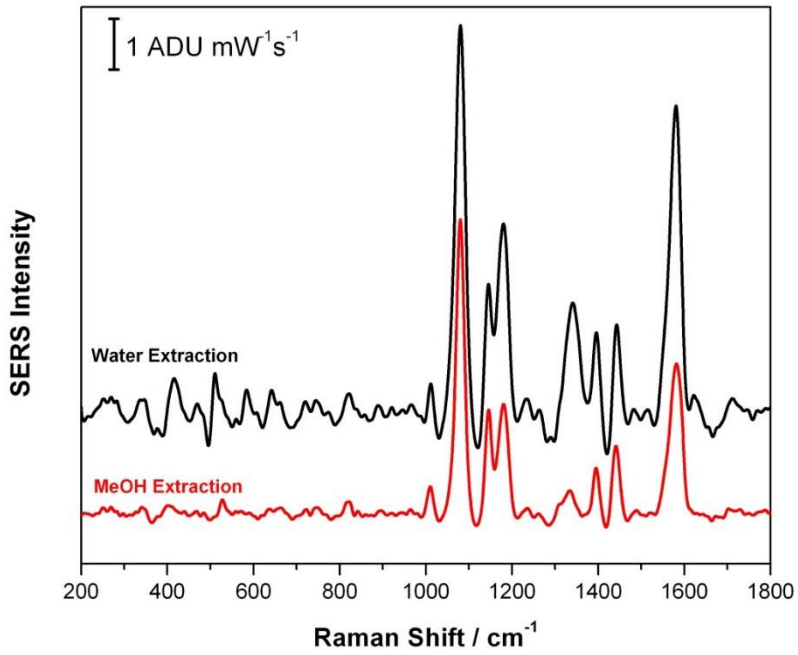

Figure 5.17: SERS of 1 mM p-ATP on AgNP made from DFE in methanol (red) and in water (black). Both spectra have been baseline corrected using the DeltaNu software. 785nm laser used (30 s, 22.3 mW).

Another issue to consider is that fruits at different stages of ripeness will contain different amounts of antioxidants and sugar.[101] Karikari and colleagues showed that green bananas have about 20% starch, but when fully ripened almost all of the starch is hydrolysed to sucrose, glucose, and fructose.[102] These changes affect the colour of the edible part of the banana. While the peel is green, the flesh is white due to the high starch content and has great adhesion to the peel, but this adhesion is lost due to solubilisation of the pectic substances that follows the hydrolysis of starch.[101] The rich colour of the banana peel is due to the presence of a branch of antioxidants referred to as carotenoids, in particular xanthophyll lutein.[104] While the exact percentage of antioxidants in the banana peel has not been followed from green to ripened banana, it has been noted that a

greater amount of antioxidants exist in the ripened yellow peel.[104] Therefore, banana peels will likely demonstrate varying efficiencies in colloidal nanoparticle synthesis depending on what stage of ripeness they are at. Three banana peels at various stages of ripeness were investigated using water as the solvent to obtain the extract; those peels can be seen in Figure 5.18.

Figure 5.18: The peels of differing degree of ripeness for bananas, from most ripened (yellow) on the left to least ripened (green) on the right.

Figure 5.19 shows the relative SERS performance of the three banana peel extracts. It is clear that the AgNPs produced from the most ripened peel (BPE Y) least starch, richest antioxidant content) was the least SERS active, while the least ripened peel ((BPE G) highest starch and least antioxidant content) was the best suited for SERS. The quantities of reduced sugar in yellow peels do not seem to contribute as much as the starch content of greener peels to the overall colloidal synthesis. Clearly, banana ripeness is an important consideration for any future applications involving banana peel extracts for the facile synthesis of AgNPs. For sustainability considerations, green banana peels are less likely to be a readily available waste material as compared to ripened banana peels, due to the fact that green bananas are not generally eaten.

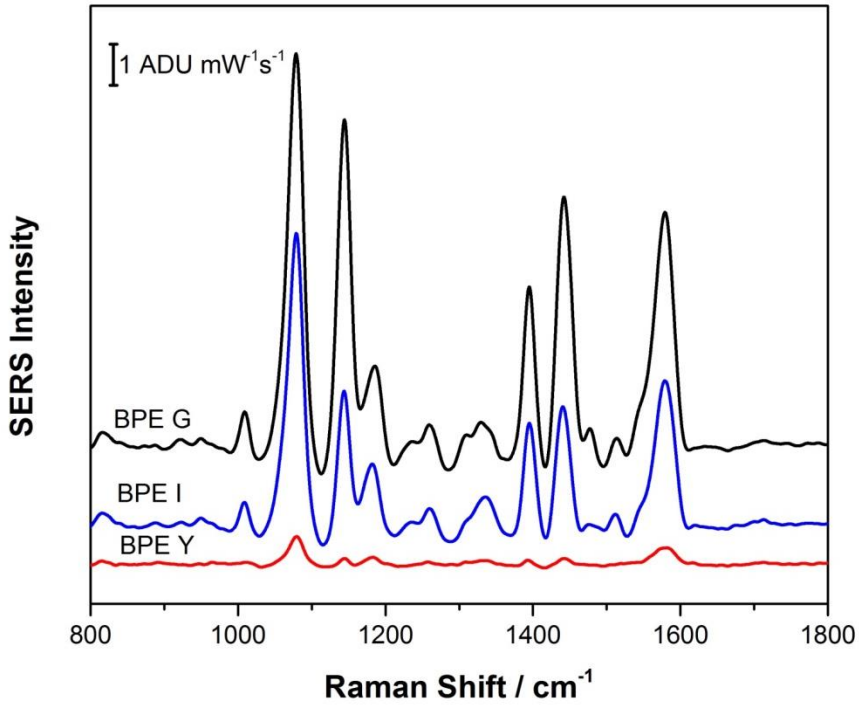

Figure 5.19: SERS of 1mM p-ATP on green (BPE G), intermediate (BPE I) and yellow (BPE Y) AgNPs. 785 nm laser was used. (30 s, 22.3 mW)

In terms of catalysis, the peaks identifying DMAB can be observed in all three spectra in Figure 5.19. There was no noteworthy spectral interference from the biogenic corona and all Ag SERS substrates regardless of the stage of ripened banana peel used clearly showed successful plasmon-assisted catalysis.

5.1.4.1 Avocado (*Persea Americana*) Pit Extract AgNPs

The final extract investigated in this thesis work was the avocado pit extract, referred to as APE in this work. The avocado pit is mostly regarded as a food waste product that is known for its antioxidant activity attributed to the presence of phenolic compounds.[105] The lack of a biogenic corona made the APE AgNPs relatively easy to image *via* SEM which can be seen in Figure 5.20. The mean nanoparticle size was 50 nm

with a standard deviation of 8 nm for a sample size of 50 nanoparticles. The SERS substrates produced from APE rivalled the best performing extract thus far (DFE); this is shown in Figure 5.21. It should be mentioned that APE, like the BPE could produce colloidal NPs in the absence of heating but to keep everything equivalent the plot in Figure 5.21 is an APE SERS substrate made under the influence of heating. Since it was easy to view the APE *via* the SEM it was thought that the lack of a thick capping agent or biogenic corona would make it easy to obtain SERS activity for 4,4'-bipyridine. Since it is usually difficult to get SERS for non-thiolated probe molecules, two APE AgNP substrates were made. One substrate was treated with KCl to displace whatever capping agent remained on the surface and the other was left untreated. It was expected that the KCl treated substrate would be more SERS active since there would be less distance between the probe molecule and the SERS substrate. This is indeed demonstrated in Figure 5.22.

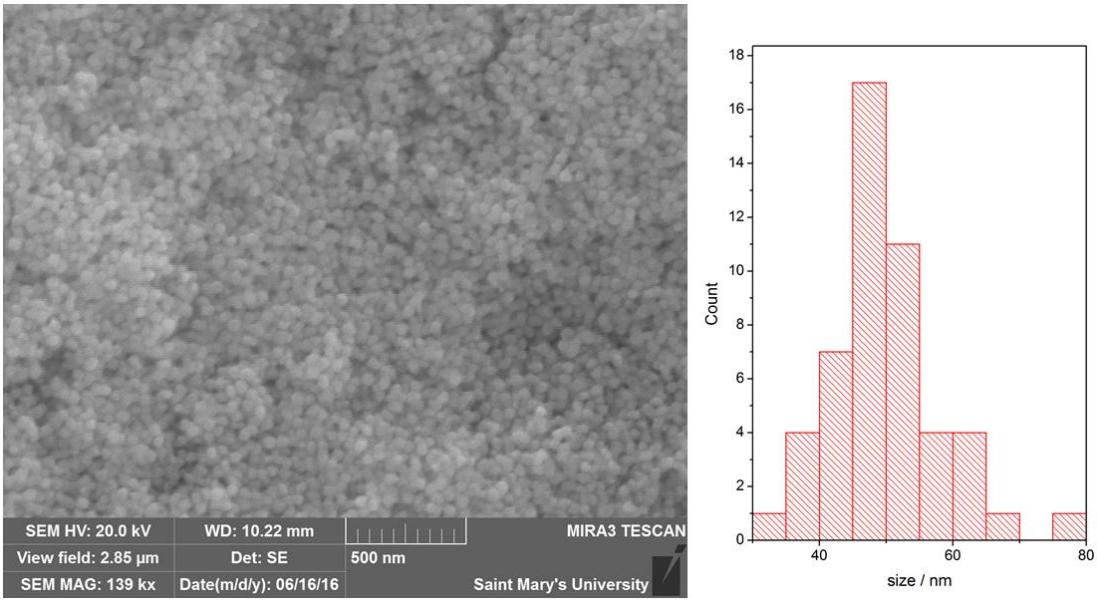

Figure 5.20: SEM of APE synthesised AgNPs on the left and size distribution on the right.

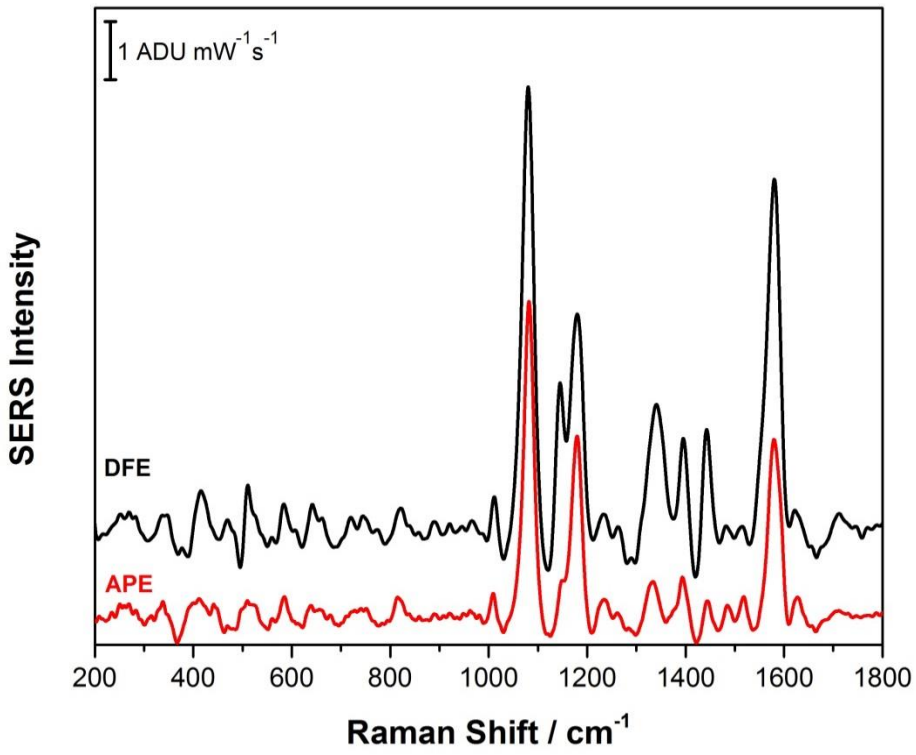

Figure 5.21: SERS of 1 mM p-ATP on DFE and APE AgNPs 785 nm laser was used. (30 s, 22.3 mW)

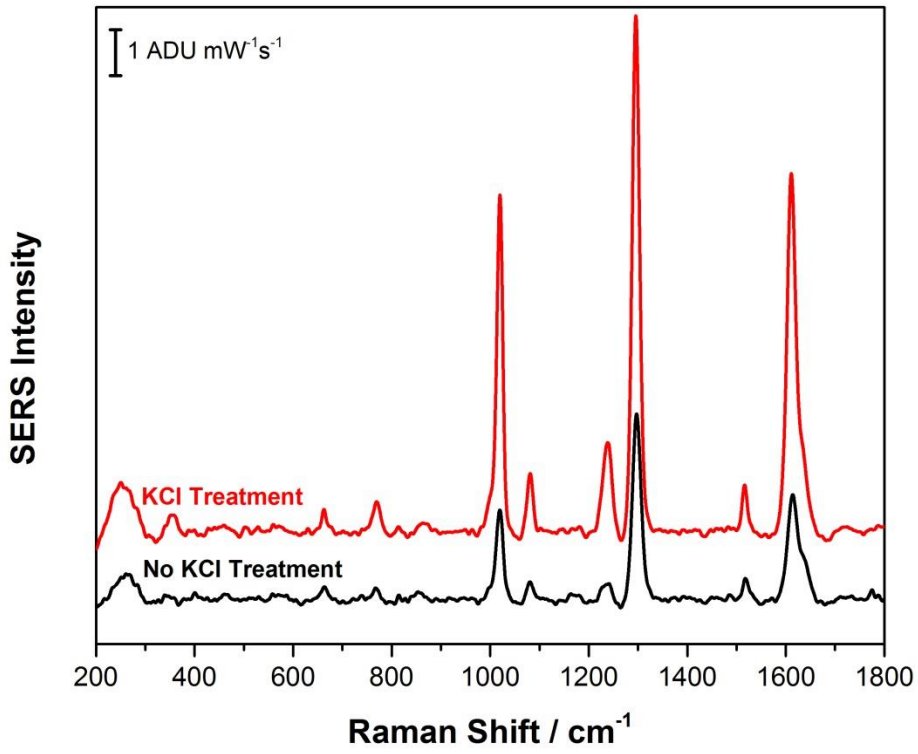

Figure 5.22: SERS of 1 mM 4,4'-bipyridine on APE AgNPs treated with KCl prior to adding the probe (red) and with no pre-treatment (black)

APE is the greenest of the extracts used to make AgNPs in this thesis because it could be obtained with an aqueous extraction and produced colloidal silver from Ag^+ in approximately 15 minutes in the absence of heating. In addition, the avocado pit is a very common food waste product that is not particularly suited for human nutrition due to the very high levels of antioxidants and vitamins.[106] APE AgNP substrates had very little biogenic corona, which made characterisation *via* electron microscopy straightforward which translated into no notable spectral interference. Removal of the capping layer through KCl treatment facilitated the collection of slightly more intense SERS spectra. Additionally, APE AgNP SERS substrates were the most uniform in morphology and

rendered the most spot to spot uniformity in SERS signal as seen in Figure 5.23. This low level of spot-to-spot variation was not observed for any of the other green synthetic strategies evaluated in this thesis work. Hence, the AgNP SERS substrate produced using the avocado pit extract shows the most promise from both the point of view of sustainability as well as performance as the more reproducible signal brings SERS one step closer to being a quantifiable tool that can be expolited for medical diagnositic testing.

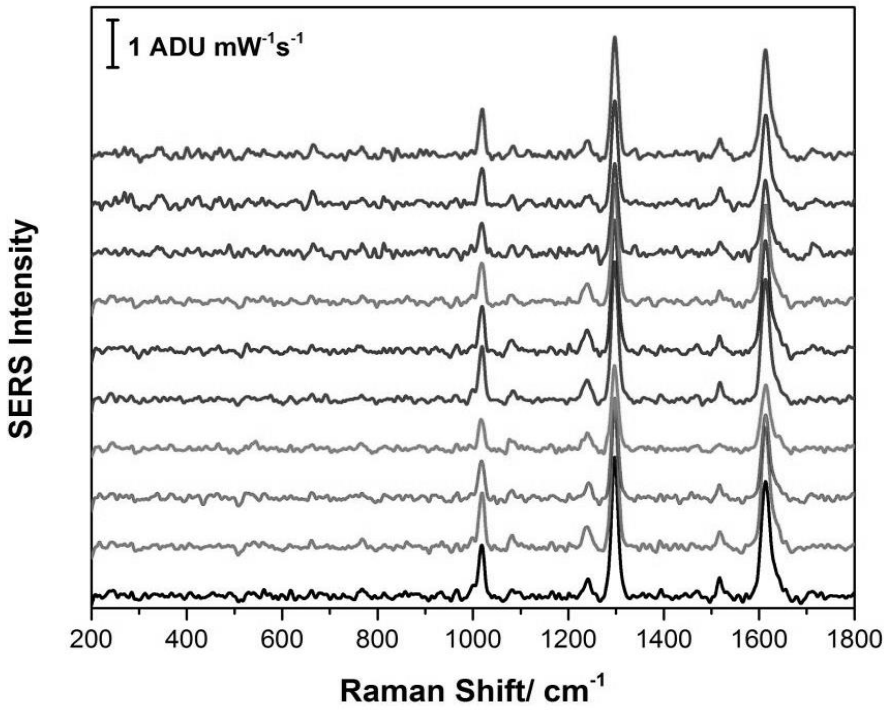

Figure 5.23: Ten spots on APE SERS substrate treated with 10 mM 4,4'-bipyridine. 785 nm laser, 30 s acquisition, 22.3 mW.

In summary, this part of the thesis research explored a variety of different plant and fruit extracts for the facile and green synthesis of silver nanoparticles. Important factors that needed to be considered were sustainability of the source and potential

competition with food resources, local availability, choice of extraction solvent and the generation of an interfering biogenic corona on the nanoparticle surface. Of all extracts evaluated, avocado pit extract showed the most promise.

5.2 Bioscaffolds

There is excellent consensus in the literature that multidimensional plasmonic nanostructures, which have order in two or three dimensions, have much better performance than stand-alone single dimension nanostructures such as non-ordered nanospheres.[34-38] This improved performance is due to the uniform arrangement of SERS active hot-spots that can exist for architectures that have long-range order at the nanoscale. A uniform arrangement of hot-spots leads to a much more uniform and robust SERS signal that is amenable to quantitative analysis, and thus useful for sensing platforms. Unfortunately, there are limited ways in which such multidimensional nanostructures can be created. Some methods exist to fabricate simple structures such as electron beam lithography, physical vapor deposition, or reactive ion etching, however these methods are energy intensive, expensive, and require highly purified materials such as gases and metals. In addition, these methods are far from scalable. Hence, there is a great need for new methods that can be used for the reliable, cost-effective, and sustainable fabrication of nanoscale materials.

This section will explore inexpensive and sustainable avenues to create three-dimensional SERS platforms based on natural biomaterials that exhibit nanoscale order. The first scaffold investigated was the micro/nano ordered pore system of the diatom. It was noted that to adhere the metal nanoparticles to the surface of this bioscaffold some

type of entrainment molecules like complementary DNA strands would have to be applied, one to the metal nanoparticle and the other to the surface of the diatom.[34] This would bind the metal nanoparticles to the surface of the scaffold creating a relatively inexpensive 3D SERS sensor.[35] The following investigations were geared at eliminating this extra step thereby making the process greener and utilizing those substrates to see if they facilitated an improved catalysis of p-ATP to DMAB.

5.2.1 Diatomaceous earth

As shown in the SEM images (Figure A.2.1), commercially available diatomaceous earth (Celite®) is composed of several different types of diatoms. The pore sizes varied from ~120 nm to ~680 nm. The first strategy to incorporate AgNPs on the diatom structure was to prepare them *in situ*; during the Lee-Miesel colloidal Ag synthesis the siliceous structures would be added directly to the reaction vessel. Two things were noted immediately through the SEM investigations: 1) the AgNPs produced with Celite® present in the reaction vessel had less of a surface capping layer, which made for better resolved SEM images of individual AgNPs as seen in Figures 5.24 C & D compared to AgNPs void of diatoms in their reaction vessel in Figures (5.24 A & B). The nanoparticles synthesized in the presence of the diatoms were also less aggregated.

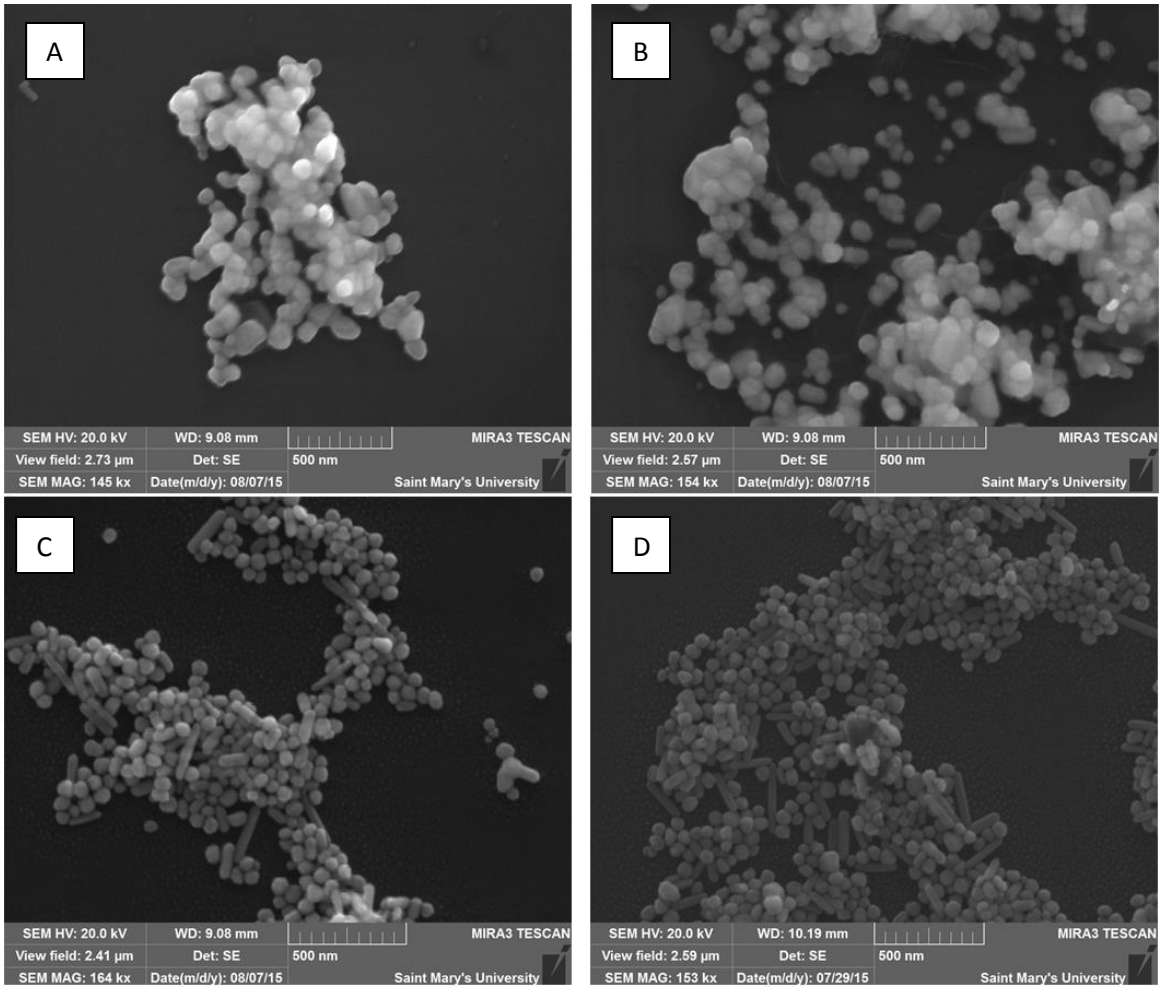

Figure 5.24 SEM image of citrate-reduced AgNPs (a) & (b), *In situ* diatom-citrate-reduced AgNPs (c) & (d).

2) the AgNPs were clearly capable of covering the diatom structure without the need of a pre-treatment with a coupling agent (e.g. complementary DNA strands). The AgNPs became more densely packed on the surface of the diatom once the colloidal sols were centrifuged as seen in Figure 5.25 B & D compared to prior to centrifugation (Figure 5.25. A & C).

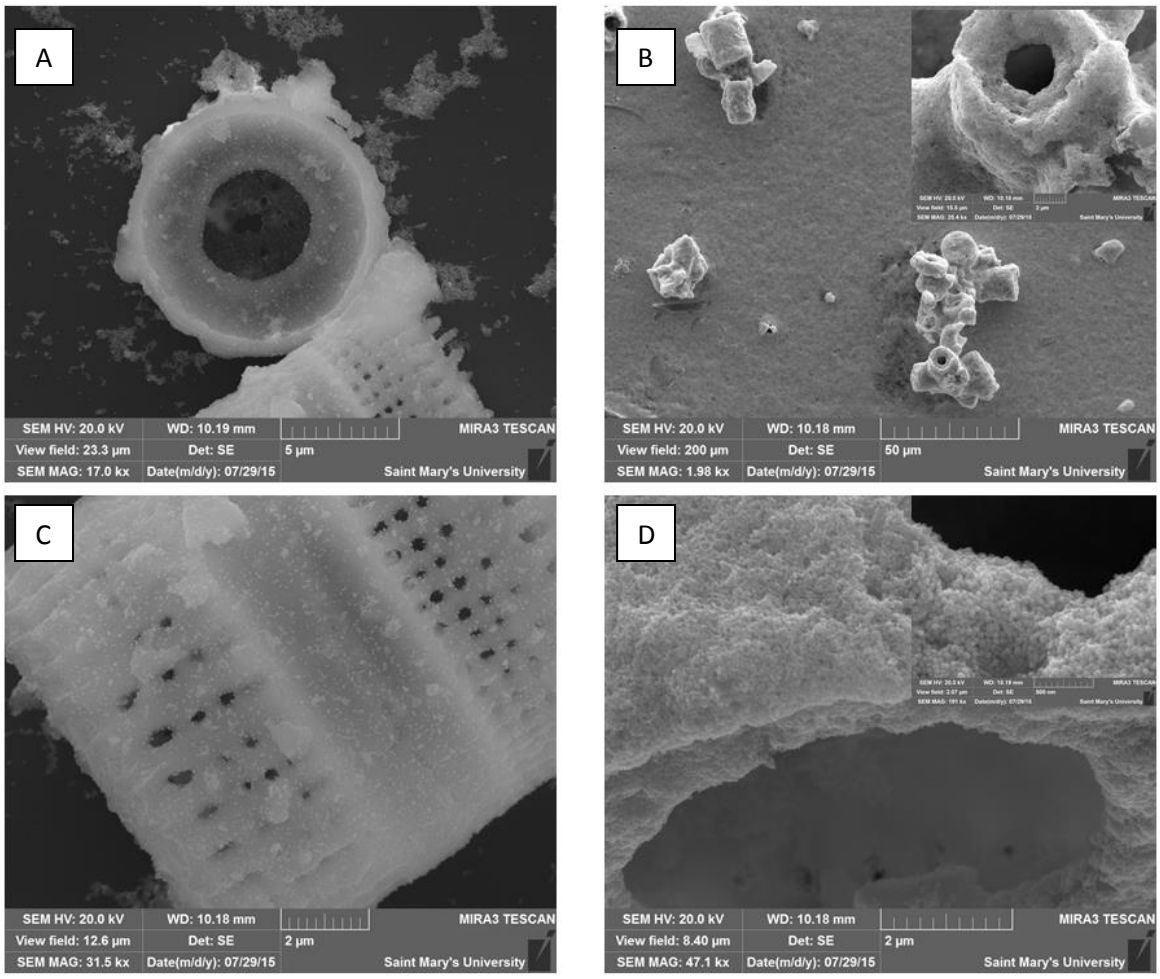

Figure 5.25: SEM images of diatom-AgNP 3D SERS substrate directly from the bulk colloidal mixture (A) & (C), and post centrifugation (B) & (D).

The benefits of these observations can be appreciated in the added SERS benefit. SERS spectra of p-ATP using the diatom-AgNPs were not only more intense than the AgNPs in the absence of the diatoms but the interfering citrate signal was also not observed. Additionally, it can be noted by the SERS spectra of 1 mM p-ATP in Figure 5.26 that the diatom-AgNP successfully demonstrated plasmon-assisted catalysis. This observation is highlighted by the stars above the catalytic DMAB peaks at 1390 cm^{-1} and 1434 cm^{-1} in the red spectrum in Figure 5.26. At the same time it is obvious that the same

catalytic response cannot be noted from the black spectrum obtained for the citrate reduced AgNPs in the absence of the diatoms.

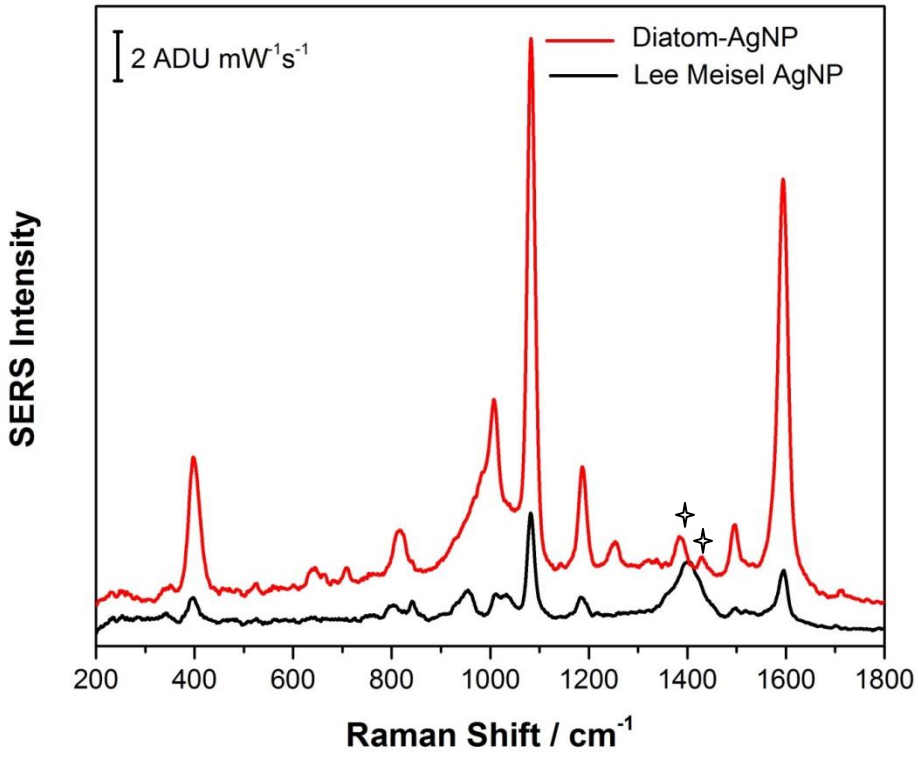

Figure 5.26: SERS of 1 mM p-ATP on citrated-reduced silver nanoparticles (black) and on diatom-AgNPs (red). 785 nm laser-line was used. (30 s, 22.3 mW (black) 10.6 mW (red))

For the citrate-reduced AgNP substrates to facilitate catalysis they would have to be pretreated with KCl to displace the citrate or conditioned using EC-SERS where the citrate could be removed electrochemically. The fact that such benefits are attainable with the inexpensive and readily available diatomaceous earth makes this synthesis inherently greener. In addition to the noted improvement in SERS intensity when on the scaffold, the fact that the citrate signal is not enhanced was suspicious. The catalytic peaks were a bit weak, that plus the well resolved SEM images (lack of a corona due to the citrate capping

agent) leads one to think that the surface of the diatomaceous earth (SiO_2), to some extent displaced the citrate capping agent. A full removal of citrate on the surface of diatom-AgNPs was not the case; this was confirmed by changing the probe molecule from p-ATP (thiol; strong adsorption to Ag) to 4,4'-bipyridine which would bind less strongly to the surface of the AgNPs. When this was done, the citrate spectral interference was noted in Figure 5.27 (citrate peak noted by asterisks), [107] hence citrate was indeed still on the surface diatom-AgNPs.

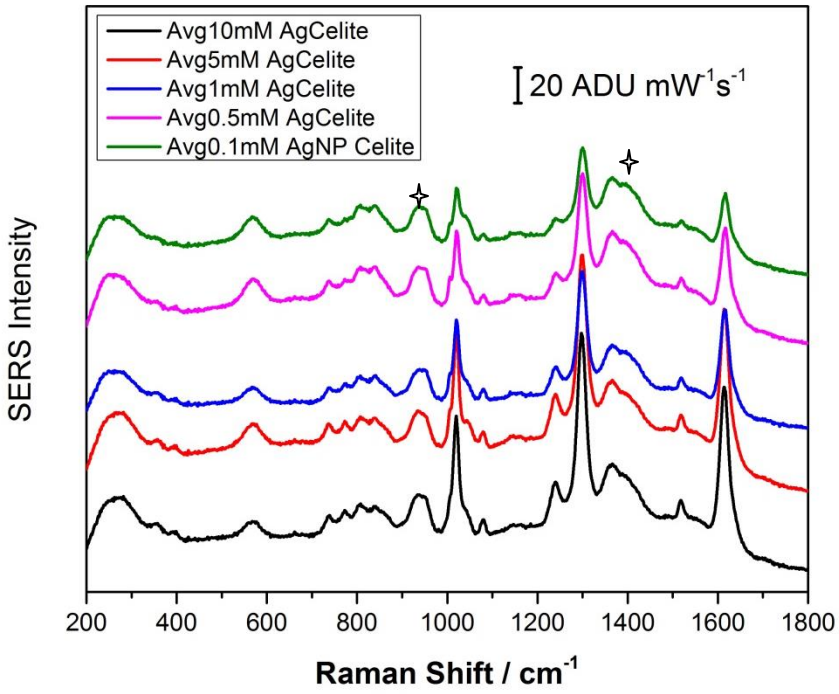

Figure 5.27: SERS of 4,4'-bipyridine on citrate reduced diatom-AgNPs using a 785 nm laser line.(30 s, 2.93 mW) Each spectra is the average of 10 spectra collected from 10 different spots on the SERS substrate.

The last thing to investigate for the diatom-AgNP substrates was its performance in an electrochemical environment when fashioned into a SERS-active electrode. Figure 5.28 demonstrates that the electrochemical reduction of the catalytic peaks is maintained.

Again, upon returning to more positive voltages the peaks due to the oxidation product are observed. Overall, this diatom-AgNP substrate has ~2x more intense SERS signal as compared to the AgNP in the absence of the diatoms.

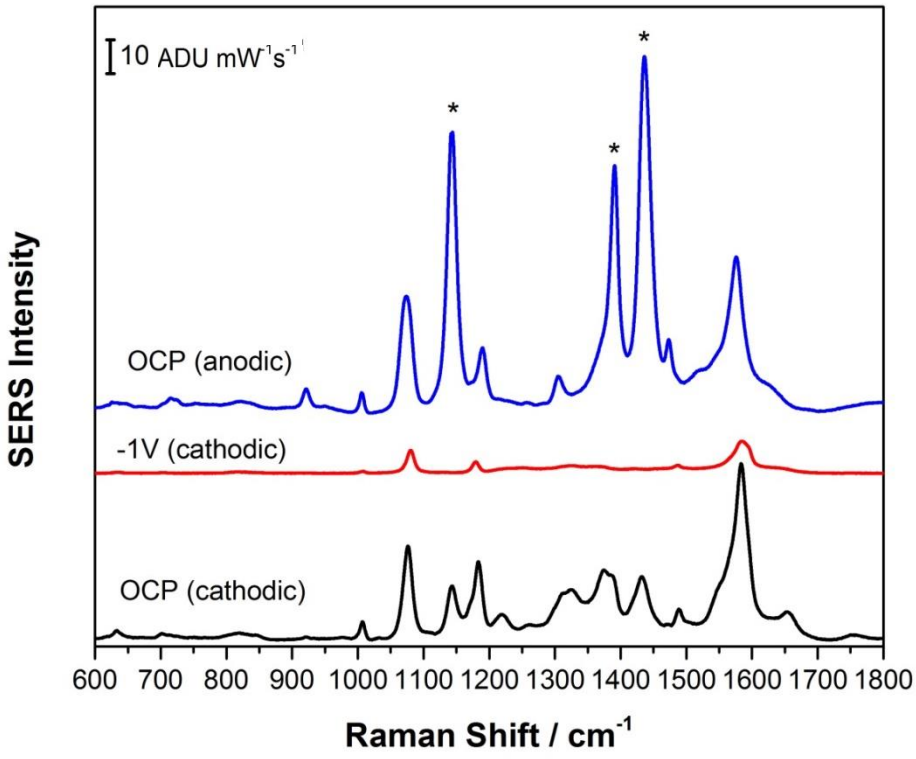

Figure 5.28: EC-SERS p-ATP on Ag-diatom SERS substrates made from citrate reduction. 532 nm laser 30 s, 3 mW. Asterisks indicated catalytic peaks due to DMAB.

The next diatom study was geared at using the smaller more uniform AgNPs produced *via* $NaBH_4$-reduction. To achieve this, *in situ* preparation was repeated, this time adding the Celite® to the reaction vessel for the borohydride reduction. The AgNPs were not as densely packed on the diatom surface as those from the citrate *in situ* reduction displayed in Figure 5.25. These $NaBH_4$ reduced diatom-AgNPs were then used to carry out all the same studies as the citrate reduced diatom AgNP SERS substrates

shown previously. The following figure shows the cathodic (0.0 V → -1.0 V Ag/AgCl) EC-SERS cycle for 0.1 mM 4,4'-bipyridine.

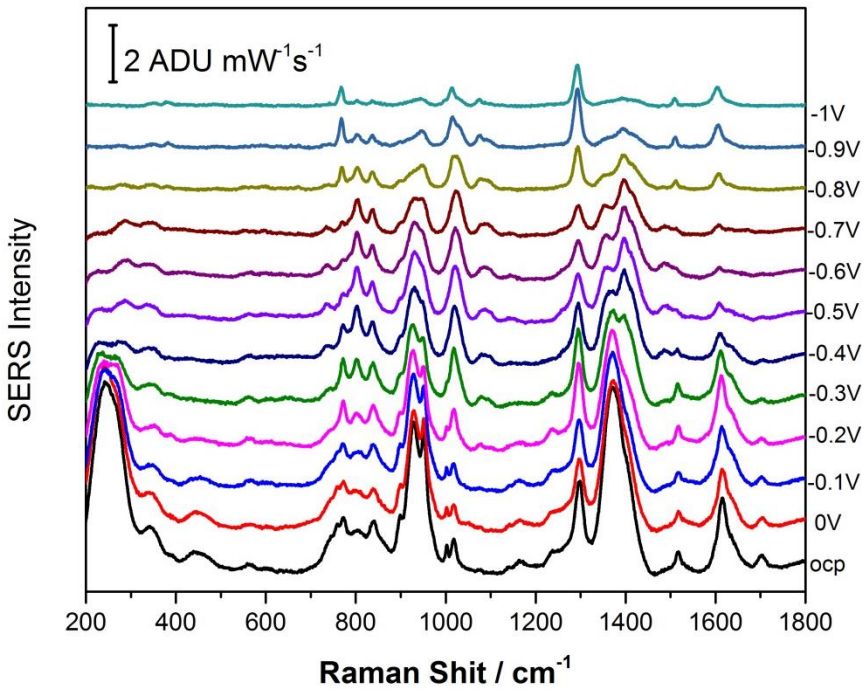

Figure 5.29: Cathodic EC-SERS of 0.1 mM 4,4'-bipyridine in 0.1 M NaF on diatom-AgNP substrates made from *in situ* $NaBH_4$ reduction. 532 nm laser was used at 3 mW for 30 seconds for each spectrum.

As the system approached -1.0 V the spectral background was significantly reduced. In addition, the peaks are observed to change dramatically with applied potential. Peaks due to citrate (which is used as a capping agent in the $NaBH_4$ synthesis) are clearly observed at ~1400 cm^{-1} and ~930 cm^{-1}, and disappear as the potential becomes more negative. This is due to the decreasing surface charge on the surface of the silver as the potential of zero charge is approached, which makes citrate adsorption less and less favourable due to electrostatic repulsion.

Equally important to note is that the $NaBH_4$ reduced diatom-AgNPs were incapable of reversing DMAB to p-ATP even at very negative applied voltages (data not

shown). Upon SEM investigation of this substrate it was found that the *in situ* $NaBH_4$ reduced AgNP showed relatively inferior coverage of the diatoms when compared to the citrate reduced preparation. This would account for the inability to electrochemically reduce DMAB to p-ATP since the partially-covered diatom is acting as an insulator and preventing electron transfer, thus possibly short circuiting the electrochemical cell.

Figure 5.30 shows the SERS signal for p-ATP on the sodium borohydride reduced AgNP diatom composite substrates prepared *in situ*. It is clear that there is a reduction of peak intensity at 1580 cm^{-1} as the 4,4'-bipy concentration is lowered. This peak is attributed to a C=C aromatic ring stretching vibration of the benzene ring which makes it a good indicator peak for quantitative assessment as it remains unperturbed by the plasmon assisted catalysis. In Figure 5.31 the intensity of the 1615 cm^{-1} peak increases linearly with 4,4'-bipyridine concentration. An r^2 value of 0.86 is testament to the best linear fit achieved by the diatom silver nanoparticle substrates and an indication that quantitative analysis may be a future possibility for these substrates.

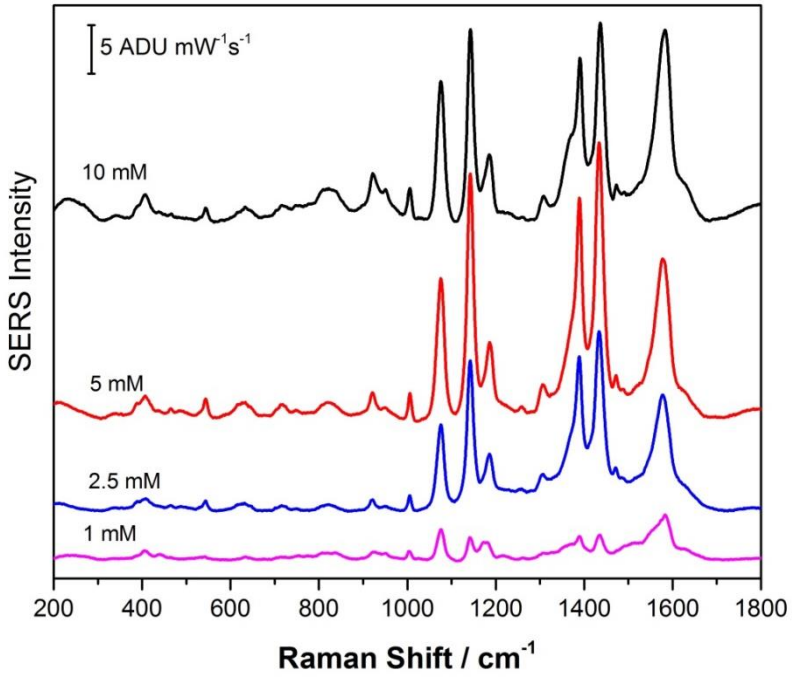

Figure 5.30: Plot of EC-SERS measurements of p-ATP collected on diatom-AgNP substrates made from *in situ* $NaBH_4$ reduction. The measurements were taken with a 532 nm laser, power of 3 mW for 30 s at open circuit potential (OCP) in 0.1 M NaF.

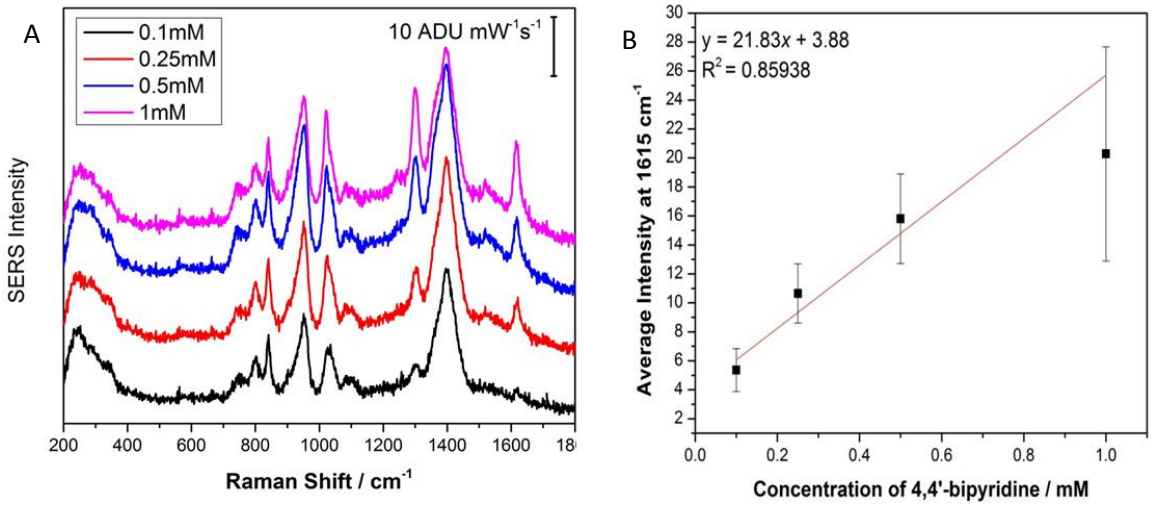

Figure 5.31 SERS measurements of 4,4'-bipyridine collected on diatom-AgNP substrates made from *in situ* $NaBH_4$ reduction (A). Linear relationship between the intensity at 1615 cm^{-1} and concentration (B). The measurements were taken with a 785 nm laser. (2.93 mW and acquisition time of 30 seconds)

With an aim of achieving even higher levels of reproducibility the aqueous suspension of Celite® was centrifuged (1000 rpm for 5 minutes), forcing the heavier, more complete diatoms to form a pellet, leaving the lighter broken fractions in the supernatant to be easily discarded.[41] The $NaBH_4$-reduced AgNPs were then drop-coated onto dried layers of diatoms instead of the *in situ* preparation that had previously resulted in poor surface coverage. Through drop-coating it was expected that the presence of more uniform layers of diatoms would allow a more densely packed biotemplate. This would provide more uniform signal since the scaffolds (diatoms) were more uniform than in the previous strategy (*in situ*). The SERS signal, while still more intense than for the AgNPs in the absence of diatoms, varied within the same margin of error as the first strategy and had a significant spectral background; this can be seen in Figure 5.27.

As a potential bioscaffold, diatomaceous earth was shown to have great promise. The most promising approach in using this biotemplate for the creation of sustainable SERS substrates was through the *in situ* citrate reduction of Ag^+ in the presence of the diatoms. In addition, this work illustrated that binding agents are not needed to attach the AgNPs to the siliceous structures. The $NaBH_4$ pathways were found to not be ideal because of poor surface coverage of the AgNPs on the diatoms leading to inconsistencies in signal as well as the inability to do spectroelectrochemistry.

5.2.2 Fruit Fly (*Drosophila Melanogaster*) Wings as SERS Templates

The nanoscale structural features that give butterfly wings their colour has already been explored for the improvement of plasmonic platforms. The transparent iridescent nature of fruit fly wings made them an interesting candidate as a bioscaffold for this thesis work. Additionally, availability of *Drosophila melanogaster* as a waste product from the genetics teaching laboratories at Saint Mary's University provided a route for sustainability. Figure 5.32 (A) shows an SEM image of a fruit fly wing revealing a well ordered surface with regular hair-like projections. The base of these projections had an average diameter of 1200 nm while the tip diameter was about 100 nm. The fruit fly wings were removed from the fly, mounted on a flat carbon surface and $NaBH_4$-reduced silver nanoparticles were drop-coated directly on top of the wings, as can be seen in Figure 5.32 (B). Aggregates of the silver nanoparticles are shown to form around the base of the hair projections while some of the nanoparticles form partial clusters along the lower region of the shaft.

Figure 5.33 shows the SERS signal for 1 mM p-ATP on the surface of the fruit fly wing SERS substrate (red) and the $NaBH_4$-AgNP SERS substrate (black). Clearly the incorporation of the fruit fly wing enhances the SERS signal considerably. Additionally, SERS of the wing reveals no significant background interference due to the organic composition of the wing. The fruit fly wing adds an alternative to the butterfly wings currently being explored as templates, particularly since fruit flies are more readily available and generated in genetics labs the world over as a waste product.

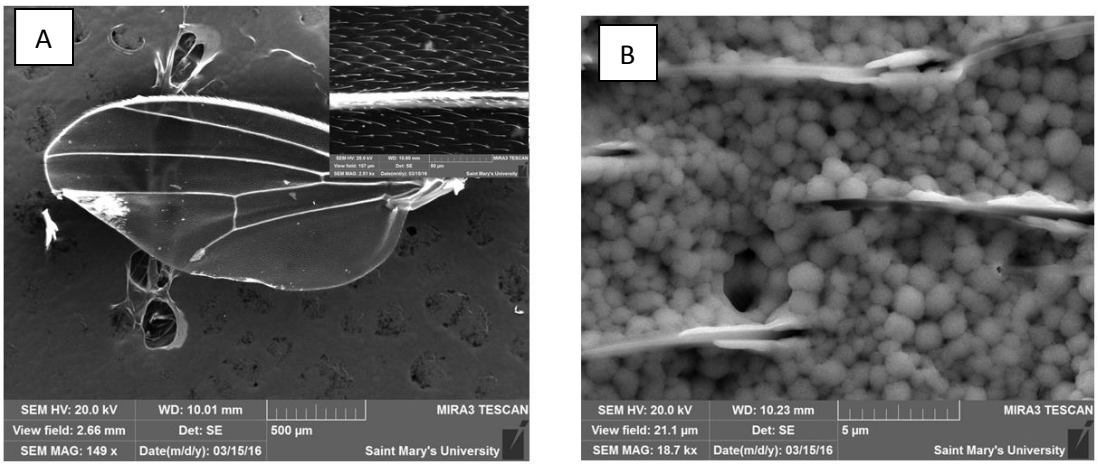

Figure 5.32: SEM images of drosophila wings on the left and $NaBH_4$ reduced AgNP coated drosophila wings on the right.

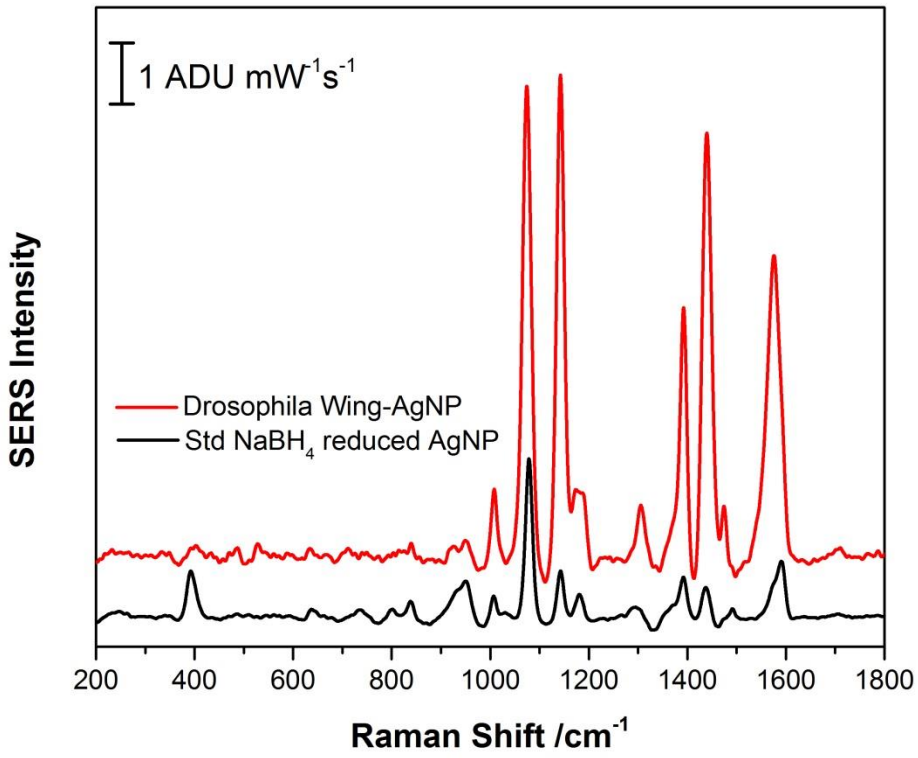

Figure 5.33: SERS of 1 mM p-ATP on $NaBH_4$ reduced AgNP-Fruit fly wing substrate (red), on $NaBH_4$-reduced AgNPs (black).(785nm, 30 sec, 10.6 mW (black) and 2.93 mW (red).

5.3 Copper SERS substrates

A lack of reported Cu nanostructures and the relative ease of oxidation compared to other plasmonic metals has limited the progress of copper plasmonics, despite it being a more sustainable option compared to Ag and Au. In this section copper substrates fabricated using controlled electrochemical deposition were explored as potential substrates for SERS. The investigations presented in this section explored a number of different parameters including electrodeposition potential, time, counter ions, additives, etc. In addition, electrodeposited bimetallic structures were also evaluated for SERS applications.

Initial studies all involved copper electrodeposition from a deaerated 0.1 M $CuSO_4$ solution. A series of different potentials were explored for varying time intervals as listed in Table 5.3.

Table 5.3: Electrochemical potential versus Ag/AgCl and deposition time that was used for the initial trials. Y indicates a Cu deposit was noted, N indicates no Cu deposit was present. All observations were initially made by visual inspection.

Applied Potential vs Ag/AgCl	Time / minutes	Deposit observed?	SERS Active
-0.1 V	1	N	N
	5	N	N
	20	N	N
-0.3 V	1	Y	N
	2	Y	N
	3	Y	Y
	8	Y	N
	10	Y	N
-0.5 V	1	Y	N
	2	Y	N
	4	Y	N

It was recognised that at an applied potential of -0.3 V for a period of 3 minutes, SERS signal could be observed for a monolayer p-ATP deposited onto the electrodeposited Cu substrate. However, the SERS signal was non-uniform and had a large background as shown in Figure 5.35 in red. The SERS signal collected on the Cu substrate (-0.3 V, 3 mins) only positively identified the p-ATP by two peaks (1079 and 1174 cm^{-1}) the rest of the spectrum was obscured by the huge spectral background. Li and coworkers demonstrated that a smooth copper surface could be electrochemically roughened through the application of square wave voltammetry (SWV).[53] It was this idea that was then used to improve the number of identifiable nanoscale features on the poorly performing Cu SERS substrate in the present work. The same parameters (0.1 M $CuSO_4$, -0.3 V, 3 mins) was used to reproduce the Cu deposits, followed by SWV between 0.0 V

and -1.4 V (0.2 mV/s, pulse 0.02500 s) as reported by Li.[53] When the SWV is at the 0.000 V step, the deposits on the electrode are expected to form copper oxide, which upon the -1.4 V step reduces back to the zero valent copper metal. Purposely forming the surface oxide allows nanoscale imperfections to form during the rapid reduction step; this can be appreciated from Figure 5.36, which shows the SEM images for the electrodeposited copper SERS substrates before and after the SWV treatment. The additional nanofeatures noted in Figure 5.36 B are accredited with the slight improvement of the SERS performance noted in black in Figure 5.35.

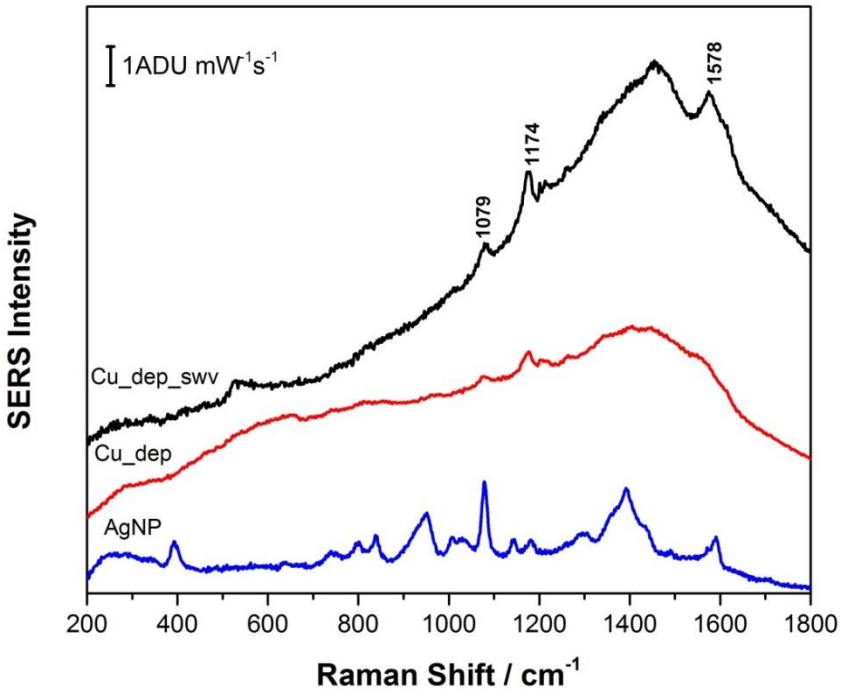

Figure 5.34: SERS of 1 mM p-ATP on citrate-reduced AgNPs (blue), copper deposits created at -0.3 V for 3 mins in 0.1 M $CuSO_4$ (red), copper deposits created at -0.3 V for 3 mins in 0.1 M $CuSO_4$ followed by SWV (0.00 V to -1.4 V) (black).

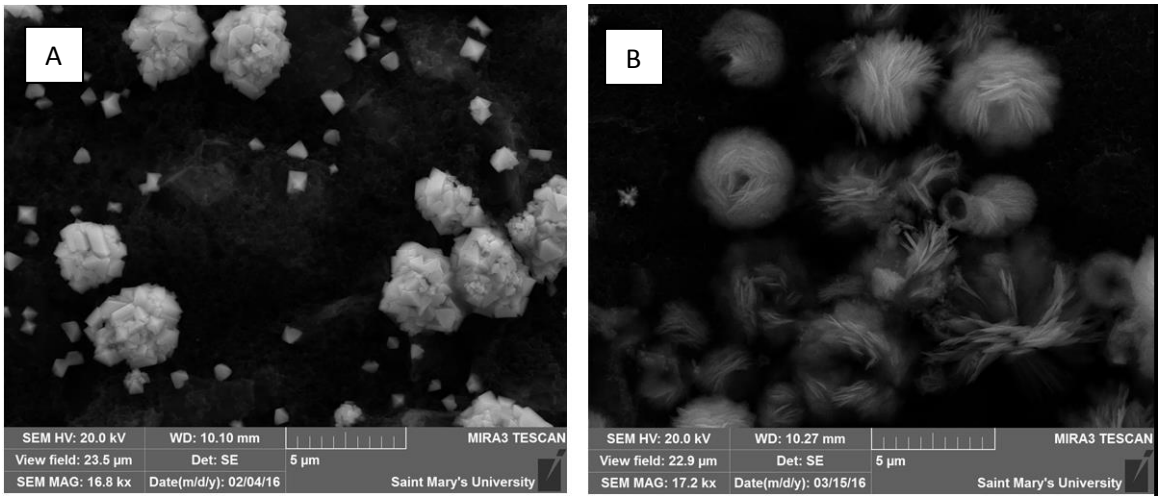

Figure 5.35: Cu deposits formed from electrodeposition in 0.1 M $CuSO_4$ at a potential of -0.300V vs Ag/AgCl for 3 minutes (A) and the same substrate after a SWV treatment between 0.000 V and -1.400 V (B).

All the electrodeposited Cu substrates formed at -0.3 V were a combination of octahedral crystalline structures ranging in diameter from 1.5 to 3 µm and aggregates of these octahedral crystalline structures ranging between 7 to 16 µm in diameter as shown in Figure 5.36 A. These octahedral structures are consistent with Cu_2O.[51] The clusters were observed to have nanoscale roughness to them that were as small as 60 nm on some aggregates. Once the SWV treatment was applied, these deposits developed a plate-like appearance as shown in Figure 5.36 B. It is this nanoscale roughness on the clusters that is believed to be responsible for the enhanced SERS activity of the Cu substrates. The baseline corrected SERS spectra for the Cu substrate shown in Figure 5.37 (orange) shows that all the peaks are due only to p-ATP while the SERS peaks on the $NaBH_4$-reduced AgNP shows evidence of both p-ATP as well as DMAB. The greater affinity of the amino terminated end of p-ATP to adsorb onto the Cu substrates as opposed to the thiolated end likely limits the ability of the p-ATP to dimerize to DMAB on Cu.[87] Work done by Matejka and coworkers supports these findings, adding that the plasmon-assisted

catalysis is possible on Cu substrates at 633 nm or more energetic laser lines.[87] However, any formed DMAB on Cu using such short laser lines will not be able to be followed spectroscopically, *in situ*, *via* SERS because of the limiting interband transitions at such energetic wavelengths.[2] While showing some initial promise, the SWV modified electrodeposited Cu substrates were difficult to reproduce and so were not considered further as a viable substitution for traditional Ag or Au SERS substrates. Therefore, all further studies reported in this thesis used the bulk electrodeposition step only, with no SWV treatment.

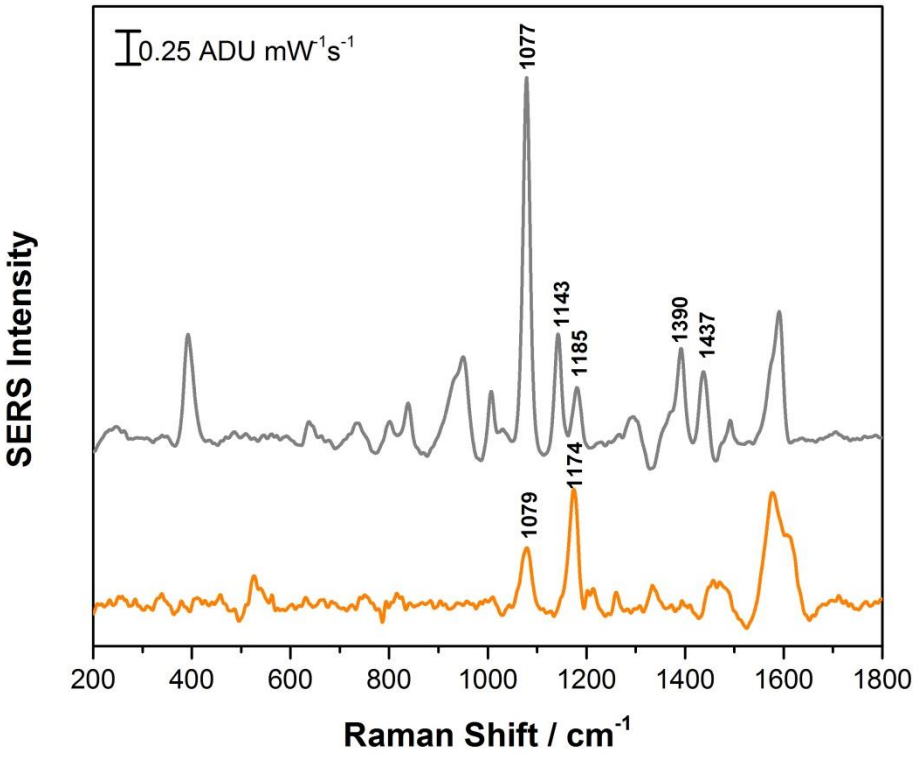

Figure 5.37: SERS of 10 mM p-ATP on Cu substrate made from 0.1 M $CuSO_4$ -0.3 V, 3 minute deposition followed by SWV (0.00 V to -1.4 V) (orange) and $NaBH_4$ AgNP (grey). 785 nm laser, 30 s, 10.6 mW orange, 2.93 mW (grey) (spectral baseline correction performed using NuSpec software)

In search of a more uniform and reproducible Cu SERS substrate the same parameters were used (-0.3 V for 3 minutes), however the copper salt was replaced with

$Cu(NO_3)_2$ to see if there would be a change in the morphology of the deposits when the counter ion was varied. The copper deposits from the $Cu(NO_3)_2$ were in the form of tip-truncated cubes and it was noted that flower-like growths were present on the faces of the Cu deposits as shown in Figure 5.38. The faces had a mean width of ~630 nm while the individual "petals" of the flower-like growths ranged in size from 50-125 nm. Interestingly enough the SERS spectra for p-ATP collected from these substrates with the 785 nm laser line showed the signature peaks for the plasmonic assisted catalytic product DMAB, namely; 1141, 1390 and 1443 cm^{-1}. Not only are those peaks exclusive to SERS on Ag and Au substrates but the Cu SERS substrate at the 785nm laser line appeared to outperform the monodispersed sodium borohydride reduced Ag substrates as shown in Figure 5.39.

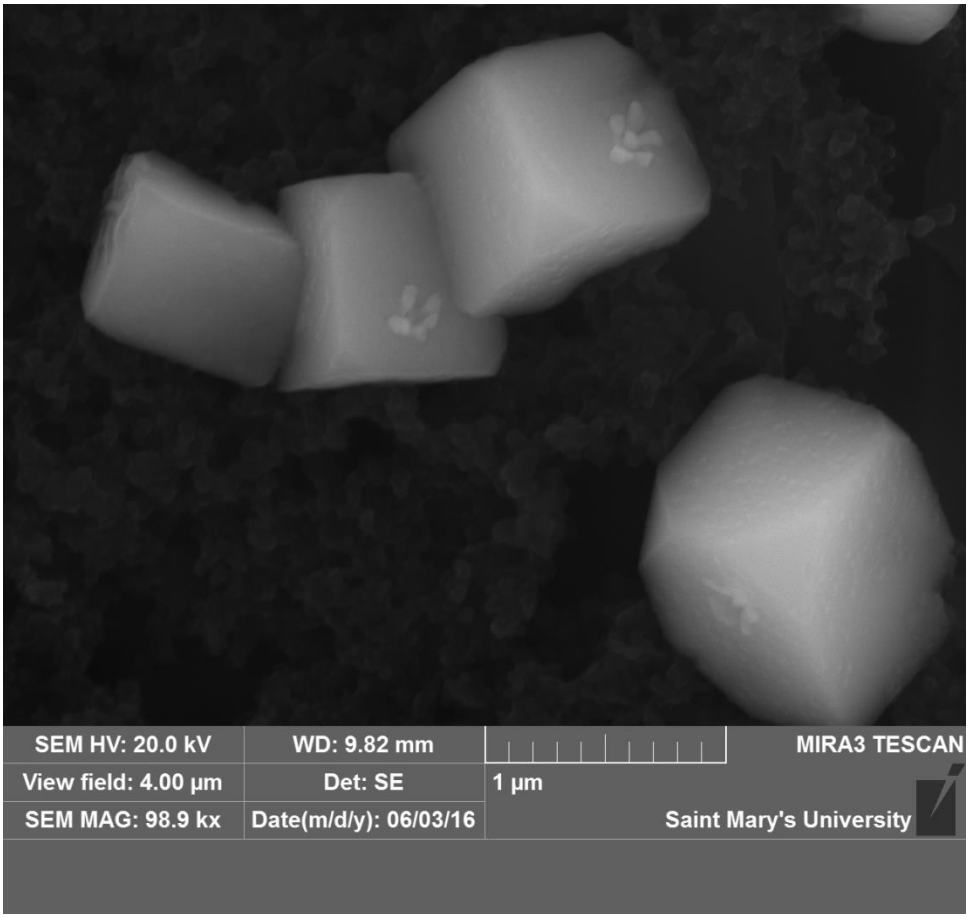

Figure 5.38: Cu deposits produced with a -0.3 V potential for a period of 3 minutes from a purged 0.1 M $Cu(NO_3)_2$ aqueous solution.

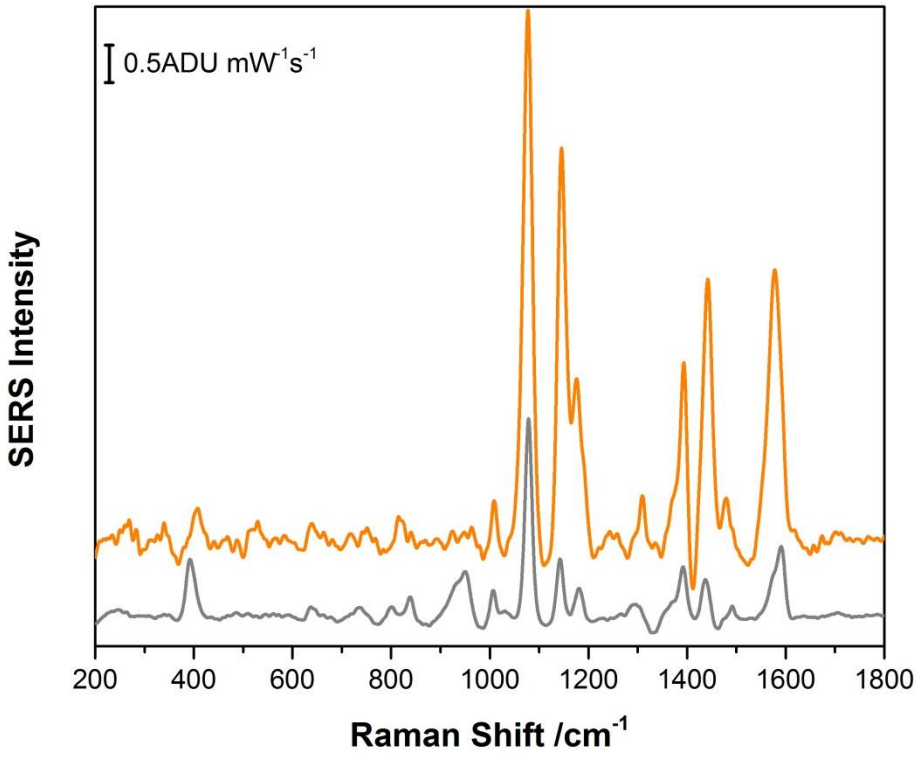

Figure 5.39: SERS of 1 mM p-ATP on Cu substrate made from 0.1 M $Cu(NO_3)_2$ -0.3 V, 3 minute deposition (orange) and $NaBH_4$ AgNP (grey). 785 nm laser, 30 s, 2.93 mW (Spectra are baseline corrected using NuSpec software)

While the SERS of p-ATP on the Cu substrates at 785 nm made from the $Cu(NO_3)_2$ solution was promising, a strong SERS response from the Cu SERS substrate at the 532 nm laser line was suspicious as only Ag substrates are technically capable of SERS responses at such short wavelengths. Figure 5.40 shows a relatively weak SERS spectrum from the Cu substrate but the strength is not in question, the fact that any SERS response was achieved with that more energetic laser line is surprising. Initially EDX was not considered given the copper salts were ultra pure (99.999%) but all this evidence mandated such an analysis. The EDX spectra revealed that the copper deposits had

growths of Ag on them. The flower-like patterns on the face of each Cu deposit were confirmed to be Ag, suggesting all of the SERS response was in fact coming from these Ag deposits as opposed to the copper. The contamination of the copper substrate with silver most likely resulted from improperly washed glassware used in the extensive amount of AgNPs substrate studies. This was not a total loss as the bimetallic Cu-Ag substrates certainly outperformed the uniform monometallic $NaBH_4$ AgNP substrates as shown in Figure 5.39. Rao and colleagues have demonstrated that such bimetallic substrates have improved SERS efficiency due to a charge transfer mechanism.[107] The surface copper oxide layer of the Cu deposits facilitates a charge transfer from the oxide layer to the Ag.[107] This allows the induction of a larger electromagnetic field hence a more sensitive SERS response for the 785 nm laser line as noted above. At 532 nm the interfering interband transitions in Cu are clearly attenuating the SERS response for the bimetallic system. In terms of sustainability, only trace amounts of the endangered Ag metal would have to be used to create these bimetallic nanostructures and far less solvent is required per substrate for the electrodeposition strategy. The next phase of this research project therefore explored the idea of Cu/Ag bimetallic SERS substrates further.

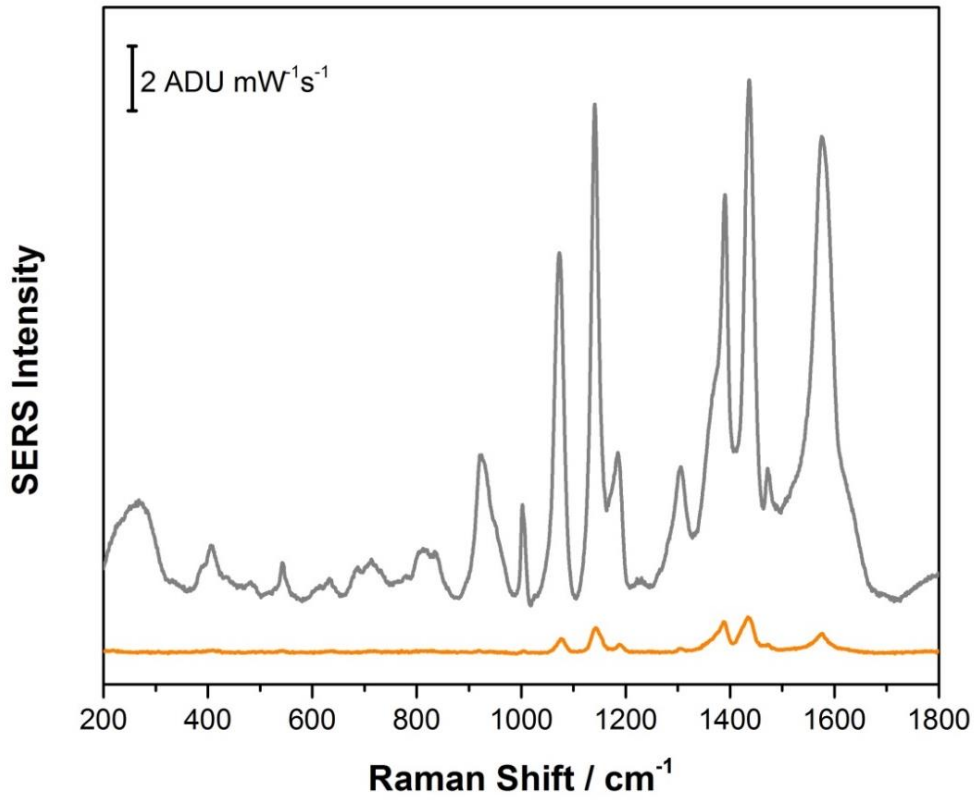

Figure 5.40: SERS of 1 mM p-ATP on Cu substrate made from 0.1 M $Cu(NO_3)_2$ -0.3 V, 3 minute deposition (orange) and $NaBH_4$ AgNP (grey). 532 nm laser, 30 s, 3 mW (Spectra were baseline corrected using NuSpec software)

To recreate the highly SERS active bimetallic copper-silver substrates two things were tried. Firstly, the 0.1 M copper salt ($Cu(NO_3)_2$) solution was purposely spiked with varying amounts of silver nitrate. These studies resulted in large deposits of silver and copper in separate areas as seen by Figure 5.41 which shows dentritic Ag deposits on the screen printed electrode.

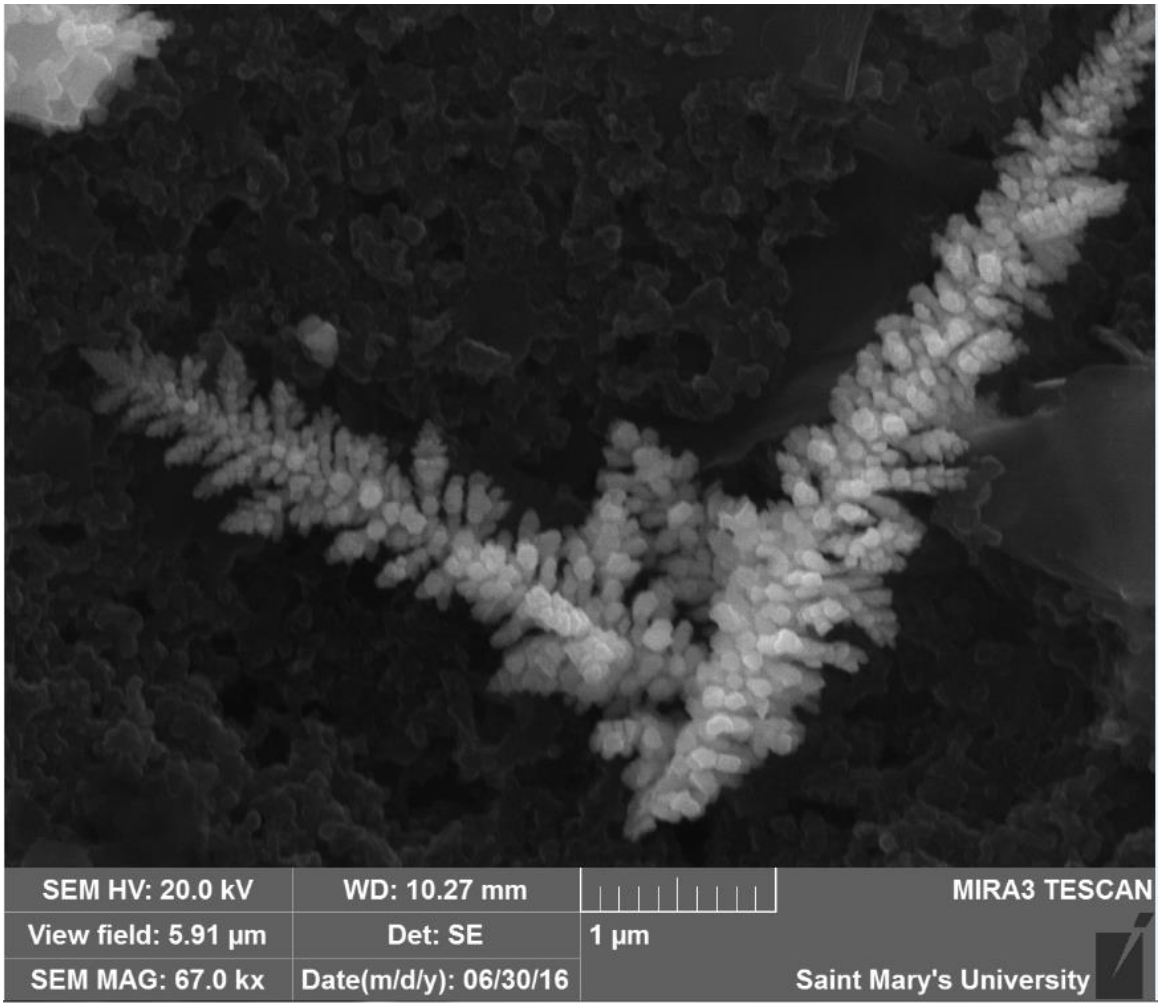

Figure 5.41: Ag dendrite deposit on SPE formed during a mixed copper-silver deposition study.

The SERS signal for p-ATP recorded for these deposits were reasonable but the signals were coming solely from the Ag deposits, which were often masked by the copper deposits or appeared in largely spaced island-like deposits; there was no observed bimetallic nature to the deposits. The second attempt to recreate the bimetallic Cu-Ag SERS substrate was based on a sequential electrodeposition. The Cu was first electrodeposited as outlined above, followed by a spike of the electroplating solution with 0.1 mM $AgNO_3$ between 200 µl and 1000 µl. The SERS response of the two attempts to recreate the bimetallic substrate were similar. However the distribution of silver in the

latter was much greater, therefore a more uniform signal could be obtained from the sequentially electrodeposited bimetallic Cu-Ag synthesis.

At +0.337 V vs SHE (Cu^{2+}/Cu^{0}), Cu^{2+} has a lower standard reduction potential than Ag^{+}, which is +0.799 V vs SHE, hence an electrochemical cell that has sufficient applied potential to deposit Cu will also automatically co-deposit Ag.[128] Hence, when both Cu^{2+} and Ag^{+} are present, Ag will electrodeposit first. When silver is added after the Cu electrodeposition step, this allows the Ag to electrodeposit onto the Cu structures in a more controlled fashion. It can be noted from Figures 5.42 and 5.43 below, that the flower-like structures that grow on the faces of the Cu deposits can be controlled as the amount of silver nitrate added to the electroplating bath after the initial deposition of Cu directly affects the size of the flower-like Ag that appears on the Cu deposits. Figure 5.42 where 250 µl of the silver nitrate was added to the electroplating bath has smaller flowers on the copper base metal than Figure 5.43, which used 500 µl of the silver nitrate.The accompanying EDX spectra in Figure 5.42 B and C confirmed that the base metal deposit was Cu microstructures and the flower-like nanostructures were predominantly Ag.

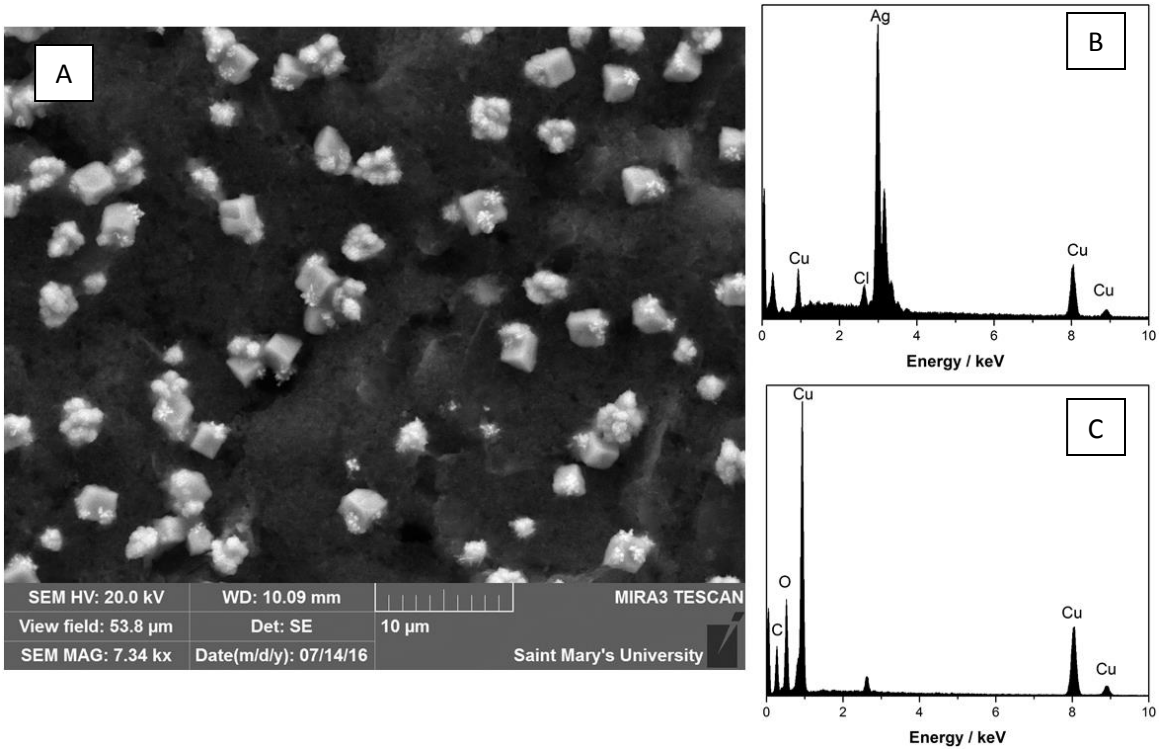

Figure 5.42: SEM of sequentially deposited Cu-Ag deposit using 250 µl 1 x 10^{-4} M $AgNO_3$ (A), EDX of cube deposit face with flower-like growth (B), and EDX of cube without growth (C).

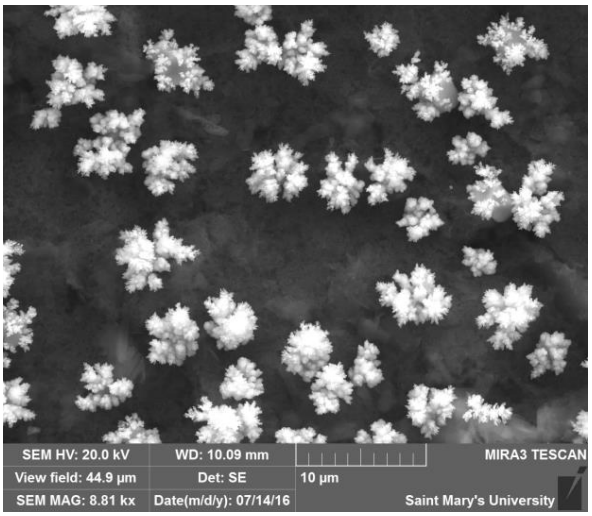

Figure 5.43: SEM of sequentially deposited Cu-Ag using 500 µl 1 x 10^{-4} M $AgNO_3$.

The SERS activity of these bimetallic Cu-Ag substrates was assessed in EC-SERS measurements using p-ATP as the Raman reporter molecule. Figures 5.44 and 5.45 show the cathodic and anodic spectra, respectively for the Cu-Ag substrates prepared using 500 µl of the 0.1 mM $AgNO_3$. It is difficult to note in those two figures whether the DMAB peaks completely disappear at more negative potentials since the intensity of the overall spectra gets significantly weaker at negative applied potentials.[98] The electrochemical reduction of DMAB back to p-ATP can be better appreciated in Figure 5.46 where the intensity of the spectrum collected at -1 V is amplified to highlight the disappearance of the DMAB fingerprint peaks as it has been fully reduced back to p-ATP at this potential. This demonstrates that the bimetallic substrates maintain the excellent SERS performance of the traditional AgNPs, even under electrochemical control, preserving the ability to follow a surface redox process at an electrified interface *in situ*. Since this substrate uses ~ 2000 times less silver metal ion, the route can be considered more sustainable compared to the traditional AgNP SERS substrates we well. To our knowledge, this work represents the first facile method for the production of cheap, robust and sustainable SERS bimetallic Cu/Ag substrates on a screen printed electrode. By coupling this novel technique to electrochemical systems, many potential applications can be explored, ranging from rapid and sensitive biosensing to fundamental investigation pertaining to plasmon-assisted catalysis.

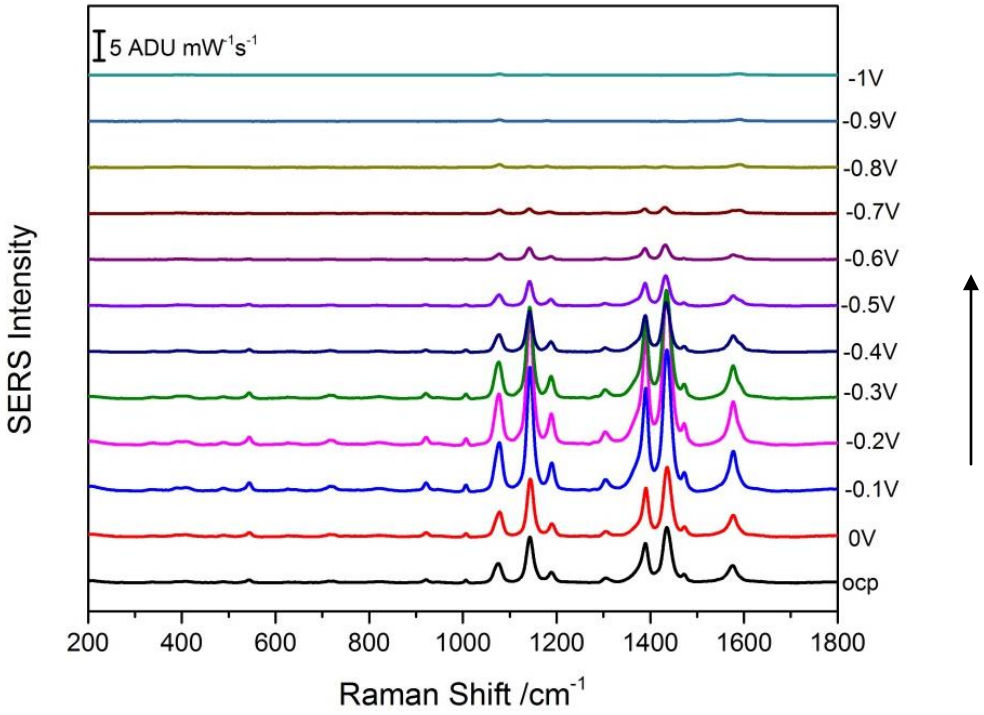

Figure 5.44: EC-SERS of 1 mM p-ATP in the cathodic direction on Cu-Ag (500 µl of the 0.1 mM $AgNO_3$) sequential substrates using the 532nm laser line. 0.1 M NaF was used as the electrolyte.

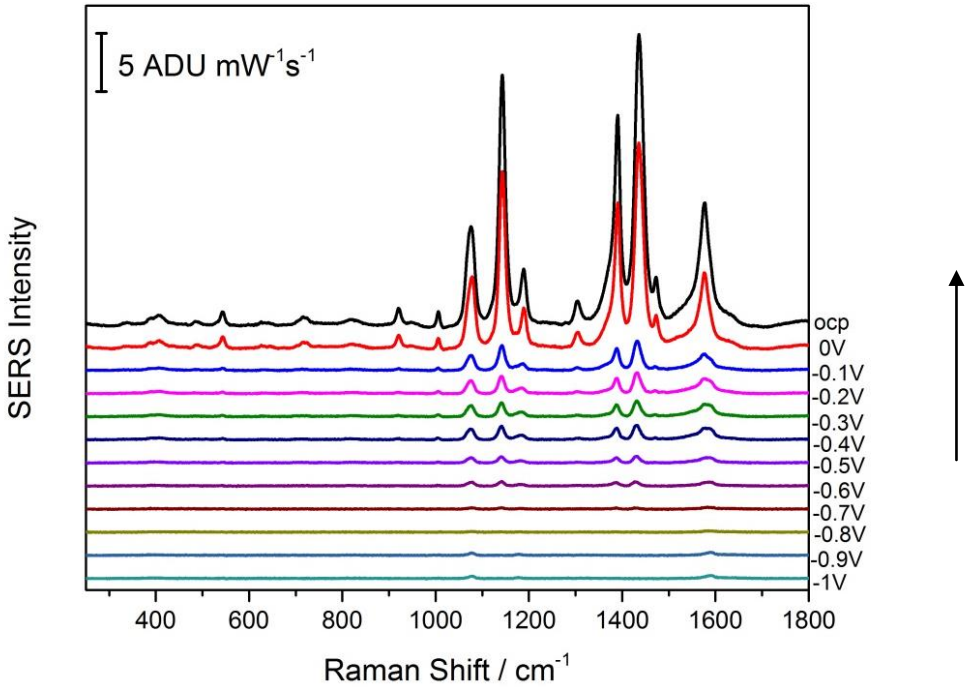

Figure 5.45: EC-SERS of 1 mM p-ATP in the anodic direction on Cu-Ag (500 µl of the 0.1 mM $AgNO_3$) sequential substrates using the 532 nm laser line. 0.1 M NaF was used as the electrolyte.

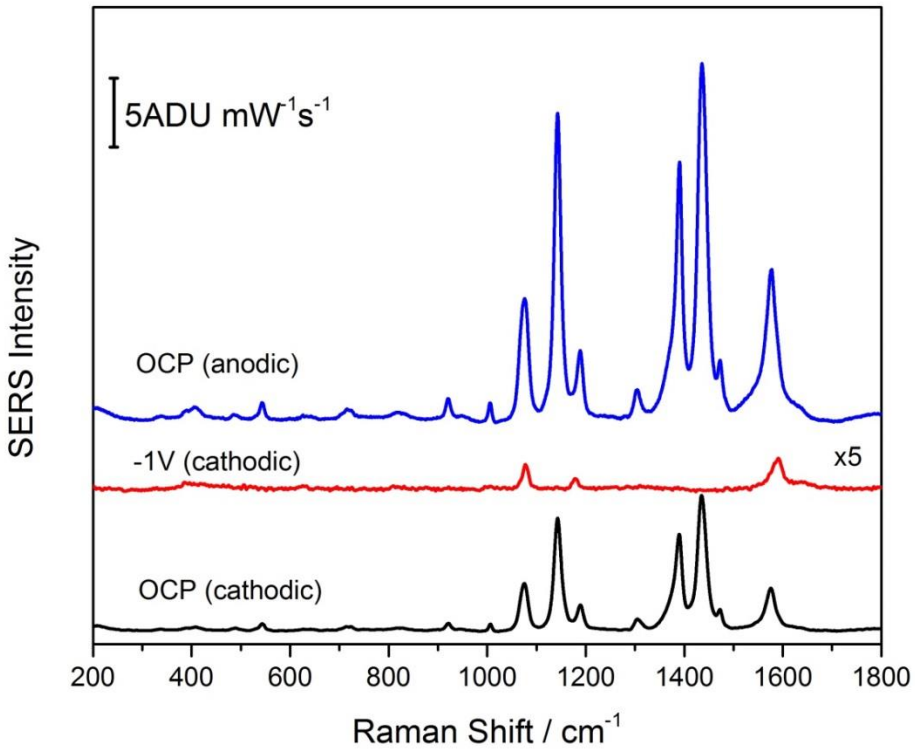

Figure 5.46: EC-SERS of 1 mM p-ATP on Cu-Ag sequential substrates at OCP in black, -1 V in red and OCP at the end of the anodic collection in blue using the 532 nm laser line. 0.1 M NaF was used as the electrolyte.

5.3.2 PEG and KCl as additives

In an attempt to create more nanofeatures in a pure copper electrochemical deposit many additives have traditionally been added to the electroplating baths. Most of these additives are used to enhance the appearance of the bulk features of copper in the mining industry. In this section, the commonly used additives polyethylene glycol (PEG) and KCl were explored in an effort to produce Cu only SERS substrates with more abundant nanoscale features.

Combinations of varying amounts of 0.2 mM cholesterol–PEG 600 and 0.5 M KCl were added to 10 ml of 0.1 M $Cu(NO_3)_2$ as shown in Table 5.4 below.

Table 5.4 Combinations of additives investigated for Cu electrodeposition

Volume of 0.2 mM Cholesterol-PEG-600 (ml)	Volume of 0.5 M KCl (ml)
1	0.05
1	0
0.5	0.05
0.5	0

A potential of -0.3V Ag/AgCl for 3 minutes was applied to each combination and SERS of 10 mM p-ATP was attempted on all with no success. While no useful SERS signals were obtained during these additive studies, the SEM images revealed that the additives provided some degree of shape and size control for the Cu deposits. It has already been established that under these electrodeposition parameters void of any additives, Cu deposits are octahedral when copper (II) sulphate is used, and form tip-truncated cubes / complete cubes when a copper (II) nitrate solution is used. When PEG and KCl were added to the $Cu(NO_3)_2$ solution, deposits resembling a rose bush formed with cube-like crystals forming on and in between the rose "bushes". In the absence of KCl the majority of the deposits were in the form of dodecahedra as seen in Figure 5.47. It was noted that when 1 ml of PEG and 0.05 ml of KCl were added, the cubes that formed in and around the rosebush-like deposits had a mean size of 740 nm, but when the

amount of PEG was decreased to 0.5 ml the cube size averaged about 265 nm. The combination of the two additives was supposed to reduce the grain size which was observed.[55] This is demonstrated by the very narrow sheets that make up the deposit shown in Figure 5.48.[55] In addition, KCl inhibits the formation of dendritic growth according to work done by the Bartlette group.[56] Different size and shape particles can be formed using the same capping agent, which is the case with PEG.[109] Simply put, PEG can tune the deposition rate depending on its concentration in the electroplating bath which ultimately provides some degree of control over the size of the deposits. A lower concentration of PEG would correlate to a situation where there is less copper complexation with the ethylene oxide ligand ($-CH_2-CH_2-O-$) of the PEG; thus copper ion transport in the overall volume of the electroplating bath and subsequent passage through the electrical double layer would not be as slow as in a plating bath with more PEG.[107] More work is required to release the copper ion complexed with the PEG to the electrode surface but this is reduced when chloride ion is added to the bath.[107] This results in more efficient ionic transport which accounts for the differences between the deposits formed with both PEG and KCl (rosebush and cubes) vs those formed with just PEG (octahedral).[107] The lack of a SERS response for p-ATP on all the substrates made with PEG as an additive was attributed to them being very well capped by the PEG molecule, therefore blocking the surface to thiol adsorption and therefore any SERS signal.

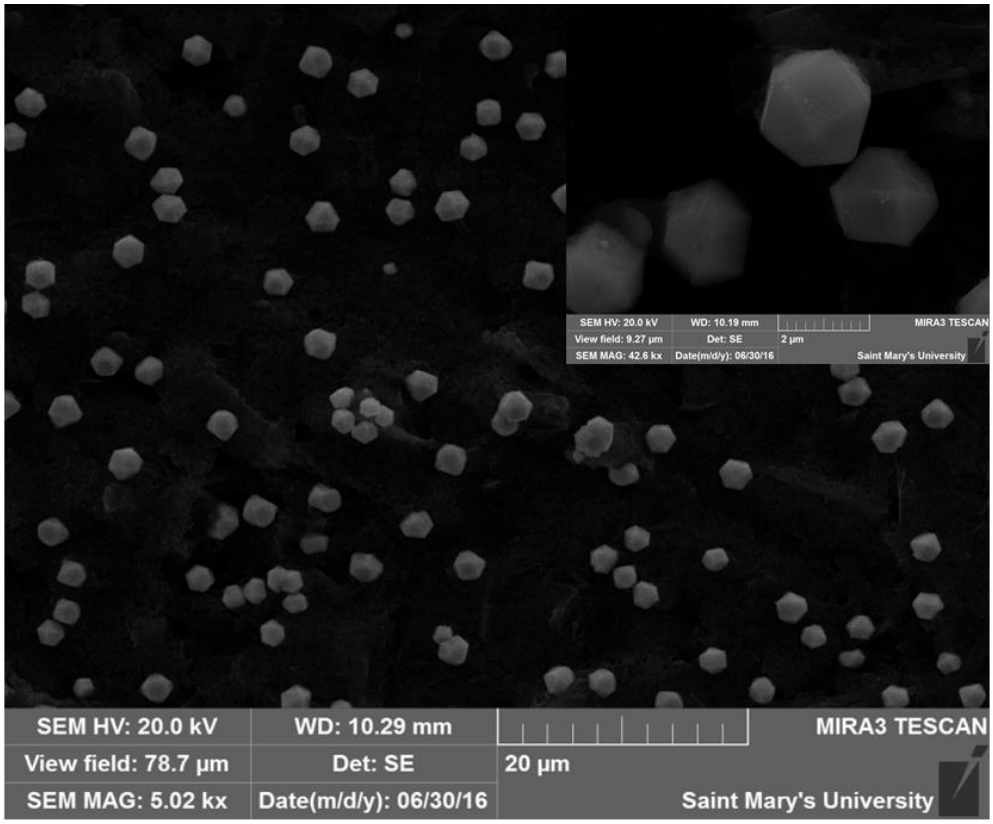

Figure 5.47 : SEM image of Cu deposit on SPE from an electroplating bath of 0.5 ml 0.2 mM cholesterol-PEG and 10 ml 0.1 M $Cu(NO_3)_2$. (-0.3 V Ag/AgCl for 3 minutes).

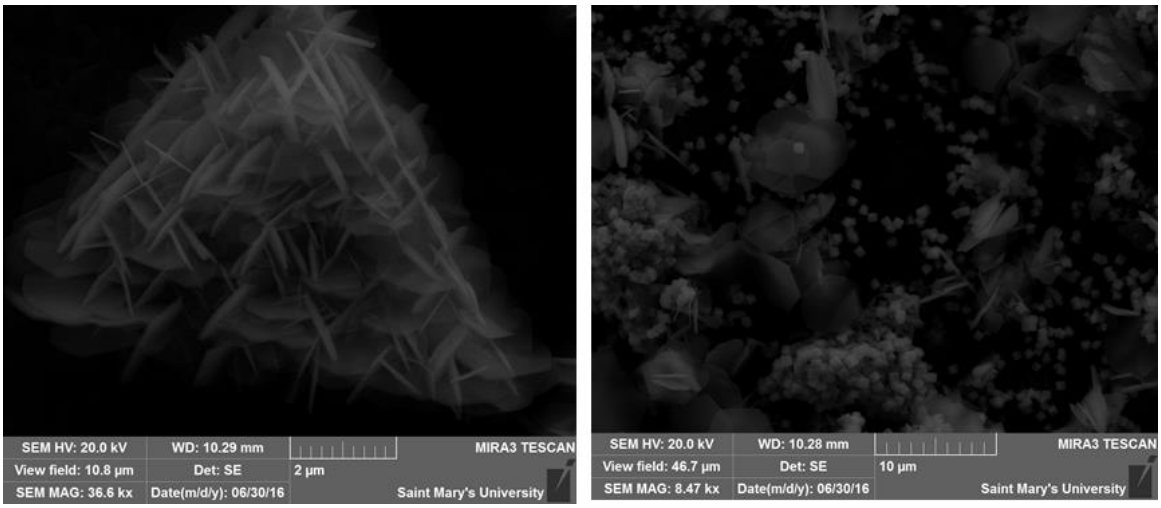

Figure 5.48 Electrodeposition of Cu from a 10 ml 0.1 M copper nitrate electroplating bath containing 1 ml PEG and 0.05 g KCl. Applied potential -0.3 V for 3 minutes. On the left rosebush-like deposit and on the right cubic deposits shown on and in-between the rosebush deposit.

In summary, while electrodeposition of Cu was fast, easy and cost-effective, limited success was achieved in creating monometallic SERS-active copper substrates. This research work showed that oxidation of copper is rapid, even under deaerated conditions, and nucleation of Cu was difficult to promote over growth. The majority of electrodeposited copper obtained in this study was micron in scale, as opposed to nanoscale, and thus not suitable for plasmonic applications. The bimetallic Cu-Ag structures produced through sequential electrodeposition, were very promising, showing excellent SERS activity using ~2000 times less Ag metal than the traditional monometallic AgNP SERS substrates.

Chapter 6 Conclusions and Future Work

6.1 Green Synthesis of Ag Nanoparticles for SERS

In conclusion, viable Ag SERS substrates could be made from all of the plant/ fruit extracts explored in this research work. In some cases heat and the addition of base were necessary in order to increase the rate of reaction and form the AgNPs within a reasonable period of time. Some of the extracts however, resulted in AgNPs that were heavily coated in an organic layer (biogenic corona), which hampered their use in SERS studies as the surface of the metal was blocked. In addition, while all of the investigated extracts produced AgNPs that were useful for SERS of thiols (i.e. p-ATP) not all of them could be used on molecules void of this sulfur functionality. As a result, only a few of the extracts could be used for making SERS substrates with broad applicability, such as for the sensing of non-thiolated analytes. The extracts with the least significant biogenic coronas were the easiest to image *via* SEM as there was less non-conductive mass present to weaken the resolution of the electron microscope. It was demonstrated that smaller sugars could participate in the reduction and capping of Ag^{+} but were not independently as useful for the production of SERS active Ag substrates. It was also determined through the exploration of banana peels at varied levels of ripeness that complex sugars such as starch may play a more crucial role in the production of SERS-active AgNP than the simpler sugars like glucose. From a green chemistry perspective, the best extracts were the banana peel, the dandelion flower, and the avocado pit, as they were all non-edible renewable materials and outperformed the standard citrate reduced AgNPs when it came to SERS analysis of p-ATP. Only the dandelion flower extract and avocado pit extract were capable of detecting non-thiolated molecules, and as a result, these two extracts are the ones that should be further pursued for SERS sensing applications. Finally, only the

avocado pit extract produced very monodisperse AgNPs, and correspondingly uniform SERS signals. Therefore, only the avocado pit extract should be pursued for SERS sensing applications where a quantitative analysis of analyte is required.

In summary, natural extracts that are high in antioxidant levels are very promising for the green synthesis of AgNPs for the creation of SERS substrates. Important considerations should include energy requirements for the synthesis (heat vs. no heat, *etc*.) as well as the extent to which the AgNPs are left coated with a biogenic corona. When natural materials are being considered, one should always first consider foodstuff materials that do not complete with a food resource, or which are a waste product of the food industry. In addition, the materials should be widely available, plentiful throughout the year, and easy to process.

Future work in this area will seek to move both the dandelion flower extract and avocado pit extract forward in terms of SERS based sensing. In particular, non-thiolated analytes will be assessed using the avocado pit extract AgNPs, to determine important figures of merit such as limit of detection and dynamic linear range. In addition, the long term stability of both the extracts as well as the AgNPs synthesized using the extracts should be evaluated.

6.2 Bioscaffolds

The incorporation of both diatoms and drosophila wings with the traditional AgNPs offered a clear advantage with regards to SERS signal intensity. By incorporating the sodium borohydride AgNPs into the frame-work of the diatoms *via* an *in situ* preparation, a highly functional SERS substrate was created using a low-cost, readily available biomaterial. In addition, the catalytic product peaks for DMAB were far more

intense on the bioscaffolds than for any of the silver nanoparticle SERS substrates alone. As a result, bioscaffold / biotemplated plasmonic substrates may show great promise in the future as surface plasmon assisted catalysis becomes more commonplace.

In summary, it was shown in this thesis work that natural materials, such as biomaterials, can have regular micron to nanoscale order that can be exploited for next generation plasmonic substrates. In this way, multidimensional architectures can be fashioned that are not possible even with today's most sophisticated instrumentation. For large scale plasmonic applications, such as plasmon-assisted solar cells, this bioscaffold approach may prove very advantageous and much more sustainable and scalable.

Future work in this area should seek to optimize the diatom-AgNP platform, and move forward with SERS-based sensing of non-thiolated analytes. In addition, other biomaterials should be evaluated, such as peacock feathers, which have structural color and are renewable, as well as green crab shells, which have nanoscale features and represent an invasive species in Nova Scotia.

6.3 Cu SERS substrates

The synthesis of stable and SERS-active Cu nanoparticles was the most challenging but also most rewarding part of this thesis work. The shape and size of copper deposits formed on screen printed electrodes can be manipulated not only by varying the electrodeposition parameters, but also by varying the choice of copper salt (type of anion) as well as through the addition of additives. Cu^{2+} from copper (II) nitrate deposited at -0.3 V vs Ag/AgCl has a tendency to form tip-truncated cubes or complete cubes while Cu^{2+} deposited from $CuSO_4$ under identical conditions forms octahedral deposits. Square wave

voltammetry was found to be a potentially useful electrochemical tool for introducing nanoscale features to the copper deposits. Different combinations of the two additives explored in this work (PEG and KCl) afforded some further control over particle morphology but attempts to use the resultant substrates for SERS were ultimately unsuccessful.

The bimetallic Cu-Ag substrates displayed major promise for SERS and EC-SERS. Despite using only a trace amount of silver in the electrodeposition, the resultant bimetallic substrate exhibited SERS enhancement at 785 nm that was greater than for monometallic silver substrates. This represented a significant improvement for the long term sustainability of plasmonic substrates. For example, for the production of 20 SERS substrates, the Cu-Ag bimetallic substrates require nearly 100,000 times less silver ion.

In summary, copper does hold promise as a plasmonic metal for future applications, however significant challenges remain with regards to reliable, facile and low energy methods of fabricating Cu nanostructures. In addition, the ease of oxidation of copper remains a significant issue in the field. This thesis research has highlighted the potential of electrodeposition and voltammetric techniques for this purpose, however little success was achieved for the monometallic copper substrates. Instead, bimetallic metal nanostructures that incorporate trace amounts of silver appear to show great promise and will be explored further.

Future work in this area will continue to focus on the creation of stable and nanoscale copper structures through electrochemical approaches. In particular, future work will explore alternate additives as well as ionic liquids for enhanced morphological

control. As well, the Cu-Ag bimetallic structures reported in this work should be explored from a computational point of view through finite-difference time-domain (FDTD) calculations; this would allow one to fully understand the near-field coupling between the two metals and examine the theoretical origin of the SERS enhancement for these structures.

6.4 Final Thoughts

In summary, this thesis work represents an exploration into the very new area of *sustainable* plasmonics. Many applications of plasmonics are poised to make significant advancement in essential areas such as renewable energy, catalysis, and environmental protection. This thesis work has explored three central themes: (i) green synthesis of metal nanoparticles (ii) bioscaffold-based templating for multidimensional plasmonics, and (iii) Cu-based plasmonics. In all three areas successes were noted, and ideas for future work have been suggested. Perhaps most importantly, this thesis work starts a conversation that must take place in the field of plasmonics if any of the future applications of this technology are to be realized in a sustainable and long term way.

References

1. Garcia, M. A. *J. Phys. D: Appl. Phys*. **2011**, 44, 283001
2. Rycenga, M.; Cobley, C.M.; Zeng, J.; Li, W.; Moran, C. H.; Zhang, Q.; Qin, D.; Xia, Y. *Chem Rev*. **2011**, 111, 3669-3712
3. Duan, H.; Wang, D.; Li, Y. *Chem. Soc. Rev.* **2015**, *44*, 5778-5792.
4. Sharma, V. K.; Yngard, R. A.; Lin, Y. *Adv. Colloid Interface Sci.* **2009**, *145*, 83-96.
5. Iravani, S. *Green Chem.* **2011**, *13*, 2638-2650.
6. de Souza Porto, M. F.; de Freitas, C. M. *Risk analysis : an official publication of the Society for Risk Analysis* **1996**, *16*, 19-29.
7. Gunster, D. G.; Bonnevie, N. L.; Gillis, C. A.; Wenning, R. J. *Ecotoxicol. Environ. Saf.* **1993**, *25*, 202-213.
8. Walt Bodanich and Eric Koli. Tainted Exports: 2 Paths of Bayer Drug in 80's: Riskier Type Went Overseas. *New York Times*. May 22, **2003**, 1-7.
9. Anastas, P. T.; Kirchhoff, M. M. *Acc. Chem. Res.* **2002**, *35*, 686-694.
10. Anastas, P.; Eghbali, N. *Chem. Soc. Rev.* **2010**, *39*, 301-312.
11. Warner, J. C. *Abstracts of Papers of the American Chemical Society* **2012**, *244*.
12. Clark.J.H; Smith,P. *Innov. Pharmaceut. Technol*.,**2005**, 94.
13. Sheldon, R. A. Catalysis: *J. Chem. Technol. Biotechnol.* **1997**, *68*, 381-388.
14. Mendum, T.; Stoler, E.; VanBenschoten, H.; Warner, J. C. *Green Chem. Lett Rev.* **2011**, *4*, 81-86.
15. Hehn, R. S. *Environ. Sci. Technol.* **2016**, *50*, 397-404.

16. Greimel, K. J., Perz, V., Koren, K., Feola, R., Temel, A., Sohar, C.; Guebitz, G. M.*Green Chem*. **2013**, *15*(2), 381-388.
17. Gavankar, S.; Suh, S.; Keller, A. F. *Int. J. Life Cycle Assess.* **2012**, *17*, 295-303.
18. Gilbertson, L. M.; Zimmerman, J. B.; Plata, D. L.; Hutchison, J. E.; Anastas, P. T. *Chem. Soc. Rev.* **2015**, *44*, 5758-5777.
19. Dhingra, R.; Naidu, S.; Upreti, G.; Sawhney, R. *Sustainability*, **2010**, 210, 3323-3338
20. Subramanian, V.; Sermenzin, E.; Hristozov, D.; Marcomini, A.; Linkov, I. *Nanotoday*, **2014**, 9, 6-9
21. Fadeel, B.; Garcia-Bennett, A. E. *Adv. Drug Deliv. Rev.* **2010**, *62*, 362-374
22. Stewart, M. E.; Anderton, C. R.; Thompson, L. B.; Maria, J.; Gray, S. K.; Rogers, J. A.; Nuzzo, R. G. *Chem. Rev.* **2008**, *108*, 494-521.
23. Upadhyay, L. S. B.; Verma, N. *Anal. Lett.* **2015**, *48*, 2676-2692.
24. Jenkins, R.L.; Carley, A, F.; Knight, D.; Kiely, C.J.; Hutchings, G. J. *Nat. Chem*, **2011**, 3, 551-555.
25. Satoh, N.; Nakashima, T.; Yamamoto, K. *Nat. Nanotechnol*. **2008**, 3, 106-111
26. You, H.; Yang, S.; Ding, B.; Yang, H. *Chem. Soc. Rev*. **2013**, 4, 2880-2904.
27. Xie, J.P.; Lee, J. Y.; Wang, D. I. C.; Ting, Y.P. *ACS Nano*, **2007**, 1, 429-439.
28. Tan, Y. N.; Lee, J. Y.; Wang. D. I. C. *J. Am. Chem. Soc*. **2010**, 132, 5677-5686
29. Sheldon, R. A. *Green Chem*, **2005**, 7, 267.
30. Chung, I.; Park, I.; Seung-Hyun, K.; Thiruvengadam, M.; Rajakumar, G. *Nanoscale Res. Lett.* **2016**, 11, 40.

31. Metz,K. M.; Sanders, S. E.; Pender, J. P.; Dix, M. R.; Hinds, D. T.; Quinn, S. J.; Ward, A. D.; Duffy, P. I.; Cullen, R. J.;Colavita, P. E. *ACS Sustainable Chem. Eng.*, **2015**, 3, 1610-1617

32. Zhou, H.; Fan, T.; Zhang, D. *Chemsuschem* **2011**, *4*, 1344-1387.

33. Hoffert, M. I.; Caleira, A, K.; Haites, E, F.; Harvey, L.D.; Potter, S. D.; Schneider, S. H.; Watts,R. G.; Wigley, T.M.L.; Wuebbles, D. J. *Nature*. **1998**, 395, 881-884.

34. Chen, J.; Qin, G.; Chen, Q.; Yu, J.; Li, S.; Cao, F.; Yang, B.; Ren, Y. *J. Mater. Chem. C* **2015**, *3*, 4933-4944.

35. Fernandes, F. M.; Coradin, T.; Aime, C. *Nanomater.* **2014**, *4*, 792-812.

36. Kroeger, N.; Brunner, E. *Wiley Interdisciplinary Rev. Nanomed. Nanobiotech.* **2014**, *6*, 615-627.

37. Ren, F.; Campbell, J.; Wang, X.; Rorrer, G.; Wang, *Opt. Express* **2013**, *21*, 15308-15313.

38. Yang, J.; Zhen, L.; Ren, F.; Campbell, J.; Rorrer, G. L.; Wang, A. X. *J. Biophotonics* **2015**, *8*, 659-667.

39. Garrett, N. L.; Sekine, R.; Dixon, M. W. A.; Tilley, L.; Bambery, K. R.; Wood, B. R. *Phys. Chem. Chem. Phys.* **2015**, *17*, 21164-21168.

40. Jakšić, Z.; Pantelić, D.; Sarajlić, M.; Savić-Šević, S.; Matović, J.; Jelenković, B.; Vasiljević-Radović, D.; Ćurčić, S.; Vuković, S.; Pavlović, V.; Buha, J.; Lačković, V.; Labudović-Borović, M.; Ćurčić, B. *Opt. Mat.* **2013**, *35*, 1869-1875.

41. Lv, M. Y.; Teng, H. Y.; Chen, Z. Y.; Zhao, Y. M.; Zhang, X.; Liu, L.; Wu, Z.; Liu, L. M.; Xu, H. J. *Sens. Actuators B Chem.* **2015**, *209*, 820-827.

42. Yan, R.; Chen, M.; Zhou, H.; Liu, T.; Tang, X.; Zhang, K.; Zhu, H.; Ye, J.; Zhang, D.; Fan, T. *Sci. Rep.* **2016**, *6*, 20001.

43. Blau, S.K. *Phys. Today*, **2004**, 57, 18

44. Liu, H.; Wang, X.; Cui, W.; Dou, Y.; Zhao, D.; Xia, Y. *J. Mat. Chem.* **2010**, *20*, 4223-4230.

45. Meng, Y.; Gu, D.; Zhang, F. Q.; Shi, Y. F.; Yang, H. F.; Li, Z.; Yu, C. Z.; Tu, B.; Zhao, D. Y. *Angew. Chem. Int. Ed.* **2005**, *44*, 7053-7059.

46. Payne, E.K.; Rosi, N.L.; Xue, C.; Mirkin, C.A. *Angew Chem Int Ed*. **2005**, 44, 5064-5067

47. Davis, S.C.; Sheppard, V.C.; Begum, G.; Cai, Y, Fang, Y.; Berrigan J.D, Kroger, N.; Sandhage, K,H. *Adv. Funct. Mater*. **2013**, 23, 4611-4620.

48. Periodic table of endangered elements.http://www.compoundchem.com/2015/08/19/endangered-elements/ (Accessed August 11, 2016)

49. Wang,J.; He, S.; Jiang, Y. Iron nitride permanent magnet and technique for forming iron nitride permanent magnet.US20140299810 A1, Oct 9,**2014**

50. Zhang, Q.; Zhang, K.; Xu, D.; Yang, G.; Huang, H.; Nie, F.; Liu, C.; Yang, S. *Progress. Mat. Sci.* **2014**, 60, 208-337.

51. Neupane, M. P.; Kim, Y. K.; Park, I. S.; Kim, K, Lee, M. H, Bae, T.S. *Surf Interface Anal.* **2009**, 41 259-263.

52. Outokesh, M.; Hosseinpour, M.; Ahmadi, S. J.; Mousavand, T.; Sadjadi, S.; Soltanian, W. *Ind Eng. Chem. Res.* **2011**, 50, 3540-3554

53. Guo, M.; Lie, M.; Zhao, W.; Xia, Yue.; Huang, Wei.; Li, Z. *Appl. Surf. Sci*. **2015**,353, 1277-1284.

54. Chen, L.; Yu, J.; Fujita, T.; Chen, M. *Adv. Funct. Mater*. **2009**,19, 1221-1226.

55. Bassetto, V. C.; Russel, A. E. ; Kubota, L.T. ; Bartlette, P.N. *Electrochimica Acta*. **2014**, 144, 400-405

56. Weber, C.; Patterson, Z.; Zhao, M.; Balachandran, R.; Gouk, R.; Verhaverbeke, S.; Shadman, F.; Keswani, M. *Mat. Sci. Semiconductor Processing*. **2015**, 30, 578-584

57. Lee, P. C.; Meisel, D. *J. Phys. Chem*. **1982**, 86, 339

58. Dong,X.; Ji, X.; Wu, H.; Zhao, L.; Li, J.; Yang, W. *J. Phys. Chem. C*, **2009**, 113 16, 6573–6576.

59. Dong, X, Ji, X.; Wu, H.; Zhao, L.; Li, J.; Yang, W. *J. Phys. Chem. C.* **2009**, 113, 673.

60. Zhang, Q.; Zhang, K.; Xu, D.; Yang, G.; Huang, H.; Nie, F.; Liu, C.; Yang, S. *Progress. Mat. Sci* **2014**, 60, 208-337.

61. Pushpavanam, K.; Santra, S.; Rege, K. *Langmuir* **2014**, *30*, 14095-14103.

62. Haes, A. J.; Zou, S.; Schatz, G. C.; Van Duyne, R. P. *J. Phys. Chem. B*, **2004**, 108, 109–116

63. Zhou, J.; Zhu, F.; Wang, Y.; Wang, Tao. *Chem. Phys. Lett*. **2015**, 627, 96-100

64. Everett, D.H. Definitions, Terminology and Symbols in Colloid and Surface Chemistry: Part 1. *Pure and Applied Chemistry*, **1972**,31, 579-638.

65. Nützenadel, C. *Eur. Phys. J. D.* **2000**, 8, 245-250

66. Cao, G.; Wang, Y. Nanostructures and Nanomaterials: Synthesis, Properties, and Applications. 2ndED. University of Washington, USA.**2011.**

67. Polte, J. *CrystEngComm* **2015**, *17*, 6809-6830.

68. Brett, C. M.A.; Brett, A.M. O. Electrochemistry Principles, Methods, and Applications, Oxford University. **1993.**

69. Rotello, V. Nanoparticles: Building Blocks for Nanotechnology. *Plasmonic Nanomaterials*. Wei. A. University of Massachusetts, Amherst Massachusetts. **2004.**

70. Aroca, R. Surface-Enhanced Vibrational Spectroscopy. University of Windsor, Ontario, Canada, **2006.**

71. Xie, W.; Schlucker, S.; *Nat. Commun.* **2015**, 6, 770.

72. Alison M. Funston, Carolina Novo, Tim J. Davis, and Paul Mulvaney. *Nano Lett.* **2009,** 9, 1651-1658.

73. Robatjazi, H.; Bahauddin, S. M.; Doiron, C.; Thormann, I. *Nano Lett*. **2015**, 15, 6155-6161.

74. Sun, M. Nanoparticle Catalysis by Surface Plasmon: *Catalysis by Nanoparticles*: University of Connecticut Press, **2013.**

75. Kneipp, K.; Kneipp, H.; Itzkan, I.; Dasari, R. R.; Feld, M. S. *J. Phys.Condensed Mat.* **2002**, *14*, R597-R624.

76. Ferraro, J. R.; Nakamoto, K. In *Basic Theory;* Introductory Raman Spectroscopy; Academic Press: 1250 Sixth Avenue, San Diego, CA, **1994**, 1-90.

77. Pelletier, M. J. In *Introduction to Applied Raman Spectroscopy;* Analytical Applications of Raman Spectroscopy; BlackwellnScience: Ann Arbor, Michigan, USA, **1999**, 1-44.

78. Jeanmaire, D. L.; Van Duyne, R. P. *J. Electroanal. Chem. Int. Electrochem.* **1977**, *84*, 1-20.

79. Creighton, J.; Albrecht, M.; Hester, R.; Matthew, J. *Chem. Phys. Lett.* **1978**, *55*, 55-58.

80. Kennedy, B.; Spaeth, S.; Dickey, M.; Carron, K. *J. of Phys. Chem. B* **1999**, *103*, 3640-3646.

81. Cai, W. B.; Ren, B.; Li, X. Q.; She, C. X.; Liu, F. M.; Cai, X. W.; Tian, Z. Q. *Surf. Sci.***1998**, *406*, 9-22.

82. Skoog. A. Douglas; West. M. Donald; Holler. F. James; Crouch. Stanely. R., Eds.; In *Fundamentals of Analytical Chemistry eighth edition;* Brook/ Cole Cengage Learning: United States of America, **2004.**

83. Kanani, N. Electrolplating, Basic Principles, Processes and Practice. Atotech Deutschland GmbH, Germany. **2004.**

84. Goodall, B.; Robinson, A. M.; Brosseau. C. L. *Phys. Chem. Chem. Phys*., **2013**,15, 1382-1388.

85. Robinson, A.M.; Harroun, S. G.; Bergman, J.; Brosseau, C. L. *Anal. Chem*., **2012**, 84 (3), 1760–1764

86. Zhao, L.; Ding, K.; Ji, X.; Li, J.; Wang, H.; Yang.W. *Colloids Surf. A*, **2011**, 386.

87. Dendisova, M.; Havranek, L.; Oncak, M.; Matejka, P. *J. Chem. C*. **2013**, 117, 21245-21253.

88. Zhao, L.; Blackburn, J.; Brosseau, C.L. *Anal. Chem,* **2015**, 87, 441-447.

89. Vidal-Iglesias, F. J.; Solla-Gullon, J.; Orts, J. M.; Rodes, A.; Perez, J. M. *Journal of Physical Chemistry C* **2015**, *119*, 12312-12324.

90. Xie, D.; Sharma, S. B.; Paiva, N. L.; Ferreira, D.; Dixon, R. A. *Science*, **2003**, 299, 396-399.

91. Giampieri, F.; Tulipani, S.; Alvarez-Suarez, J. M.; Quiles, J. L.; Mezzetti, B.; Battino, M. *Nutrition* **2012**, *28*, 9-19.

92. Halliwel, B. *Nutr. Rev*. **1997**, 55, S44.

93. Hadjipavlou-Litina, D.; Magoulas, G. E.; Bariamis, S. E.; Drainas, D.; Avgoustakis, K.; Papaioannou, D. *Bioorg. Med. Chem.* **2010**, *18*, 8204-8217.

94. Liang, E.J.; Engert, C.; Kiefer, W. *Vib. Spec*. **1995**, 8, 435-444

95. Bors, B. Comparing Haskap to other Berries. http://www.fruit.usask.ca/articles/Haskap/Haskap%20Sister%20crops.pdf. (Accesed 26,Aug, 2016).

96. Ibrahim, H. M. M. *J. Radiat. Res. Appl. Sci.* **2015**, *8*, 265-275.

97. Bankar, A.; Joshi, B.; Kumar, A. R.; Zinjarde, S. *Colloids Surf. Physicochem. Eng. Aspects* **2010**, *368*, 58-63.

98. Schlucker, S. Surface Enhanced Raman Spectroscopy: Analytical, Biophysical and life Science Applications. *Electrochemical SERS and its Application in Analytical, Biophysical and Life Science.* Ren, B.; Wu, Y. C.; Tian, Z. University of Wurzburg and Eisingen.**2011.**

99. Nostro, A.; Germanò, M. P.; D'Angelo, V.; Marino, A.; Cannatelli, M. A. *Lett. Appl. Microbiol*. **2000**, 30, 379-384.

100. Stashenko, E. E.; Jaramillo, B. E.; Martínez, J. R. *J. Chromatography A.* **2004**, 1025, 93-103.

101. Zheng, W.; Wang, S.Y. *J. Agric. Food Chem*., **2001**, 49, 5165–5170

102. Marriott, J.; Robinson, M.; Karikari, S.K. *Sci. Food Agri*. **1981**, 32, 1021-1026.

103. Salvador, A.; Sanz, T.; Fiszman, S. M. *Postharvest Biol. Technol.* **2007***, 43*, 319-325.

104. González-Montelongo, R.; Gloria Lobo, M.; González, M. *Food Chem.* **2010***, 119*, 1030-1039.

105. Soong, Y.; Barlow, P. J. *Food Chem.* **2004***, 88*, 411-417.

106. Rodríguez-Carpena, J.; Morcuende, D.; Andrade, M.; Kylli, P.; Estévez, M. *J. Agric. Food Chem.***2011**, *59*, 5625-5635.

107. Kerker, M.; Siiman, O.; Bumm, L.; Wang, D..*Appl. Opt.* **1980***, 19*, 3253-3255.

108. Jayram, N. D.; Aishwarya, D.; Sonia, S.; Margalaraj, D.; Kumar, P. S.; Rao, G. M. *J. Colloid and Interface Science*. **2016**, 477, 209-119.

109. Huang, M. H.; Chiu, C. *J. Mater. Chem. A*, **2013**, 1, 8081-8092.

110. Stoychev, D.; Tsvetanov,C. *J. Appl. Electrochem*, **1996**, 26, 741-749.